Prädiktive Regelung der Strömung in Rohrnetzwerken solarthermischer Kraftwerke

Predictive Control of the flow in Networks of Tubes in Solar Thermal Power Plants

Masterarbeit
Mathematik

März 2019

Vorgelegt von Presented by	Annika Sachtje Wirichsbongardstraße 65 52062 Aachen Matrikelnummer: 319110 annika.sachtje@rwth-aachen.de
Erstprüfer First examiner	Prof. Dr. rer. nat. Michael Herty Lehr- und Forschungsgebiet: Kontinuierliche Optimierung (IGPM) RWTH Aachen University
Externer Betreuer External supervisor	Dr. rer. nat. Pascal Richter Steinbuch Centre for Computing Karlsruhe Institute of Technology

Eigenständigkeitserklärung

Hiermit versichere ich, dass ich diese Masterarbeit selbstständig verfasst und keine anderen als die angegebenen Quellen und Hilfsmittel benutzt habe. Die Stellen meiner Arbeit, die dem Wortlaut oder dem Sinn nach anderen Werken entnommen sind, habe ich in jedem Fall unter Angabe der Quelle als Entlehnung kenntlich gemacht. Dasselbe gilt sinngemäß für Tabellen und Abbildungen. Diese Arbeit hat in dieser oder einer ähnlichen Form noch nicht im Rahmen einer anderen Prüfung vorgelegen.

Aachen, März 2019

Annika Sachtje

Contents

1. Introduction

As, due to climate change, nature phenomena become more and more dangerous and oil and coal deposits are limited, we are forced to think about alternative sources of energy. Alternative sources like renewable energies, such as solar power. Energy from renewable sources is rapidly taking over on the market and will continue to do so in the next years, supported by the energy level targets of the EU-governments: "This EU level target will drive continued investment in renewable energy meaning, for example, that the share of renewable energy in the electricity sector would increase from 21% today to at least 45% in 2030." [5]

To ensure that energy from renewable sources is able to meet the increasing demand or even partially replace fossil energy, the solar thermal power plants need to produce enough energy and be preferably at least as profitable as coal-fired plants, for example. Since renewable energies are still relatively young compared to energy based on fossil resources, those systems are not yet as well explored. Even among solar thermal power plants there are different types.This thesis will focus exclusively on solar thermal power plants with parabolic troughs. Those power plants work similar to coal-fired power stations, producing energy with a steam driven turbine. But rather than with coal, the water in solar thermal power plants is warmed with the help of a heat transfer fluid (short: HTF). This fluid is pumped through pipes, which are heated up by sunlight, concentrated via parabolic mirrors.

How hot the HTF gets, does not only depend on the amount of solar irradiance provided by the sun. The mass flow inside the tube plays a major role, too. When the fluid passes through the pipe more slowly, it is exposed to the sunlight for a longer period of time and thereby reaches a higher temperature. Nevertheless it is very important to keep the HTF's temperature within fluid specific thresholds to prevent irreversible decomposition.

The goal of this thesis is to optimize the control of the mass flow inside the network of tubes, keeping the fluids temperature as high as possible, while staying within those thresholds.

To do so, the physical phenomena of a solar thermal power plant must be simulated in a mathematical model. An accurate model is given by the Navier Stokes equations. However calculations based on those equations would be too complex. The considerations of this thesis will therefore be based on a simplified model, based on temperature-balance laws. This model is still very precise to ensure realistic results. It is eased to only one equation and thus keeps complexity and computational time in reasonable measures. Rather than reacting on the current situation by approximating the needed mass flow, this thesis will introduce a predictive control. Therefore the mass flow of each tube will be calculated via an optimization problem, which considers the fluid's future behavior, judged on the current temperature and irradiation level.

While optimization problems often already are hard to solve, this one also includes a partial differential equation (short: PDE), making calculations even harder. Hence the optimization problem will be solved with the Karush-Kuhn-Tucker-Method (short:

KKT-Method).

Although controling the mass flow with an optimization problem is more complex, it also gives a higher precision, providing good values without having to settle first. Thus this strategy is promising for application in reality, where the network's flow can only be regulated in periodic steps, rather than in every second.

The resulting control is then extended by the use of mirrors or valves in order to achieve a result as perfect as possible.

Hence the thesis will be organized as follows:

Section 2 will provide the foundational knowledge about the processes in a solar thermal power plant with parabolic troughs and the current state-of-the-art for control. Section 3 will then deal with the mathematical model on which the observations will be based on. After that, Section 4 gives a brief overview over the mathematical basics, which are necessary for the thesis' further calculations, before the optimization problem for a closed loop, i.e. one tube, is introduced. Moreover the section will set up the corresponding KKT-System. Furthermore it is explained how this strategy is implemented and simulated in Matlab. To get started with the consideration of a network, Section 5 will briefly summarize Cherek's theory in this regard. Based on the knowledge for a single tube, Section 6 will use Cherek's Mirror- and Valve-Control [4] and adapt the mass flow update according to the optimization problem. Moreover the control strategies are adjusted to the predictive approach. At last, in Section 7 an extensive feasibility study will be presented, comparing the results of this thesis with those of Cherek and also studying real data. This will include scenarios for the single tube case as well as the network situation.

2. A solar thermal power plant with parabolic troughs

In order to optimize the control of a solar thermal power plant, it is necessary to understand the processes operating there. On this basis the model of fluid mechanics, that is used in this thesis, becomes comprehensible.

A solar thermal power plant with parabolic troughs works similar to a coal-fired power station.
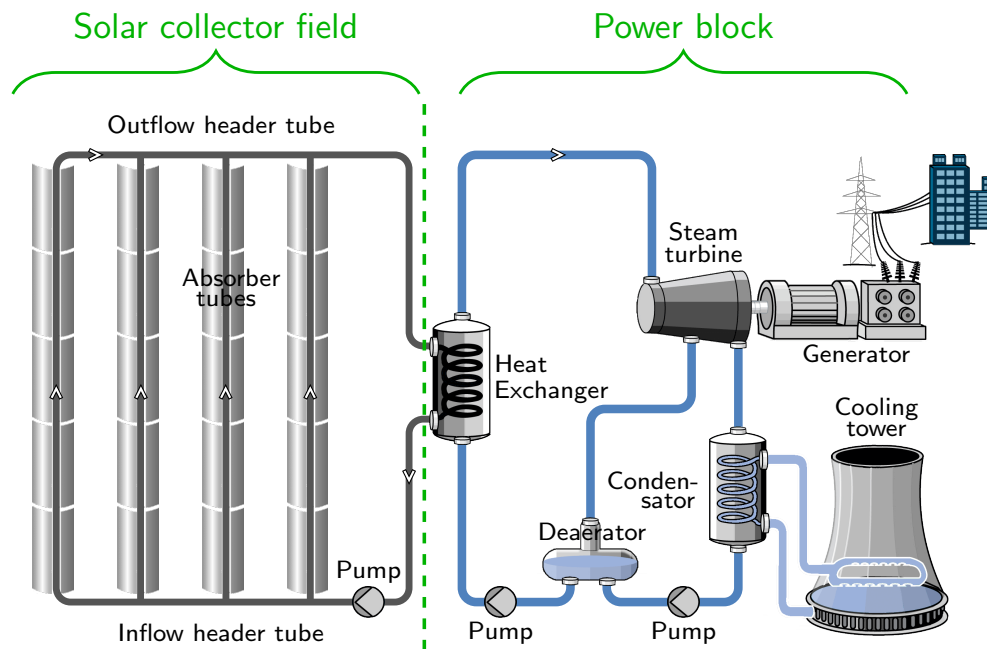

Figure 1: Conceptual drawing of a Solar thermal power plant with parabolic troughs.

The power plant is divided into two parts, the solar block or solar collector field (Figure 1, left) and the power block (Figure 1, right).
Let's consider the power block first. Rather than burning coal underneath a huge basin of water, here the water is heated up by a heat exchanger. As in coal-fired power stations, the resulting steam drives a turbine and the generator finally generates the electric power. The electic power can then be fed into the power grid. Meanwhile the steam cools down and condensates back to water with use of a condensator and cooling tower. In the water dissolved gases (excess air) are removed in the deaerator, as they would cause damage, such as rust, within the network. The removed gases are returned to the steam turbine. Now the water can again be pumped through the heat exchanger to be heated for steam generation. On the other side is the solar block of the system. In this block, the heat transfer fluid, which serves the heat exchanger as energy source, is warmed with the help of sunlight. The solar collector field consists of a network of pipes. The pipes leading to and from the network are called the inflow

and outflow header tubes. They are not exposed to sunlight and are well insulated to maintain the temperature inside the pipe. These two tubes are connected by a large number of so-called absorber or collector tubes. The absorber tubes are responsible for the temperature increase. They are surrounded by huge parabolic mirrors which reflect the sun's rays onto the pipe and thus heat the contained fluid (compare Figure 1).

To use as much sunlight as possible in the most effective way, the mirrors are attached mobile, so that they are able to follow the sun, as it moves along the sky (see Figure 2).
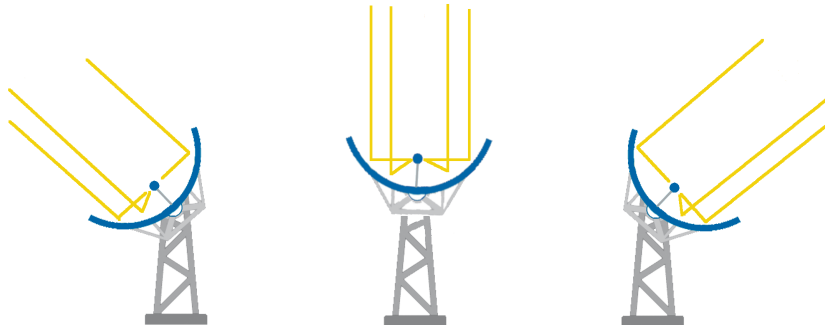

Figure 2: Conceptual drawing of a parabolic trough following the sun.

As mentioned earlier, due to the rising importance of power won by solar energy, there has already been done a lot of research on solar thermal power plants in the last years. The best location for power plants have been analyzed [6, 14], as well as design criteria that decrease the building costs [13, 2]. Research has been done, concerning used materials in the power plants, such as mirrors and tubes [8] including observations on heat loss [15]. Furthermore the impact of the heat transfer fluid has already been investigated [10, 12]. Along with this research, the solar thermal power plant had to be modeled in a mathematical way, so that for different purposes there already exist different models of the complex system, each discretized according the investigated information (compare [16],[7]).

Now the aim of all those improvements is for the heat of the fluid, which is measured at the end of the absorber field, to reach and hold the desired temperature. In case to do so, the control can manipulate the volumetric flow of the pump, the aperture of the mirrors and the valves, that already exist at the beginning of the absorber tubes. Currently those valves are only positioned once a year. So the current state-of-the-art is the following strategy:

The parabolic mirrors follow the sun as it rises along the sky. According to the weather conditions and therefore the intensity of the sun, the volumetric flow through the network is tuned by the pump. In the case when clouds overshadow parts of the network, or mirrors are broken and cannot be repaired right away, as this would shut down operations, the pump control is not sufficient anymore. As the pump control

affects all absorber tubes at once, the fluid in not overshadowed pipes would exceed the critical heat. In order to prevent this, well-functioning mirrors are defocused.

The new approach is to also use the valves to control the volumetric flow of single tubes, minimizing the number of defocused mirrors and maximizing the plants efficiency.

3. Flow in a tube

An accurate model of a solar thermal power plant, which considers all physical quantities, would be way to complex to solve. Even if such a model could be set up and solved, the computation time would exclude a practical usage in the operating plant. Hence the system has to be discretized, while always keeping the overall purpose in mind. So the aim is to find a model, which is easy enough to be calculated in reasonable time, but not simplified to an extend where its behaviour deviates too much from reality. This thesis is based on a model by Cherek [4], described in this section.

As the energy input of the solar thermal power plant is provided by the sun, it needs to be represented in an optical model. On top of that the dynamic of the fluid inside the pipes is described by the thermodynamic model. Lastly the model is expanded to a network of tubes.

3.1. Optical model

To model the rise of the sun across the sky, as well as tubes being partly overshadowed, the solar irradiation is simulated by a function $I(x,t)$ dependent on space and time. Further variables considered in the optical model are the geometrical parameters of the collector field and the parameters describing the parabolic mirrors, which are used to reflect the sunlight to the absorber tubes.

Parameter	Description	Unit
$I(x,t)$	Direct solar irradiation	$\mathrm{W\,m^{-2}}$
η_{col}	Global efficiency factor	-
G	Aperture of the mirrors	m
$\phi(x,t)$	Defocus factor	-
N	Number of collector rows	-
N_{mirror}	Number of mirrors per collector row	-
ℓ_{a}	Length of the collector rows	m
ℓ_{mirror}	Length of the mirrors	m
ℓ_{h}	Length of the header tubes	m
ℓ_{d}	Distance between the absorber tubes	m
A_{h}	Cross sectional area of the header tubes	$\mathrm{m^2}$
A_{a}	Cross sectional area of the absorber tubes	$\mathrm{m^2}$
D_{h}	Inner diameter of the header tubes	m
D_{a}	Inner diameter of the absorber tubes	m

Table 1: Parameters of the optical and geometrical model.

Here the defocus factor $\phi(x,t)$ states whether the mirror at position x is defocused in time step t or not. Thereby broken mirrors can be modelled as permanently defocused.

The length of the tubes are given via

$$l_a = \ell_{\text{mirror}} \cdot N_{\text{mirror}} \text{ and } \ell_{\text{h}} = N \cdot \ell_{\text{d}}. \tag{1}$$

And finally the inner diameters of the tubes are calculated using the cross sectional areas

$$D = \sqrt{\frac{A}{\pi}} \cdot 2, \tag{2}$$

for absorber and header tubes respectively.

3.2. Thermodynamic model

As for the thermodynamic processes, Cherek began with the conservation laws of mass, momentum and energy and combined them with a model of the energy input from the sun:

$$\rho_t + (\rho\nu)_x = 0 \tag{3}$$

$$(\rho\nu)_t + (\rho\nu^2 + p)_x = -\frac{\xi}{D}\frac{\rho\nu|\nu|}{2} + \frac{4}{3}(\mu\nu_x)_x \tag{4}$$

$$E_t + (\nu(E + p))_x = \frac{\xi}{D}\frac{\rho\nu^2|\nu|}{2} + \frac{4}{3}(\mu\nu\nu_x)_x + (kT_x)_x + \frac{4}{D}H^t(T_m - T) \tag{5}$$

$$\rho_m \cdot c_m \cdot A \cdot (T_m)_t = \eta_{\text{col}} \cdot \phi(x,t) \cdot G \cdot I(x,t) - P_{rc} - D\pi H^t(T_m - T) \tag{6}$$

The used parameters are denoted in Table 2.

Parameter	Description
ρ, ρ_m	Density of the fluid/ the wall of the tube
c_{v}, c_m	Specific heat capacity of the fluid/ the wall of the tube
ν	Velocity of the fluid
p	Pressure of the fluid
μ	Dynamic viscosity of the fluid
E	Total energy of the fluid
k	Thermal conductivity of the fluid
T	Temperature of the fluid
H^t	Convective heat transfer coefficient
T_m	Temperature of the tube wall
ω	Surface roughness of the tube
P_{rc}	Convective thermal losses
η_{therm}	Thermodynamic efficiency factor
ξ	Aperture of the valves

Table 2: Parameters of the thermodynamic model.

Due to the size ratio of tube length to width, the flow model is kept one dimensional.

Scale Analysis

Then Cherek performed a scale analysis to discard terms with no notable influence. Moreover he changed equation (5), so it models the temperature rather than the total energy, as the temperature is what is going to be controlled. This leads to the following model of three partial differential equations:

$$\rho_t + (\rho\nu)_x = 0 \,, \tag{7}$$

$$(\rho\nu)_t + \left(\rho\nu^2 + \frac{p_\mathrm{r}}{\rho_\mathrm{r}\nu_\mathrm{r}^2}p\right)_x = -\frac{\omega}{D_\mathrm{a}}\ell_\mathrm{a}\frac{\rho\nu|\nu|}{2}\,, \tag{8}$$

$$(\rho T)_t + \left(\nu\rho T + \frac{p_\mathrm{r}}{\rho_\mathrm{r}T_\mathrm{r}c_\mathrm{v}}p\nu\right)_x = \frac{\xi}{D_\mathrm{a}}\frac{\nu_\mathrm{r}^2\ell_\mathrm{a}}{c_\mathrm{v}T_\mathrm{r}}\frac{\rho\nu^2|\nu|}{2} - \frac{4H_\mathrm{r}^\mathrm{t}T_\mathrm{m,r}}{D_\mathrm{a}\rho_\mathrm{r}c_\mathrm{v}T_\mathrm{r}}H^\mathrm{t}T_\mathrm{m} + \frac{4H_\mathrm{r}^\mathrm{t}}{D_\mathrm{a}\rho_\mathrm{r}c_\mathrm{v}}H^\mathrm{t}T\,. \tag{9}$$

Here, parameters indexed with an r are reference parameters. The parameters are given in the tables below and characterize the typically used specifications of solar thermal power plants. These are also the parameters, that will be used in the simulations.

Quantity		Value
Length of the absorber tube	ℓ_a	$1000\,\mathrm{m}$
Inner diameter of the absorber tube	D_a	$0.070\,\mathrm{m}$
Inner diameter of the header tube	D_h	$0.1\,\mathrm{m}$
Surface roughness	ω	$0.024\,\mathrm{mm}$

Table 3: Reference parameters for the network of tubes.

Quantity		Molten salt	Thermal oil	Unit
Temperature	T_r	[523.2, 710]	[353.2, 673.2]	K
Pressure	p_r	[1, 10]	[70, 100]	bar
Velocity	u_r	[0.68, 0.74]	[1.28, 1.87]	$\mathrm{m\,s^{-1}}$
Temperature of the wall	$T_\mathrm{m,r}$	[523.2, 710]	[353.2, 673.2]	K
Heat transfer coefficient	H_r^t	[2023400, 200450]	[1299100, 193490]	$\mathrm{W\,m^{-2}\,K^{-1}}$
Density	ρ_r	[1901.4, 1761.3]	[1014.4, 693.6]	$\mathrm{kg\,m^{-3}}$
Dynamic viscosity	μ_r	[0.0041, 0.0010]	[0.0012, 0.00015]	$\mathrm{kg\,m^{-1}\,s^{-1}}$
Specific heat capacity	c_v	[2120.6, 1764.9]	[1715.8, 2635.6]	$\mathrm{m^2\,s^{-2}\,K^{-1}}$
Thermal conductivity	k_r	[0.4557, 0.3696]	[0.1300, 0.0756]	$\mathrm{W\,m^{-1}\,K^{-1}}$

Table 4: Reference parameters for the HTF.

Finally, to reduce complexity and computation time, Cherek scales down the system

to one last PDE

$$T_t + \nu T_x = \frac{\eta_{\mathrm{col}} \cdot \eta_{\mathrm{therm}} \cdot G}{\rho \cdot c_{\mathrm{v}} \cdot A} \phi(x,t) I(x,t) \; . \tag{10}$$

Therefore we are going to neglect equations of mass and momentum and assume an incompressible flow with negligible axial conduction. Furthermore we are also neglecting heat losses and diffusion, but introducing a thermodynamic efficiency factor $\eta_{col} \in [0,1]$ to consider thermodynamic losses.

Closure Equations

For closure equations Cherek considered Therminol VP1 and molten salt as heat transfer fluids. Their properties density, viscosity, thermal conductivity and specific heat capacity are given by the following equations [17],[3].

Therminol VP1

$$\begin{aligned}
\rho(T) = &- 0.90797 \, (T - 273.15) + 0.00078116 \, (T - 273.15)^2 \\
&- 2.367 \cdot 10^{-6} \, (T - 273.15)^3 + 1083.25 \; ,
\end{aligned} \tag{11}$$

$$\mu(T) = \exp\left(\frac{544.149}{(T - 273.15) + 114.43} - 2.59578 \right) \cdot 10^{-6} \, \rho \; , \tag{12}$$

$$\begin{aligned}
k(T) = &- 8.19477 \cdot 10^{-5} \, (T - 273.15) - 1.92257 \cdot 10^{-7} \, (T - 273.15)^2 \\
&+ 2.5034 \cdot 10^{-11} \, (T - 273.15)^3 - 7.2974 \cdot 10^{-15} \, (T - 273.15)^4 \\
&+ 0.137743 \; ,
\end{aligned} \tag{13}$$

$$\begin{aligned}
c_{\mathrm{v}}(T) = &(0.002414 \, (T - 273.15) + 5.9591 \cdot 10^{-6} \, (T - 273.15)^2 \\
&- 2.9879 \cdot 10^{-8} \, (T - 273.15)^3 \\
&+ 4.4172 \cdot 10^{-11} \, (T - 273.15)^4 + 1.498) \cdot 10^3 \; .
\end{aligned} \tag{14}$$

Molten Salt (NaNO$_3$-NaNO$_2$-KNO$_3$)

$$\rho(T) = 2293.6 - 0.7497T \; , \tag{15}$$

$$\mu(T) = 0.4737 - 2.297 \cdot 10^{-3} T + 3.731 \cdot 10^{-6} T^2 - 2.019 \cdot 10^{-9} T^3 \; , \tag{16}$$

$$k(T) = 0.6966 - 4.6055 \cdot 10^{-4} T \; , \tag{17}$$

$$c_{\mathrm{v}}(T) = 5806 - 10.833T + 7.2413 \cdot 10^{-3}T^2 \ . \tag{18}$$

3.3. Solver

In order to simulate the flow, the remaining PDE (10) has to be solved numerically. To do so, Cherek suggested a finite volume method, in particular an upwind scheme, since information is only forwarded in the positive x-direction. Therefore the homogeneous part of the equation is solved by

$$T_i^{n+1,-} = T_i^n - \Delta t \left(\nu \, T_x^- \right), \tag{19}$$

with the indices i denoting the cell and n denoting the current time step. Furthermore Δt is the time step size and the temperature gradient T_x^- is defined by numerical differentiation

$$T_x^- = \frac{T_i^n - T_{i-1}^n}{\Delta x} \ , \tag{20}$$

with Δx being the spatial step size. Lastly the right-hand side of equation (10) is solved by an explicit Euler step in Δt:

$$T_i^{n+1} = T_i^{n+1,-} + \Delta t \, \frac{\eta_{\mathrm{col}} \cdot \eta_{\mathrm{therm}} \cdot G}{\rho_i^n \cdot c_{v,i}^n \cdot A} I_i \phi_i^n \ . \tag{21}$$

When using upwind schemes, it is important to consider stability. In order to be stable, the used upwind scheme has to satisfy the Courant-Friedrichs-Lewy condition (short: CFL condition). In this model, this implies that for the CFL number c the inequality

$$c = \left| \frac{\nu \Delta t}{\Delta x} \right| \leq 1 \tag{22}$$

has to hold. Practice has shown, that the CFL number c should also satisfy a lower bound

$$0.5 \leq c \leq 1 \tag{23}$$

since otherwise, due to the numbers representation of computers, undesired numerical effects can occur.
The use of the explicit Euler method to solve the right-hand side finally excludes the case $c = 1$, to be able to guarantee stability for this method as well.

Instead of using the explicit Euler method to solve the right-hand side, it could be usefull to use the implicit Euler method. This method is stable but significantly slower than the explicit Euler. The formula to solve the right-hand side implicitly is

$$T_i^{n+1} = T_i^{n+1,-} + \Delta t \, \frac{\eta_{\mathrm{col}} \cdot \eta_{\mathrm{therm}} \cdot G}{\rho_i^{n+1} \cdot c_{v,i}^{n+1} \cdot A} I_i \phi_i^n \ . \tag{24}$$

Comparisons regarding computation time and accuracy of both approaches will be given in Section 7.

4. Closed-loop control

Before we show the control of an entire network of tubes, the temperature control of a fluid in one single tube is shown.

This will be the aim of this section. We will therefore give a brief overview on the mathematical theory that will be used. As the control will be based on an optimization problem, the next step is to first formulate this optimization problem. The rest of the section will than complete the theoretical observations on the control of one tube and give some information on the implementation in Matlab code.

4.1. Mathematical theory

The KKT-Method is a common strategy for solving optimization problems.
The general optimization problem is given as follows:

$$
\begin{aligned}
\min_{y} \quad & f(y) \\
\text{s.t.} \quad & h_i(y) \leq 0 \quad i \in \{1, ..., m\} \\
& g_j(y) = 0 \quad j \in \{1, ..., p\}
\end{aligned}
\tag{25}
$$

Then the corresponding Lagrange-Function is given by

$$
\mathscr{L}(y, \lambda, \mu) = f(y) + \sum_{i=1}^{m} \mu_i h_i(y) + \sum_{j=1}^{p} \lambda_j g_j(y) = f(y) + \langle \mu, h \rangle + \langle \lambda, g \rangle.
\tag{26}
$$

From this, due to duality and in case the functions are differentiable, the following KKT-system can be set up:

$$
\begin{aligned}
\nabla \mathscr{L}(y, \lambda, \mu) = \quad & \nabla f(y) + \sum_{i=1}^{m} \mu_i \nabla h_i(y) + \sum_{j=1}^{p} \lambda_j \nabla g_j(y) = 0, \\
& h_i(y) \leq 0, && \forall i \in \{1, ..., m\} \\
& g_j(y) = 0, && \forall j \in \{1, ..., p\} \\
& \mu_i \geq 0, && \forall i \in \{1, ..., m\} \\
& \mu_i h_i(y) = 0 && \forall i \in \{1, ..., m\}
\end{aligned}
\tag{27}
$$

When certain constraint qualifications are fulfilled, those equations can easily be solved, then they build an optimal solution for the original optimization problem [9, Chapter 5]. In other cases, when the constraint qualifications do not hold, the solution can be approximated by one or multiple gradient steps.

The method of gradient descent takes a minimization problem

$$
\min f(x) ,
\tag{28}
$$

where f is a real-valued function. The iterative method now starts with a well guessed starting point x_0 and determines the next value by going one step in the direction of the negative gradient

$$
x_{i+1} = x_i + \alpha_i \cdot (-\nabla f(x_i)) ,
\tag{29}
$$

with a positive step size α, which has to be adjusted in each step. This can be done by numerous strategies [9]. As this is not the main topic of this thesis, those strategies will not be further discussed.

4.2. Optimization problem

After this theoretical excurs the setting of the solar thermal power plant and the underlying model are to be considered. The model consists of one partial differential equation, describing the fluids temperature.

To start out this section will focus on a single closed loop, instead of the whole network. The given situation is shown in Figure 3. The volume flow is regulated by the pump at the beginning of the inflow-header pipe. This is where the control applies. In the absorber tube, which is lined with mirrors, the fluid is then exposed to the sunlight and warms up. The mirrors are not yet required in this scenario, as the temperature can already be sufficiently controlled by the volume flow. The temperature of the fluid is measured at the end of the absorber tube. This measurement serves as the basis for the next control step.

The power plants objective is to maximize the fluids temperature, reaching a desired threshold, while not exceeding it. Therefore the problem can be described as a minimization of the difference between the demanded and the actual temperature, measured at each end of an absorber tube. The only control option considered in this situation is a change in volumetric flow.

In conclusion, the optimization problem can be given as:

Figure 3
Solar block with
one absorber tube

$$\min_{q} \quad f(T, q)$$

$$\text{s.t.}$$

$$g(T, q) = \frac{\partial}{\partial t} T(x, t) + \frac{q(t)}{A} \cdot \frac{\partial}{\partial x} T(x, t) - \underbrace{\frac{\eta_{col} \cdot \eta_{therm} \cdot G}{A \cdot \rho(T) \cdot c_{\mathrm{v}}(T)} \phi(x, t) I(x, t)}_{=:S(T, x, t)} = 0 \qquad (30)$$

Where $T = T(x, t)$ is the fluid's temperature, depending on space and time and $q(t)$ is the volumetric flow of the pump, depending on the time. Here the temperature T implicitly depends on the volumetric flow q, so $T(x, t)$ is actually rather $T_q(x, t)$. To avoid confusion, the indexed q will be omitted.

The constraint is the partial differential equation, modelling the whole system, taken from [4] (compare Section 3). To be able to work with this constraint, all dependencies and derivations have been written out. Furthermore the velocity ν has been replaced, because $\nu = \frac{q(t)}{A}$ holds and the volumetric flow $q(t)$ as well as the pipe's cross-sectional area A are known.

At last the objective function still needs to be chosen.

Consider the temperature difference in time at the end of the tube

End-tube-function:

$$f(T, q) = \int_0^{t_{end}} (T(x_{end}, t) - T_{demand})^2 \ dt + \frac{\beta}{2} \int_0^{t_{end}} q^2(t) \ dt \ , \tag{31}$$

or the difference in time and space

Full-tube-function:

$$f(T, q) = \int_0^{t_{end}} \int_{x_0}^{x_{end}} (T(x, t) - T_{demand})^2 \ dx \ dt + \frac{\beta}{2} \int_0^{t_{end}} q^2(t) \ dt \ . \tag{32}$$

Both considered objective functions include the following term:

$$\frac{\beta}{2} \int_0^{t_{end}} q^2(t) \ dt \qquad\qquad \text{(Volumetric weight)}$$

with $\beta \in [0, \infty)$.

This is a general approach of optimization to assure the consideration of the flow itself and punish a to high rate of volumetric flow [9, Chapter 11]. Here, the weight β is a constant that still needs to be set, judged by experience. If β is chosen too big, the share of the temperature difference becomes neglectable and the optimization problem would no longer serve its purpose. On the other hand, if β is chosen too small, the control barely changes the volumetric flow of the pump, not actually controlling anything anymore.

4.3. KKT-System

Given this optimization problem, we can now start to examine the corresponding KKT-System analogous to [18].

Let

$$\Omega := \{ \ (x, t) \ | \ x \in [x_0, x_{end}] \ \text{and} \ t \in [0, t_{end}] \ \} \subset \mathbb{R}^2 \tag{33}$$

and

$$\Gamma := \{ \ t \ | \ t \in [0, t_{end}] \ \} \subset \mathbb{R}. \tag{34}$$

Notice that $T, \lambda \in L^2(\Omega)$ and $q \in L^2(\Gamma)$.

Hence the Lagrange-Function contains a double integral, resulting from the inner product of λ and the only constraint $g(T, q)$:

$$\mathscr{L}(T, q, \lambda) = f(T, q) - \int_0^{t_{end}} \int_{x_0}^{x_{end}} \lambda(x, t) \left(\frac{\partial}{\partial t} T(x, t) + \frac{q(t)}{A} \frac{\partial}{\partial x} T(x, t) - S(T, x, t) \right) dx \ dt \quad (35)$$

According to that, the KKT-System can be set up as:

$$\nabla_T \mathscr{L}(T, q, \lambda) = \nabla_T f(T, q) + \nabla_T \langle \lambda(x, t), g(T, q) \rangle = 0, \quad (36)$$

$$\nabla_q \mathscr{L}(T, q, \lambda) = \nabla_q f(T, q) + \nabla_q \langle \lambda(x, t), g(T, q) \rangle = 0, \quad (37)$$

$$\nabla_\lambda \mathscr{L}(T, q, \lambda) = \nabla_\lambda f(T, q) + \nabla_\lambda \langle \lambda(x, t), g(T, q) \rangle = g(T, q) = 0, \quad (38)$$

As the source term $S(T, x, t)$ of equation (30) depends on the temperature $T = T(x, t)$, derivating the Lagrange-Function (35) after T might get complicated. Thus, as a start, the source term will be simplified by setting the density ρ and the specific heat capacity c_v to constant values:

$$\rho(T) \equiv \tilde{\rho} \ \text{const.} \quad \text{and} \quad c_v(T) \equiv \tilde{c}_v \ \text{const.} \quad (39)$$

To visualize the degree of simplification, the corresponding correlations are plotted in the following figures (Figure 4 and 5). The figures show the density and specific heat capacity functions and the value for temperature $T = 600$ Kelvin, which will be the constant used in the simplification. Moreover a linear approximation is plotted. This will help the considerations without simplification in Section 4.3.2.

First consider the plots for Therminol VP1.
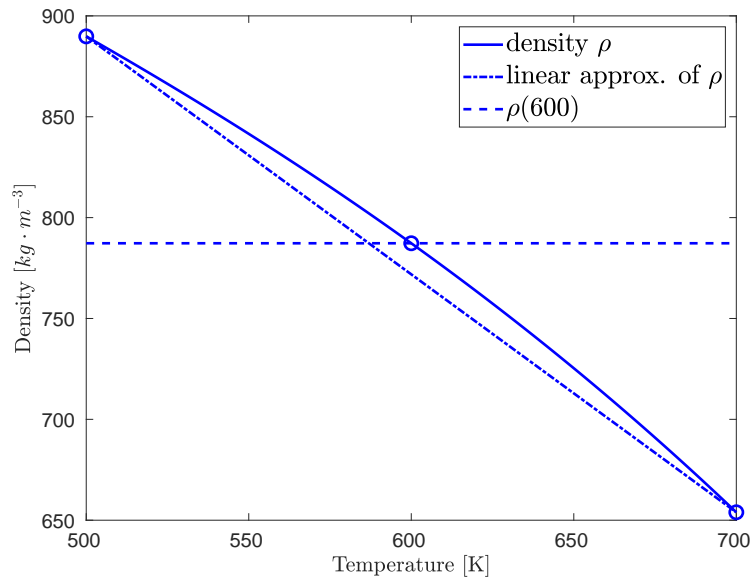
(a) Therminol VP1: Density in dependency of temperature.
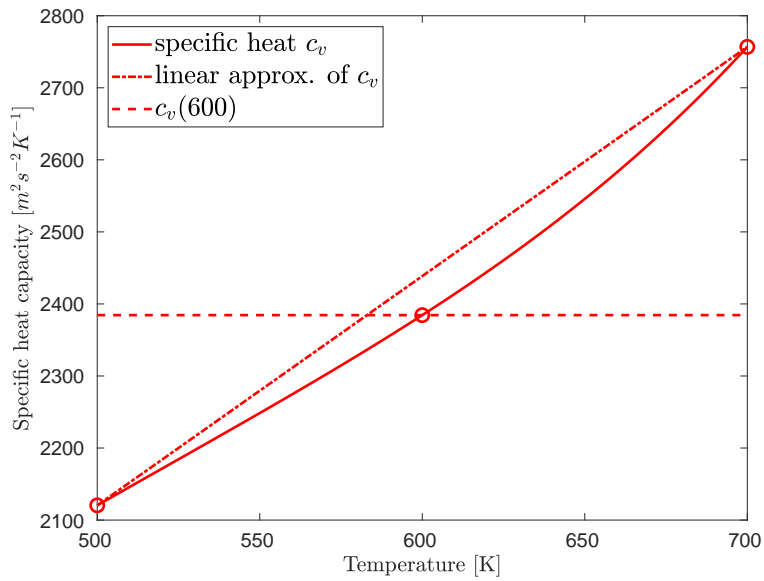
(b) Therminol VP1: Specific heat capacity.

Figure 4: Density and specific heat capacity for Therminol VP1

And also for molten salt. As the density function of molten salt is already linear, there is no need for approximation.
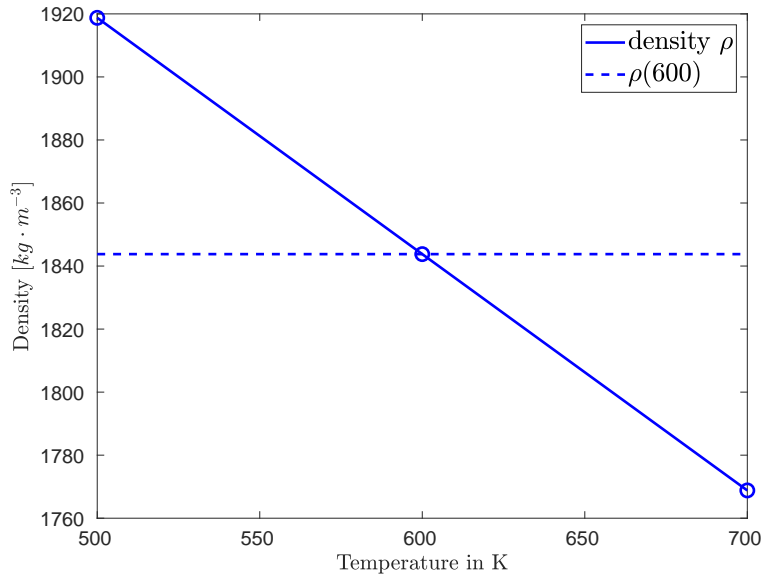
(a) Molten salt: Density in dependency of temperature.
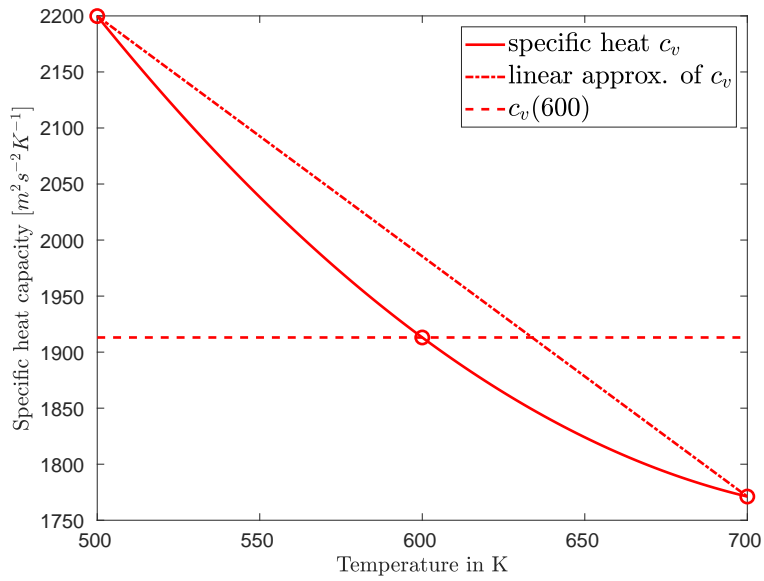
(b) Molten salt: Specific heat capacity.

Figure 5: Density and specific heat capacity for molten salt

So, the source term $S(T, x, t)$ in the constraint $g(T, q)$ from (30) does no longer depend

on $T(x,t)$. It follows:

$$g(T,q) \approx \tilde{g}(T,q) = \frac{\partial}{\partial t}T(x,t) + \frac{q(t)}{A} \cdot \frac{\partial}{\partial x}T(x,t) - \underbrace{\frac{\eta_{col} \cdot \eta_{therm} \cdot G}{A \cdot \tilde{\rho} \cdot \tilde{c}_{\mathrm{v}}}\phi(x,t)I(x,t)}_{=:S(x,t)} = 0. \quad (40)$$

4.3.1. KKT with simplifications of the source term

After these observations we can finally start to calculate the KKT-System. We will begin with the KKT-System for the optimization problem with simplified source term. Both possible objective functions will be considered, starting with the End-tube-function.

End-tube-function

For the End-tube-function (31) as objective function, the simplified minimization problem looks like this:

$$\min_q \quad \int_0^{t_{end}} (T(x_{end},t) - T_{demand})^2 \ dt + \frac{\beta}{2}\int_0^{t_{end}} q^2(t) \ dt$$
$$\text{s.t.}$$
$$\tilde{g}(T,q) = \frac{\partial}{\partial t}T(x,t) + \frac{q(t)}{A} \cdot \frac{\partial}{\partial x}T(x,t) - \underbrace{\frac{\eta_{col} \cdot \eta_{therm} \cdot G}{A \cdot \tilde{\rho} \cdot \tilde{c}_{\mathrm{v}}}\phi(x,t)I(x,t)}_{=:S(x,t)} = 0 \quad (41)$$

The corresponding Lagrange-function is then given as

$$\mathcal{L}(T,q,\lambda) = \int_0^{t_{end}} (T(x_{end},t) - T_{demand})^2 \ dt + \frac{\beta}{2}\int_0^{t_{end}} q^2(t) \ dt \quad (42)$$
$$- \int_0^{t_{end}}\int_{x_0}^{x_{end}} \lambda(x,t)\left(\frac{\partial}{\partial t}T(x,t) + \frac{q(t)}{A}\frac{\partial}{\partial x}T(x,t) - S(x,t)\right) \ dx \ dt$$

For the KKT-System the derivatives (36) - (38) will now be examined one after the other (compare [18]).

Step 1 Solve $\nabla_T \mathcal{L}(T,q,\lambda)$, by considering $\frac{\partial \mathcal{L}}{\partial T}\delta T \overset{!}{=} 0 \ \forall \ \delta T(x,t) \in L^2(\Omega)$.

$$\frac{\partial \mathcal{L}}{\partial T}\delta T = \int_0^{t_{end}} \frac{\partial}{\partial T}(T(x_{end},t) - T_{demand})^2 \delta T(x_{end},t) \ dt + \frac{\beta}{2}\int_0^{t_{end}} \frac{\partial}{\partial T}q^2(t)\delta T(x_{end},t) \ dt$$
$$- \int_0^{t_{end}}\int_{x_0}^{x_{end}} \frac{\partial}{\partial T}\lambda(x,t)\left(T_t(x,t) + \frac{q(t)}{A}T_x(x,t) - S(x,t)\right)\delta T(x,t) \ dx \ dt$$
$$= \int_0^{t_{end}} \frac{\partial}{\partial T}(T(x_{end},t)^2 - 2T(x_{end},t)T_{demand} + T_{demand}^2)\delta T(x_{end},t) \ dt$$

18

$$- \int_{0}^{t_{end}} \int_{x_0}^{x_{end}} \frac{\partial}{\partial T} \lambda(x,t) \left(T_t(x,t) + \frac{q(t)}{A} T_x(x,t) - S(x,t) \right) \delta T(x,t) \; dx \; dt \quad (43)$$

$$= \int_{0}^{t_{end}} (2T(x_{end},t) - 2T_{demand}) \delta T(x_{end},t) \; dt$$

$$- \int_{0}^{t_{end}} \int_{x_0}^{x_{end}} \frac{\partial}{\partial T} \lambda(x,t) \left(T_t(x,t) + \frac{q(t)}{A} T_x(x,t) - S(x,t) \right) \delta T(x,t) \; dx \; dt$$

By numerical differentiation we can dissolve the integrand of the last summand as follows:

$$\frac{\partial}{\partial T} \lambda(x,t) \underbrace{\left(T_t(x,t) + \frac{q(t)}{A} T_x(x,t) - S(x,t) \right)}_{=:j(T)} \delta T(x,t)$$

$$= \lim_{h \to 0} \frac{1}{h} \left(j[T(x,t) + h\lambda(x,t)\delta T(x,t)] - j[T(x,t)] \right)$$

$$= \lim_{h \to 0} \frac{1}{h} \left(\left(\frac{\partial}{\partial t}(T(x,t) + h\lambda(x,t)\delta T(x,t)) + \frac{q(t)}{A}\frac{\partial}{\partial x}(T(x,t) + h\lambda(x,t)\delta T(x,t)) - S(x,t)) \right) \right.$$

$$\left. - \left(\frac{\partial}{\partial t}T(x,t) + \frac{q(t)}{A}\frac{\partial}{\partial x}T(x,t) - S(x,t) \right) \right) \quad (44)$$

$$= \lim_{h \to 0} \frac{1}{h} \; h \left(\frac{\partial}{\partial t}\lambda(x,t)\delta T(x,t) + \frac{q(t)}{A}\frac{\partial}{\partial x}\lambda(x,t)\delta T(x,t) \right)$$

$$= \frac{\partial}{\partial t}\lambda(x,t)\delta T(x,t) + \frac{q(t)}{A}\frac{\partial}{\partial x}\lambda(x,t)\delta T(x,t)$$

Therefore we get:

$$\frac{\partial \mathcal{L}}{\partial T}\delta T = \int_{0}^{t_{end}} (2T(x_{end},t) - 2T_{demand})\delta T(x_{end},t) \; dt$$

$$- \int_{0}^{t_{end}} \int_{x_0}^{x_{end}} \frac{\partial}{\partial t}\lambda(x,t)\delta T(x,t) + \frac{q(t)}{A}\frac{\partial}{\partial x}\lambda(x,t)\delta T(x,t) \; dx \; dt \quad (45)$$

As $\delta T(x,t)$ is arbitrary, the following holds

$$\frac{\partial}{\partial t}\lambda(x,t) + \frac{q(t)}{A}\frac{\partial}{\partial x}\lambda(x,t) = 0. \quad (46)$$

19

Furthermore, partly integrating numerically leads to initial values:

$$\frac{\partial \mathscr{L}}{\partial T}\delta T = \int_0^{t_{end}} (2T(x_{end}, t) - 2T_{demand})\delta T(x_{end}, t) \ dt - \int_{x_0}^{x_{end}} \lambda(x, t_{end})\delta T(x, t_{end}) \ dx$$

$$- \int_0^{t_{end}} \lambda(x_{end}, t)\frac{q(t)}{A}\delta T(x_{end}, t) \ dt$$

$$= \int_0^{t_{end}} \left(2T(x_{end}, t) - 2T_{demand} - \lambda(x_{end}, t)\frac{q(t)}{A}\right)\delta T(x_{end}, t) \ dt \tag{47}$$

$$- \int_{x_0}^{x_{end}} \lambda(x, t_{end})\delta T(x, t_{end}) \ dx \qquad \overset{!}{=} 0 \ \forall \ \delta T(x, t)$$

$$\Rightarrow \qquad \lambda(x, t_{end}) = 0 \qquad \wedge \qquad \lambda(x_{end}, t)\frac{q(t)}{A} = 2T(x_{end}, t) - 2T_{demand} \tag{48}$$

Step 2 Solve $\frac{\partial \mathscr{L}}{\partial q}\delta q \overset{!}{=} 0 \ \forall \ \delta q(t) \in L^2(\Gamma)$.

$$\frac{\partial \mathscr{L}}{\partial q}\delta q(t) = \int_0^{t_{end}} \frac{\partial}{\partial q}(T(x_{end}, t) - T_{demand})^2\delta q(t) \ dt + \frac{\beta}{2}\int_0^{t_{end}} \frac{\partial}{\partial q}q^2(t)\delta q(t) \ dt$$

$$- \int_0^{t_{end}}\int_{x_0}^{x_{end}} \frac{\partial}{\partial q}\lambda(x, t)\left(\frac{\partial}{\partial t}T(x, t) + \frac{q(t)}{A}\frac{\partial}{\partial x}T(x, t) - S(x, t)\right)\delta q(t) \ dx \ dt$$

$$= \frac{\beta}{2}\int_0^{t_{end}} 2q(t)\delta q(t) \ dt - \int_0^{t_{end}}\int_{x_0}^{x_{end}} \frac{\partial}{\partial q}\left(\lambda(x, t)\frac{\partial}{\partial t}T(x, t)\right)\delta q(t) \ dx \ dt$$

$$- \int_0^{t_{end}}\int_{x_0}^{x_{end}} \frac{\partial}{\partial q}\left(\lambda(x, t)\frac{q(t)}{A}\frac{\partial}{\partial x}T(x, t)\right)\delta q(t) \ dx \ dt$$

$$+ \int_0^{t_{end}}\int_{x_0}^{x_{end}} \frac{\partial}{\partial q}(\lambda(x, t)S(x, t))\delta q(t) \ dx \ dt \tag{49}$$

$$= \int_0^{t_{end}} \frac{\beta}{2}2q(t)\delta q(t) \ dt - \int_0^{t_{end}}\int_{x_0}^{x_{end}} \left(\lambda(x, t)\frac{1}{A}\frac{\partial}{\partial x}T(x, t)\right)\delta q(t) \ dx \ dt$$

$$= \int_0^{t_{end}} \beta q(t)\delta q(t) - \left(\int_{x_0}^{x_{end}} \lambda(x, t)\frac{1}{A}\frac{\partial}{\partial x}T(x, t) \ dx\right)\delta q(t) \ dt$$

$$= \int_{t_0}^{t_{end}} \left(\beta q(t) - \int_{x_0}^{x_{end}} \lambda(x, t)\frac{1}{A}\frac{\partial}{\partial x}T(x, t) \ dx\right)\delta q(t) \ dt \qquad \overset{!}{=} 0 \ \forall \ \delta q(t)$$

Such that

$$\beta q(t) - \int_{x_0}^{x_{end}} \lambda(x, t)\frac{1}{A}\frac{\partial}{\partial x}T(x, t) \ dx = 0, \tag{50}$$

$$\Rightarrow \ q(t) = \frac{1}{\beta}\int_{x_0}^{x_{end}} \lambda(x, t)\frac{1}{A}\frac{\partial}{\partial x}T(x, t) \ dx. \tag{51}$$

Step 3   Solve $\frac{\partial \mathscr{L}}{\partial \lambda} \delta\lambda(x,t) \overset{!}{=} 0 \;\; \forall \; \delta\lambda(x,t) \in L^2(\Omega)$.

$$\frac{\partial \mathscr{L}}{\partial \lambda}\delta\lambda(x,t) = \int_0^{t_{end}} \frac{\partial}{\partial \lambda}(T(x_{end},t) - T_{demand})^2 \delta\lambda(x,t) \; dt + \frac{\beta}{2}\int_0^{t_{end}} \frac{\partial}{\partial \lambda}q^2(t)\delta\lambda(x,t) \; dt$$

$$- \int_0^{t_{end}} \int_{x_0}^{x_{end}} \frac{\partial}{\partial \lambda}\lambda(x,t)\left(\frac{\partial}{\partial t}T(x,t) + \frac{q(t)}{A}\frac{\partial}{\partial x}T(x,t) - S(x,t)\right)\delta\lambda(x,t) \; dx \; dt \tag{52}$$

$$= \int_0^{t_{end}} \int_{x_0}^{x_{end}} \frac{\partial}{\partial \lambda}\lambda(x,t)\left(\frac{\partial}{\partial t}T(x,t) + \frac{q(t)}{A}\frac{\partial}{\partial x}T(x,t) - S(x,t)\right)\delta\lambda(x,t) \; dx \; dt \overset{!}{=} 0 \;\; \forall \; \delta\lambda(x,t)$$

$$\Rightarrow \underbrace{\frac{\partial}{\partial t}T(x,t) + \frac{q(t)}{A}\frac{\partial}{\partial x}T(x,t) - S(x,t)}_{=g(T,q)} = 0 \tag{53}$$

So, in total the KKT-System comes down to the following formulas:

$$\text{(KKT 1)} \begin{cases} \dfrac{\partial}{\partial t}\lambda(x,t) + \dfrac{q(t)}{A}\dfrac{\partial}{\partial x}\lambda(x,t) = 0 \\ \qquad\qquad\qquad \text{with} \hfill \text{(KKT 1.1)} \\ \lambda(x_{end},t) = \dfrac{A}{q(t)}\cdot(2T(x_{end},t) - 2T_{demand}) \quad \wedge \quad \lambda(x,t_{end}) = 0, \\ \\ q(t) = \dfrac{1}{\beta}\int_{x_0}^{x_{end}}\lambda(x,t)\dfrac{1}{A}\dfrac{\partial}{\partial x}T(x,t) \; dx, \hfill \text{(KKT 1.2)} \\ \\ g(T,q) = \dfrac{\partial}{\partial t}T(x,t) + \dfrac{q(t)}{A}\dfrac{\partial}{\partial x}T(x,t) - S(x,t) = 0 \hfill \text{(KKT 1.3)} \end{cases}$$

Full-tube-function

For the Full-tube-function (32) as objective function, the simplified minimization problem looks like this:

$$\min_q \int_0^{t_{end}} \int_{x_0}^{x_{end}} (T(x,t) - T_{demand})^2 \; dt + \frac{\beta}{2}\int_0^{t_{end}} q^2(t) \; dt$$

$$\text{s.t.} \tag{54}$$

$$\tilde{g}(T,q) = \frac{\partial}{\partial t}T(x,t) + \frac{q(t)}{A}\cdot\frac{\partial}{\partial x}T(x,t) - S(x,t) = 0$$

The corresponding Lagrange-function is then given as

$$\mathscr{L}(T,q,\lambda) = \int_0^{t_{end}} \int_{x_0}^{x_{end}} (T(x,t) - T_{demand})^2 \; dx \; dt + \frac{\beta}{2}\int_0^{t_{end}} q^2(t) \; dt \tag{55}$$

$$- \int_0^{t_{end}} \int_{x_0}^{x_{end}} \lambda(x,t) \left(\frac{\partial}{\partial t} T(x,t) + \frac{q(t)}{A} \frac{\partial}{\partial x} T(x,t) - S(x,t) \right) \ dx \ dt$$

For the KKT-System again we have to calculate the derivatives.

Step 1 Solve $\nabla_T \mathscr{L}(T, q, \lambda)$, by considering $\frac{\partial \mathscr{L}}{\partial T} \delta T \stackrel{!}{=} 0 \ \forall \ \delta T(x,t) \in L^2(\Omega)$.

$$
\begin{aligned}
\frac{\partial \mathscr{L}}{\partial T} \delta T =& \int_0^{t_{end}} \int_{x_0}^{x_{end}} \frac{\partial}{\partial T} (T(x,t) - T_{demand})^2 \delta T(x,t) \ dx \ dt + \frac{\beta}{2} \int_0^{t_{end}} \frac{\partial}{\partial T} q^2(t) \delta T(x,t) \ dt \\
& - \int_0^{t_{end}} \int_{x_0}^{x_{end}} \frac{\partial}{\partial T} \lambda(x,t) \left(T_t(x,t) + \frac{q(t)}{A} T_x(x,t) - S(x,t) \right) \delta T(x,t) \ dx \ dt \\
=& \int_0^{t_{end}} \int_{x_0}^{x_{end}} \frac{\partial}{\partial T} (T(x,t)^2 - 2T(x,t)T_{demand} + T_{demand}^2) \delta T(x,t) \ dx \ dt \\
& - \int_0^{t_{end}} \int_{x_0}^{x_{end}} \frac{\partial}{\partial T} \lambda(x,t) \left(T_t(x,t) + \frac{q(t)}{A} T_x(x,t) - S(x,t) \right) \delta T(x,t) \ dx \ dt \quad (56) \\
=& \int_0^{t_{end}} \int_{x_0}^{x_{end}} (2T(x,t) - 2T_{demand}) \delta T(x,t) \ dx \ dt \\
& - \int_0^{t_{end}} \int_{x_0}^{x_{end}} \frac{\partial}{\partial T} \lambda(x,t) \left(T_t(x,t) + \frac{q(t)}{A} T_x(x,t) - S(x,t) \right) \delta T(x,t) \ dx \ dt
\end{aligned}
$$

By numerical differentiation we can dissolve the last summand as we did earlier and get:

$$
\begin{aligned}
\frac{\partial \mathscr{L}}{\partial T} \delta T =& \int_0^{t_{end}} \int_{x_0}^{x_{end}} (2T(x,t) - 2T_{demand}) \delta T(x,t) \ dx \ dt \\
& - \int_0^{t_{end}} \int_{x_0}^{x_{end}} \frac{\partial}{\partial t} \lambda(x,t) \delta T(x,t) + \frac{q(t)}{A} \frac{\partial}{\partial x} \lambda(x,t) \delta T(x,t) \ dx \ dt \\
=& \int_0^{t_{end}} \int_{x_0}^{x_{end}} \left(2T(x,t) - 2T_{demand} - \frac{\partial}{\partial t} \lambda(x,t) - \frac{q(t)}{A} \frac{\partial}{\partial x} \lambda(x,t) \right) \delta T(x,t) \ dx \ dt \quad (57) \\
\stackrel{!}{=}& \ 0 \ \forall \ \delta \lambda(x,t)
\end{aligned}
$$

$$\Rightarrow \ \frac{\partial}{\partial t} \lambda(x,t) + \frac{q(t)}{A} \frac{\partial}{\partial x} \lambda(x,t) = 2T(x,t) - 2T_{demand} \tag{58}$$

When considering this system under the given model, the starting temperature at the time point $t = 0$ is given and therefore we can assume $\delta T(x,0) \equiv 0$. As the model does not consider any backwards flow, $q > 0$ holds and we can also assume $\delta T(x_0, t) \equiv 0$. By this we can obtain the following initial values for λ:

$$\Rightarrow \ \lambda(x_{end}, t) = 0 \qquad \wedge \qquad \lambda(x, t_{end}) = 0 \tag{59}$$

Step 2 Solve $\frac{\partial \mathscr{L}}{\partial q} \delta q \overset{!}{=} 0 \ \forall \ \delta q(t) \in L^2(\Gamma)$.

This equation is the same as for the other objective function.

$$\frac{\partial \mathscr{L}}{\partial q} \delta q(t) = \int_0^{t_{end}} \int_{x_0}^{x_{end}} \frac{\partial}{\partial q}(T(x,t) - T_{demand})^2 \delta q(t) \ dx \ dt + \frac{\beta}{2} \int_0^{t_{end}} \frac{\partial}{\partial q} q^2(t) \delta q(t) \ dt$$

$$- \int_0^{t_{end}} \int_{x_0}^{x_{end}} \frac{\partial}{\partial q} \lambda(x,t) \left(\frac{\partial}{\partial t} T(x,t) + \frac{q(t)}{A} \frac{\partial}{\partial x} T(x,t) - S(x,t) \right) \delta q(t) \ dx \ dt$$

$$\tag{60}$$

$$= \int_0^{t_{end}} \left(\beta q(t) - \int_{x_0}^{x_{end}} \lambda(x,t) \frac{1}{A} \frac{\partial}{\partial x} T(x,t) \ dx \right) \delta q(t) \ dt \qquad \overset{!}{=} 0 \ \forall \ \delta q(t)$$

$$\Rightarrow \ \beta q(t) - \int_{x_0}^{x_{end}} \lambda(x,t) \frac{1}{A} \frac{\partial}{\partial x} T(x,t) \ dx = 0 \tag{61}$$

$$\Rightarrow \ q(t) = \frac{1}{\beta} \int_{x_0}^{x_{end}} \lambda(x,t) \frac{1}{A} \frac{\partial}{\partial x} T(x,t) \ dx \tag{62}$$

Step 3 Solve $\frac{\partial \mathscr{L}}{\partial \lambda} \delta \lambda(x,t) \overset{!}{=} 0 \ \forall \ \delta \lambda(x,t) \in L^2(\Omega)$.

This equation again stays the same.

$$\frac{\partial \mathscr{L}}{\partial \lambda} \delta \lambda(x,t) = \int_0^{t_{end}} \int_{x_0}^{x_{end}} \frac{\partial}{\partial \lambda} \lambda(x,t) \left(\frac{\partial}{\partial t} T(x,t) + \frac{q(t)}{A} \frac{\partial}{\partial x} T(x,t) - S(x,t) \right) \delta \lambda(x,t) \ dx \ dt$$

$$\overset{!}{=} 0 \ \forall \ \delta \lambda(x,t) \tag{63}$$

$$\Rightarrow \ \underbrace{\frac{\partial}{\partial t} T(x,t) + \frac{q(t)}{A} \frac{\partial}{\partial x} T(x,t) - S(x,t)}_{= \ g(T,q)} = 0 \tag{64}$$

Summarized we get for the KKT-System:

$$
\text{(KKT 2)}
\begin{cases}
\dfrac{\partial}{\partial t}\lambda(x,t)+\dfrac{q(t)}{A}\dfrac{\partial}{\partial x}\lambda(x,t) = 2T(x,t) - 2T_{demand} \\
\qquad\qquad\text{with} \hfill \text{(KKT 2.1)}\\
\lambda(x_{end},t) = 0 \quad \wedge \quad \lambda(x,t_{end}) = 0, \\[2mm]
q(t) = \dfrac{1}{\beta}\displaystyle\int_{x_0}^{x_{end}} \lambda(x,t)\dfrac{1}{A}\dfrac{\partial}{\partial x}T(x,t)\ dx, \hfill \text{(KKT 2.2)}\\[4mm]
g(T,q) = \dfrac{\partial}{\partial t}T(x,t)+\dfrac{q(t)}{A}\dfrac{\partial}{\partial x}T(x,t) - S(x,t) = 0 \hfill \text{(KKT 2.3)}
\end{cases}
$$

4.3.2. KKT without simplifications of the source term

In the next step we will consider the system without the simplifications. The source term $S(x,t)$ will again depend on the temperature T.
Therefore only the derivative of T needs to be reconsidered. Since the simplifications only effect the constraint, the calculation will be carried out analogue for both objective functions $f(T,q)$.
As an example the Full-tube-function will be used as objective function:

$$
\begin{aligned}
\frac{\partial \mathscr{L}}{\partial T}\delta T =& \int_0^{t_{end}}\int_{x_0}^{x_{end}} \frac{\partial}{\partial T}(T(x,t) - T_{demand})^2\delta T(x,t)\ dx\ dt + \frac{\beta}{2}\int_0^{t_{end}} \frac{\partial}{\partial T}q^2(t)\delta T(x_{end},t)\ dt\\
&- \int_0^{t_{end}}\int_{x_0}^{x_{end}} \frac{\partial}{\partial T}\lambda(x,t)\left(\frac{\partial}{\partial t}T(x,t) + \frac{q(t)}{A}\frac{\partial}{\partial x}T(x,t) - S(T,x,t)\right)\delta T(x,t)\ dx\ dt\\
=& \int_0^{t_{end}}\int_{x_0}^{x_{end}} \frac{\partial}{\partial T}(T(x,t)^2 - 2T(x,t)T_{demand} + T_{demand}^2)\delta T(x,t)\ dx\ dt\\
&- \int_0^{t_{end}}\int_{x_0}^{x_{end}} \frac{\partial}{\partial T}\lambda(x,t)\left(\frac{\partial}{\partial t}T(x,t) + \frac{q(t)}{A}\frac{\partial}{\partial x}T(x,t) \right.\\
&\left. \qquad\qquad\qquad -\frac{\eta_{col}\cdot\eta_{therm}\cdot G}{A\cdot\rho(T)c_{\mathrm v}(T)}\phi(x,t)I(x,t)\right)\delta T(x,t)\ dx\ dt
\end{aligned}
\tag{65}
$$

The formulas for $\rho(T)$ and $c_v(T)$ depend on the chosen fluid (see eq. (11) - (18)).
For simplicity and conciseness initially assume both $\rho(T)$ and $c_v(T)$ would be linear functions, given like this:

$$
\rho(T) = mT + a \qquad \text{and} \qquad c_v(T) = nT + b \tag{66}
$$

(For visualization see Figures 4 and 5.)
So the derivative of $\mathscr{L}$ with respect to $T(x,t)$ looks as follows:

$$\frac{\partial \mathscr{L}}{\partial T}\delta T = \int_0^{t_{end}} \int_{x_0}^{x_{end}} (2T(x,t) - 2T_{demand})\delta T(x,t) \ dx \ dt$$

$$- \int_0^{t_{end}} \int_{x_0}^{x_{end}} \frac{\partial}{\partial T}\lambda(x,t) \left(\frac{\partial}{\partial t}T(x,t) + \frac{q(t)}{A}\frac{\partial}{\partial x}T(x,t) \right.$$

$$\left. - \frac{\eta_{col} \cdot \eta_{therm} \cdot G \cdot \phi(x,t)I(x,t)}{A \cdot (mT(x,t)+a)(nT(x,t)+b)} \right) \delta T(x,t) \ dx \ dt$$

$$= \int_0^{t_{end}} \int_{x_0}^{x_{end}} (2T(x,t) - 2T_{demand})\delta T(x,t) \ dx \ dt \qquad (67)$$

$$- \int_0^{t_{end}} \int_{x_0}^{x_{end}} \frac{\partial}{\partial T}\lambda(x,t) \left(\frac{\partial}{\partial t}T(x,t) + \frac{q(t)}{A}\frac{\partial}{\partial x}T(x,t) + \frac{\eta_{col} \cdot \eta_{therm} \cdot G \cdot \phi(x,t)I(x,t)}{A} \right.$$

$$\left. \cdot \frac{-1}{(mT(x,t)+a)(nT(x,t)+b)} \right) \delta T(x,t) \ dx \ dt$$

In order to obtain more manageable terms, hereafter $T(x,t)$ and $\lambda(x,t)$ will be abbreviated as T and λ.

Similarly to the earlier calculations, we solve the last term by numerical differentiation:

$$\frac{\partial}{\partial T}\lambda \underbrace{\left(\frac{\partial}{\partial t}T + \frac{q(t)}{A}\frac{\partial}{\partial x}T - S(T,x,t) \right)}_{=:\,j(T)} \delta T$$

$$= \lim_{h \to 0} \frac{1}{h} \left(j[T + h\lambda\delta T] - j[T] \right) \qquad (68)$$

$$= \lim_{h \to 0} \frac{1}{h} \left(\left(\frac{\partial}{\partial t}(T + h\lambda\delta T) + \frac{q(t)}{A}\frac{\partial}{\partial x}(T + h\lambda\delta T) \right. \right.$$

$$\left. + \frac{\eta_{col} \cdot \eta_{therm} \cdot G \cdot \phi(x,t)I(x,t)}{A} \frac{-1}{(m(T + h\lambda\delta T)+a)(n(T + h\lambda\delta T)+b)} \right)$$

$$\left. - \left(\frac{\partial}{\partial t}T + \frac{q(t)}{A}\frac{\partial}{\partial x}T + \frac{\eta_{col} \cdot \eta_{therm} \cdot G \cdot \phi(x,t)I(x,t)}{A} \frac{-1}{(mT+a)(nT+b)} \right) \right)$$

$$= \lim_{h \to 0} \frac{1}{h} \left(\frac{\partial}{\partial t}(h\lambda\delta T) + \frac{q(t)}{A}\frac{\partial}{\partial x}(h\lambda\delta T) + \frac{\eta_{col} \cdot \eta_{therm} \cdot G \cdot \phi(x,t)I(x,t)}{A} \right.$$

$$\left. \cdot \underbrace{\left(\frac{-1}{(m(T + h\lambda\delta T)+a)(n(T + h\lambda\delta T)+b)} + \frac{1}{(mT+a)(nT+b)} \right)}_{(*)} \right)$$

Now, narrow the observation down on $(*)$:

$$\frac{-1}{(m(T + h\lambda\delta T)+a)(n(T + h\lambda\delta T)+b)} + \frac{1}{(mT+a)(nT+b)}$$

25

$$= \frac{-(mT+a)(nT+b) + (m(T+h\lambda\delta T)+a)(n(T+h\lambda\delta T)+b)}{(m(T+h\lambda\delta T)+a)(n(T+h\lambda\delta T)+b) \cdot (mT+a)(nT+b)} \tag{69}$$

$$= \frac{\begin{array}{c} \textcolor{blue}{-nmT^2 - mbT - anT - ab} + nmT^2 + nmTh\lambda\delta T + \textcolor{blue}{mbT} \\ + mnTh\lambda\delta T + nm(h\lambda\delta T)^2 + mbh\lambda\delta T + \textcolor{blue}{anT} + anh\lambda\delta T + \textcolor{blue}{ab} \end{array}}{\begin{array}{c} (nmT^2 + nmTh\lambda\delta T + mbT + nmTh\lambda\delta T + nm(h\lambda\delta T)^2 \\ + mbh\lambda\delta T + anT + anh\lambda\delta T + ab) \cdot (nmT^2 + mbT + anT + ab) \end{array}}$$

The blue colored terms of the sum cancel out. The remaining terms will be reorganized and partly renamed.

$$= \frac{h \cdot \delta T \cdot \overbrace{(nm(2T\lambda + h\delta T\lambda^2) + mb\lambda + an\lambda)}^{=:\ \alpha_{\text{num}}}}{\begin{array}{c} (nmT^2 + mbT + anT + ab + nm(2Th\lambda\delta T + (h\lambda\delta T)^2) \\ + mbh\lambda\delta T + anh\lambda\delta T) \cdot \underbrace{(nmT^2 + mbT + anT + ab)}_{=:\ \alpha_{\text{den}}} \end{array}} \tag{70}$$

$$= \frac{h \cdot \delta T \cdot \alpha_{\text{num}}}{(\alpha_{\text{den}} + h \cdot \delta T \cdot \alpha_{\text{num}}) \cdot \alpha_{\text{den}}}$$

So, for the numerical differentiation we get:

$$\frac{\partial}{\partial T}\lambda \ \left(\frac{\partial}{\partial t}T + \frac{q(t)}{A}\frac{\partial}{\partial x}T - S(T,x,t) \right) \ \delta T \tag{71}$$

$$= \lim_{h \to 0} \ \frac{1}{h}\left(\frac{\partial}{\partial t}(h\lambda\delta T) + \frac{q(t)}{A}\frac{\partial}{\partial x}(h\lambda\delta T) + \frac{\eta_{col} \cdot \eta_{therm} \cdot G \cdot \phi(x,t)I(x,t)}{A} \cdot \frac{h \cdot \delta T \cdot \alpha_{\text{num}}}{(\alpha_{\text{den}} + h \cdot \delta T \cdot \alpha_{\text{num}}) \cdot \alpha_{\text{den}}} \right)$$

$$= \lim_{h \to 0} \ \left(\frac{\partial}{\partial t}(\lambda\delta T) + \frac{q(t)}{A}\frac{\partial}{\partial x}(\lambda\delta T) + \frac{\eta_{col} \cdot \eta_{therm} \cdot G \cdot \phi(x,t)I(x,t)}{A} \cdot \frac{\delta T \cdot \alpha_{\text{num}}}{(\alpha_{\text{den}} + h \cdot \delta T \cdot \alpha_{\text{num}}) \cdot \alpha_{\text{den}}} \right)$$

because h still occurs in α_{num}.
All in all this finally leads to:

$$\frac{\partial \mathscr{L}}{\partial T}\delta T = \int_0^{t_{end}} \int_{x_0}^{x_{end}} (2T - 2T_{demand})\delta T \ dx \ dt$$

$$- \int_0^{t_{end}} \int_{x_0}^{x_{end}} \frac{\partial}{\partial t}\lambda\delta T + \frac{q(t)}{A}\frac{\partial}{\partial x}\lambda\delta T + \frac{\eta_{col} \cdot \eta_{therm} \cdot G \cdot \phi(x,t)I(x,t)}{A}$$

$$\cdot \lim_{h \to 0} \left(\frac{\delta T \cdot \alpha_{num}}{(\alpha_{den} + h \cdot \delta T \cdot \alpha_{num}) \cdot \alpha_{den}} \right) \ dx \ dt \tag{72}$$

$$= \int_0^{t_{end}} \int_{x_0}^{x_{end}} \left(2T - 2T_{demand} - \frac{\partial}{\partial t}\lambda - \frac{q(t)}{A}\frac{\partial}{\partial x}\lambda - \frac{\eta_{col} \cdot \eta_{therm} \cdot G \cdot \phi(x,t)I(x,t)}{A} \right.$$

$$\left. \cdot \lim_{h \to 0} \left(\frac{\alpha_{num}}{(\alpha_{den} + h \cdot \delta T \cdot \alpha_{num}) \cdot \alpha_{den}} \right) \right) \delta T \ dx \ dt$$

$$\overset{!}{=} 0 \ \forall \ \delta\lambda$$

$$\Rightarrow \frac{\partial}{\partial t}\lambda + \frac{q(t)}{A}\frac{\partial}{\partial x}\lambda + \frac{\eta_{col} \cdot \eta_{therm} \cdot G \cdot \phi(x,t)I(x,t)}{A} \cdot \lim_{h \to 0} \left(\frac{\alpha_{num}}{(\alpha_{den} + h \cdot \delta T \cdot \alpha_{num}) \cdot \alpha_{den}} \right)$$

$$= 2T - 2T_{demand} \tag{73}$$

Analogously

$$\lambda(x_{end}, t) = 0 \qquad \wedge \qquad \lambda(x, t_{end}) = 0 \tag{74}$$

still holds.
Now, observe the case of

$$\rho(T) = MT^3 + \hat{m}T^2 + mT + a \quad \text{and} \quad c_v(T) = \hat{N}T^4 + NT^3 + \hat{n}T^2 + nT + b \tag{75}$$

The numerical differentiation of the source term can be calculated analogously to the linear case and leads to the following term.

$$\lim_{h \to 0} \frac{h \cdot \delta T \cdot \alpha_{num2}}{(\alpha_{den2} + h \cdot \delta T \cdot \alpha_{num2}) \cdot \alpha_{den2}} \tag{76}$$

With

$$\alpha_{num2} = (MT^3 + \hat{m}T^2 + mT + a) \cdot (4\hat{N}T^3\lambda + 6\hat{N}T^2\lambda^2 h\delta T + 4\hat{N}T\lambda^3(h\delta T)^2 + \hat{N}\lambda^4(h\delta T)^3$$

$$+ 3NT^2\lambda + 3NT\lambda^2 h\delta T + N\lambda^3(h\delta T)^2 + 2\hat{n}T\lambda$$

$$+ \hat{n}\lambda^2 h\delta T + n\lambda) + (3MT^2\lambda + 3MT\lambda^2 h\delta T + M\lambda^3(h\delta T)^2$$

$$+ 2\hat{m}T\lambda + \hat{m}\lambda^2 h\delta T + m\lambda)$$

$$\cdot (\hat{N}T^4 + 4\hat{N}T^3 h\lambda\delta T + 6\hat{N}T^2(h\lambda\delta T)^2 + 4\hat{N}T(h\lambda\delta T)^3 + \hat{N}(h\lambda\delta T)^4 + NT^3$$

$$+ 3NT^2 h\lambda\delta T + 3NT(h\lambda\delta T)^2 + N(h\lambda\delta T)^3 + \hat{n}T^2 + 2\hat{n}Th\lambda\delta T$$

$$+ \hat{n}(h\lambda\delta T)^2 + nT + nh\lambda\delta T + b) \tag{77}$$

and

$$\begin{aligned}
\alpha_{\text{den2}} &= (MT^3 + \hat{m}T^2 + mT + a)(\hat{N}T^4 + NT^3 + \hat{n}T^2 + nT + b) \\
&= M\hat{N}T^7 + (MN + \hat{m}\hat{N})T^6 + (M\hat{n} + \hat{m}N + m\hat{N})T^5 + (Mn + \hat{m}\hat{n} + mN + a\hat{N})T^4 \\
&\quad + (Mb + \hat{m}n + m\hat{n} + aN)T^3 + (\hat{m}b + mn + a\hat{n})T^2 + (mb + an)T + ab
\end{aligned} \tag{78}$$

This term is then used as seen before.

Setting certain coefficients to zero leads directly to the quadratic result for molten salt or the simplified linear case respectively.

4.4. Control-Strategy and implementation

The above calculated KKT-Systems can now be used to regulate the pump's volumetric flow. Reconsidering the setting of the solar thermal power plant, it becomes apparent that the mathematical interesting full-tube function is not practical. Within the tube there are no precautions to react to temperature differences. So against this background the full-tube function considers information that cannot be reacted to. Hence from this point on the possibility of the full-tube function will be rejected.

Basic idea

The used control strategy in this section combines the KKT-System with one step of the gradient method and a predictive approach, resulting in the procedure that is shown in Figure 6.

Given a starting value q_0 for the flow, the fluid's temperature behavior can be calculated by solving the partial differential equation that builds the model, see (38). Those calculations are performed several times to predict the future behavior, assuming the external circumstances do not change along the way. Then equation (36) can be used to determine the Lagrange-multiplier λ. At last the new approximate volumetric flow is received by using the update formula, which evolves from equation (37).
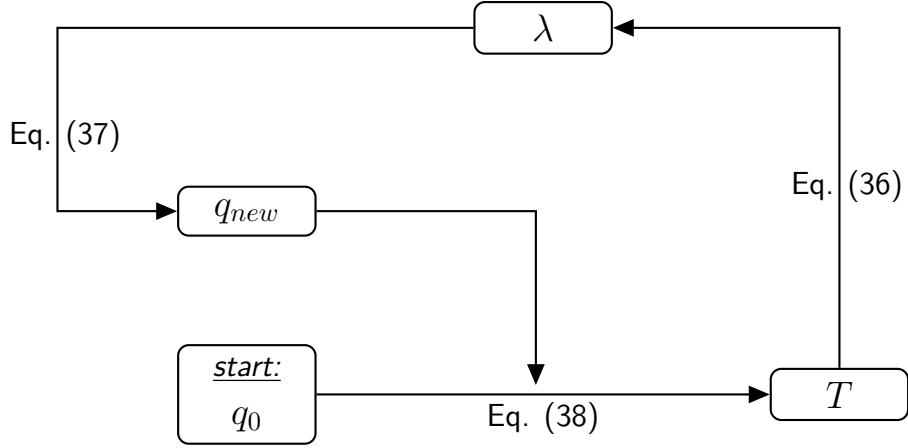
Figure 6: Basic idea to determine the regulating variables.

The realization of this strategy in code is also presented in Algorithm 1. The algorithm takes the current volumetric flow as input and consequential calculates the fluid's future temperature, given the situation that neither the flow, nor the weather conditions are changing. This calculation is carried out until a certain point in the future, given by the variable *predictiveTime*. This point can be chosen freely but is considered constant over the whole simulation. With the help of this pre-calculated temperature, the KKT-System is now solved by setting the initial values of λ and then determining its values via the upwind scheme, which is also used for the temperature calculations. As λ would actually require a downwind scheme, here an auxiliary variable $\tilde{\lambda}$ is introduced so the upwind scheme can be used. It holds:

$$\tilde{\lambda}(x') = \lambda(x_{end} - x' + x_0) \tag{79}$$

Lastly the volumetric flow is adjusted.

Algorithm 1 Control of one tube

Input: $predictiveTime$, q, $time$

1: set $timeHorizon = time + predictiveTime$;
2: set $t = time$;
3: **while** $t \leq timeHorizon$ **do**
4:      calculate new temperature T;
5: **end while**
6: set $\tilde{\lambda}(x_0) = \frac{A}{q} \cdot (2T - 2T_{demand})$;
7: calculate $\tilde{\lambda}$;
8: use $\tilde{\lambda}$ to calculate λ;
9: numerically calculate the integral $q_{int} = \int_{x_0}^{x_{end}} \lambda(x,t) \frac{1}{A} \frac{\partial}{\partial x} T(x,t) \; dx$
10: set $q_{new} = q_0 + \frac{1}{\beta} \cdot q_{int}$; $\triangleright$ update q via equation (37)

Output: new pump volumetric flow q_{new}

Implementation

The control based on this theory is implemented in Matlab. It will be included into the model implementation done by Cherek (compare [4]), so the setting described in Section 3 is adopted and then extended by the KKT-control.

Initially the simplified control will be implemented exactly as it is described in this section. Yet the full control without simplification will not be implemented. This is due to the following considerations.

The control strategy includes the principle of the gradient method, performing the next step always in the direction of the steepest descent, in order to achieve the best possible results. These results, however, are inevitably imprecise, as the whole system is already simplified for efficiency reasons (see Sections 1 and 3). Thus it makes sense to evaluate how exact the gradient step is to be executed, since solving this optimization problem also increases the complexity again. So instead, as improvement to the simplified optimization problem, the simplified KKT-system will be performed with exact predictive temperature calculations. It can already be assumed, that this induces a gradient like direction close enough to the steepest descent (see Figure 7). The corresponding results supporting the statement above can be found in Section 7.
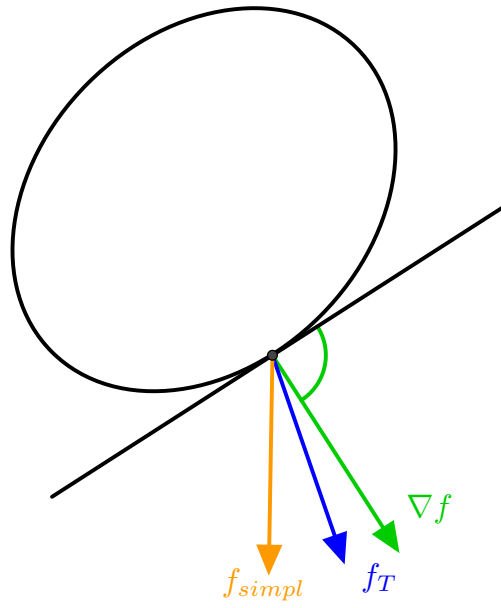
Figure 7: Assumed directions of descent for the optimization problem.
(Schematic representation)

5. Flow in a network of tubes

In Section 3 and 4 the model and control of one single tube have been observed. Before the whole network can be controlled, it needs to be modelled first. Therefore the behavior of velocity and temperature inside the junctions, which link the header- and absorber tubes, has to be specified by coupling conditions. This again has already been done by Cherek in his thesis [4] and will only be shortly reviewed here, to be able to perform the predictive network control.

Within the junctions, the conservation of mass has to hold. As the heat transfer fluid is considered to be incompressible, the condtition reduces to:

$$\sum_j A_j \nu_j = 0 \,, \tag{80}$$

with j being the indices of tubes adjacent to the observed junction. Cherek distinguishes between three types of junctions: inlet, outlet and last junctions.

Inlet junctions

Inlet junctions are those junctions, that are positioned at the inflow header and connect one incoming pipe with two outgoing pipes. Structure and indexing of those junctions are shown in Figure 8. Here ν, T, A are velocity, temperature and cross sectional area for each case. The variable ξ denotes the operating state of the valve, which is positioned at the beginning of the absorber tube. For now ξ can be considered constant, as valve control is not yet intended.
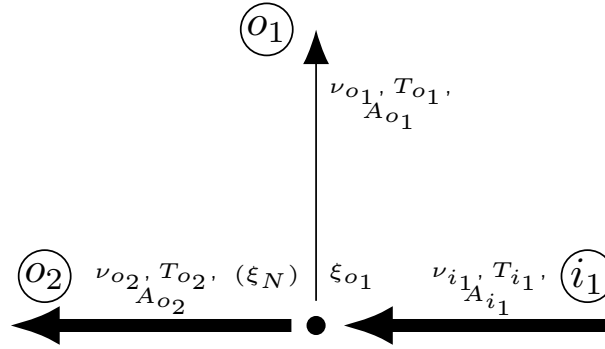
Figure 8: Junction with one incoming and two outgoing pipes. "Inlet junction" situated at the inflow header.

The velocity conditions are then given by

$$\nu_{o1,\xi} = \nu_{o2} = \nu_o = \frac{A_h \nu_{i1}}{A_h + A_a \xi_{o1}} \,. \tag{81}$$

The velocity in the absorber tube after the junction is given by $\nu_{o1} = \xi_{o1}\nu_{o1}$. As the junctions only exist at the inflow header $T_{i1} = T_{o1} = T_{o2}$ holds.

The last inlet junction is a special case. The model does not transport information backwards, so the last valve would not have any effect. Therefore the last valve is positioned at the last inlet junction instead of the last junction. Therefore in this case the velocities are calculated as follows:

$$\nu_o = \frac{A_h \nu_{i1}}{A_a(\xi_N + \xi_{o1})} \qquad \text{and} \qquad \nu_{o2} = \frac{\nu_o \xi_N A_a}{A_h} \qquad (82)$$

Last junctions

The last junctions are the junctions positioned at the last absorber tube. As mentioned earlier the valve is considered in the junction before, so that both in Figure 9 shown junctions lead to the same calculations.

(a) Junction at inflow header   (b) Junction at outflow header
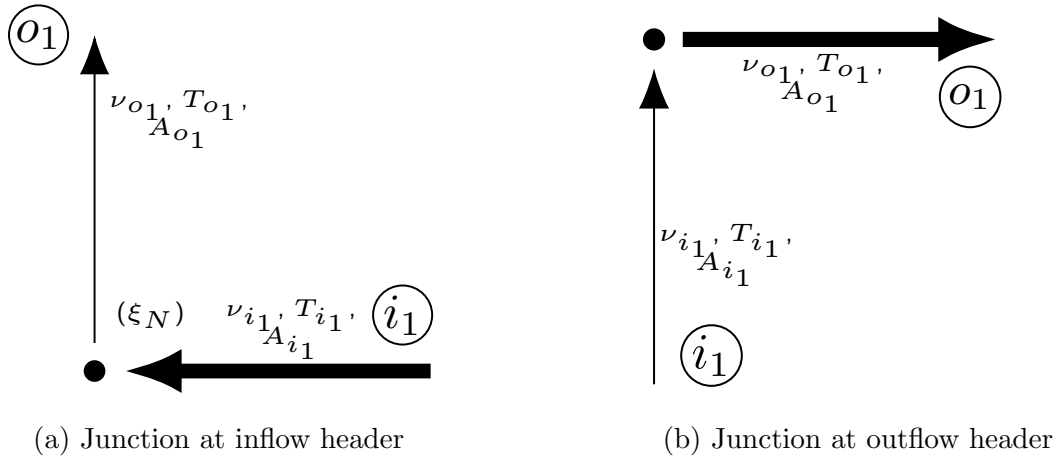
Figure 9: Junctions of type "last junction" at inflow and outflow header.

The velocity and temperature conditions are

$$\nu_{o1} = \frac{A_{i1}\nu_{i1}}{A_{o1}} \qquad \text{and} \qquad T_{i1} = T_{o1}\,, \qquad (83)$$

with $A_{i1} = A_h$ or A_a and A_{o1} respectively, depending on the case.

Outlet junctions

Lastly we consider the outlet junctions. In this junctions different velocities and temperatures gather.

The outflow velocity is calculated as follows.

$$\nu_{o1} = \frac{\nu_{i1}A_h + \nu_{i2}A_a}{A_h} \qquad (84)$$
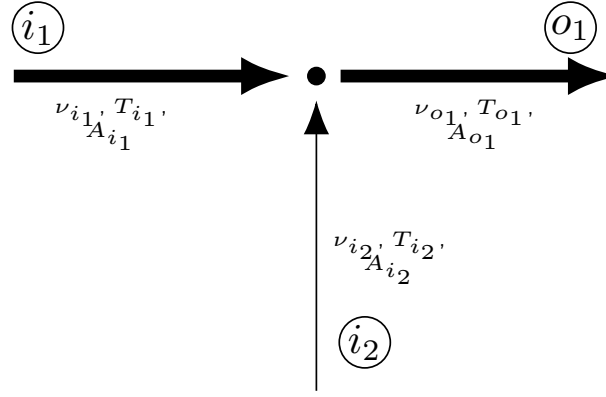
Figure 10: Junction with two incoming and one outgoing pipe. "Outflow junction" situated at the outflow header.

In order to calculate the mixed temperature Cherek suggests to first calculate the density the fluid has in the outflow tube, via

$$\rho_{o1} = \frac{\rho_{i1}\nu_{i1}A_h + \rho_{i2}\nu_{i2}A_a}{\nu_{o1}A_h} \tag{85}$$

With the density known, the temperature can be calculated using equations (11) and (15). While equation (15) can easily be inverted to get the temperature, for Therminol VP1 as heat fluid, equation (11) needs to be solved by an iterative Newton method.

6. Multiple-input multiple-output closed-loop control

Now that the network is completely modelled, we can start to consider its control. At first the state of the art control of the network will be recreated. After that the valves at the beginning of the absorber tubes will be included in the control. Before that can be done, the model needs to be slightly adjusted, to be able to control each tube of the network on its own.

6.1. Mirror Control

For the state of the art control of the network the mirrors can be defocused and, as for a single tube, the overall volumetric flow can be adjusted.
Fundamentally, the control is again based on Cherek's work [4].
His algorithm is given below.

Algorithm 2 Mirror Control

 1: **for** tube $i = 1; i \leq N; i + +$ **do**
 2:     **if** $T_i < T_{\text{demand}}$ **then**
 3:         decrease overall volumetric flow q_P;
 4:     **end if**
 5: **end for**
 6: **for** tube $i = 1; i \leq N; i + +$ **do**
 7:     **if** $T_i > T_{\text{demand}}$ **then**
 8:         calculate N_{defocus};
 9:         defocus mirrors;
10:     **end if**
11: **end for**

As long as the fluid's temperature at the end of the observed absorber tube is beneath the optimal value, the overall volumetric flow, provided by the pump, is adjusted. When the temperature in one tube increases too much, the algorithm calculates the number of mirrors that need to be defocused N_{defocus} to decrease this tube's temperature accordingly. This number is calculated via

$$N_{\text{defocus}} = \left\lceil \frac{\Delta T_{\text{demand}}}{\Delta T_{\text{mirror}}} \right\rceil , \tag{86}$$

where ΔT_{demand} is the difference between the actual and desired temperature and ΔT_{mirror} is the temperature increase over the length of one mirror.
The difference to Cherek's work will be, that the new volumetric flow is calculated by the optimization problem (see Section 4). So, for every tube which has a temperature lower than desired, an optimization problem has to be solved. It can already be assumed that this will have a significant influence on the computing time. However, more detailed statements about the computational time will be made in the feasibility

study in Section 7.

6.2. Valve Control

In the mirror control the overall volumetric flow is adjusted. However, when using the valves at the beginning of the absorber tube for control, the volumetric flow of each absorber tube has to be evaluated separately. Hence the model needs to be decoupled.

Decoupling

For the decoupling of the volume flows in the individual pipes, Cherek has investigated their relationship and was able to find the following general formula:

$$q_n = A_{\mathrm{h}}^{n-1} q_{\mathrm{P}} \frac{A_{\mathrm{a}} \xi_n}{\prod_{i=1}^{n}(A_{\mathrm{h}} + A_{\mathrm{a}} \xi_i)} \qquad \forall\, n \in \{1, ..., N-2\}\,. \tag{87}$$

This can be converted to ξ to determine the required valve position:

$$\xi_n = q_n A_{\mathrm{h}} \frac{\prod_{i=1}^{n-1}(A_{\mathrm{h}} + A_{\mathrm{a}} \xi_i)}{A_{\mathrm{h}}^{n-1} A_{\mathrm{a}} q_{\mathrm{P}} - A_{\mathrm{a}} q_n \prod_{i=1}^{n-1}(A_{\mathrm{h}} + A_{\mathrm{a}} \xi_i)} \qquad \forall\, n \in \{1, ..., N-2\}\,. \tag{88}$$

As shown in Section 6.1, the last valve is modelled in the penultimate junction. Therefore, the last two valves are directly interdependent.

$$q_k = q_{\mathrm{in}} \cdot \left(1 - \frac{\xi_j}{A_{\mathrm{a}}(\xi_k + \xi_j)}\right) \qquad \forall\, k, j \in \{N-1, N\},\ k \neq j\,, \tag{89}$$

where q_{in} is the volumetric flow into the penultimate junction, which models the last two valves. It is given by

$$q_{\mathrm{in}} = q_{\mathrm{P}} - \sum_{i=1}^{n} q_n \qquad \forall\, n \in \{1, ..., N-2\}\,. \tag{90}$$

So, the opening state of the last two valves is calculated by

$$\xi_k = \xi_j \cdot \left(\frac{q_{\mathrm{in}}}{q_{\mathrm{in}} - q_k} - 1\right) \qquad \forall\, k, j \in \{N-1, N-2\},\ k \neq j\,. \tag{91}$$

Control

So, when it comes to the valve control, for each absorber tube the needed volumetric flow is calculated as in Section 4. The difference between the current and the necessary volumetric flow is then added to the pump's volumetric flow. Now Algorithm 3 calculates the valves' opening state to guarantee that the added flow only affects the absorber tube it has been calculated for.

The new volumetric flow is calculated for each tube but in each step all valves need to be updated, due to their relation (see eq. (87) and (89)).

Algorithm 3 Valves Aperture

1: $q_{diff} = q_n - q_{old,n}$;
2: $q_P = q_P + q_{diff}$;
3: **for** i=1; i<N; i++ **do**
4:     **if** $i < N - 2$ **then**
5:         update ξ_i by equation (88);
6:     **else**
7:         update ξ_i by equation (91);
8:     **end if**
9: **end for**

While in the mirror control the optimization problem did not require to be solved for every tube, this is now mandatory for valve control. Therefore, it can be assumed that the computing time will increase again, compared to the mirror control.

6.3. Implementation

The implementation of the Valve control will be the same as Cherek's, only adjusting the approximation of the pump volumetric flow, as seen in Section 4.

The Mirror control however needs some further considerations, as the new control takes the predicted temperature into account. At this point it should be noted that the implementation of the mirror control, other than described in Cherek's thesis, always defocuses only one mirror at a time. And as the code resulting from this thesis is integrated into Cherek's code, all implementations will be oriented towards his implementation rather than his elaboration. Instead of focusing on the two cases of the temperature being too high or too low, as so far, there now are four cases to be distinguished. They are handeled as can be seen in Algorithm 4.

Algorithm 4 Predictive Mirror Control
___

1: **for** tube $i = 1; i \leq N; i++$ **do**
2:     **if** $T_i > T_{\text{demand}} + g$ **then**
3:         defocus a mirror;
4:         set waiting time to let mirrors adjust;
5:         predict future temperature $T_{i,pred}$;
6:         **if** $T_{i,pred} > T_{demand} + \tilde{g}$ **then**
7:             defocus another mirror;
8:         **else**
9:             adjust overall volumetric flow q;
10:                 by predicting the future temperature
11:                 and using Algorithm 1
12:         **end if**
13:     **else if** $T_i < T_{demand}$ **then**   ▷ if $T_i = T_{demand}$ do nothing
14:         **if** mirrors are canceled **then**
15:             focus a mirror;
16:             set waiting time to let mirrors adjust;
17:         **else**
18:             adjust overall volumetric flow
19:                 by predicting the future temperature
20:                 and using Algorithm 1
21:         **end if**
22:     **end if**
23: **end for**
___

When the current absorber's temperature is too high, actions are necessary. The control proposed in section 6.1 would react to a future temperature, thereby possibly leaving the current temperature too high, which, in the worst case, would result in serious damage of the power plant, because the fluid might gasify.

Thus the control is adapted accordingly. It reacts to a temperature that exceeds the desired temperature by g degrees and defocuses a mirror. The predictive calculations are now based on that new setting, defocusing another mirror, if the predicted temperature exceeds the desired by another $\tilde{g}$ degrees. Otherwise the overall volumetric flow q is adjusted as described in chapter 4.

On the other hand, when the absorber's temperature is beneath the demanded value, the control focuses a mirror. Either then, or when there is no more mirror to be focused again, the temperature is predicted and the pump's volumetric flow adjusted as necessary, if the predicted temperature is still too low.

7. Feasibility study

Finally, in this section the introduced controlling methods will be put to the test. Therefore two test cases will be introduced and executed. The first test case consists of a single collector row and serves as validation test for the model and the control of the volumetric flow. The second test case validates the behavior of networks of tubes, within which the collector row's volumetric flows influence each other (see Section 6.2). Thus the second case is designed as a network of four absorber tubes. Both cases will also involve shadowing of the collectors.

7.1. La Africana

The test cases, that will be used in this thesis have been constructed by Cherek [4] based on data taken from the power plant "La Africana" from Posadas, Spain.

Figure 11: Panorama view of the solar thermal power plant with parabolic troughs "La Africana" in Spain.
The plant is surrounded by eight collector fields.[1]

Some background data concerning the configuration of the power plant will be given in the Tables 5 and 6

Cherek has had access to two days amount of data about the outflow temperature of the collector field and the volumetric flow of one collector row. Taking La Africana

Background information	
Technology	Parabolic trough
Country	Spain
City	Posadas
Region	Córdoba
Land Area	252 hectares
Solar Resource	1950 MW h per year
Electricity Generation	170 000 MW h per year (estimated)
Start of Production	November 21, 2012

Table 5: Background information for solar thermal power plant La Africana in Posadas, Spain.[11]

Plant configuration	
Solar-Field Aperture Area	550 000 m^2
number of solar collector assemblies (SCAs)	672
number of absorber tubes	168
number of SCAs per absorber tube	4
SCA length	150 m
number of mirrors per SCA	12
Length of the absorber tube ℓ_a	600 m
Aperture of the mirrors G	5.45 m

Table 6: Plant configuration for the solar thermal power plant La Africana in Posadas, Spain.[11]

as an example, he has been able to construct a test case, which simulates a single absorber tube as accurately as possible. Therefore Cherek took the provided information and combined it with typical parameters of solar thermal power plants with parabolic troughs. The resulting parameters are listed in table 7.

Quantity	Value
Inner diameter of the absorber tube	$0.07\,\text{m}$
Inner diameter of the header tube	$0.1\,\text{m}$
Length of the header tube	$200\,\text{m}$
Number of mirrors per collector row	48
Length of a mirror	$12.5\,\text{m}$
Length of the absorber tube	$600\,\text{m}$
Mirrors aperture	$5.45\,\text{m}$
Global mirror efficiency	0.75
Global thermodynamic efficiency	0.7
Irradiation per area	$843.5\,\text{W}\,\text{m}^{-2}$
Desired outflow temperature	$666.36\,\text{K}$
Inflow temperature	$567.57\,\text{K}$

Table 7: Parameters for the matlab implementation of the test cases representing the power plant La Africana.

Due to the typical structure of a solar thermal power plant (see Figure 1) the following arrangement is given.

Test case	single row	network
number absorbers	1	4
number sections	3	12
number junctions	2	8

Table 8: Structure of the two considered test cases.

Assuming full intensity of solar irradiation while not considering any clouds overshadowing the collectors, Cherek calculated a design point. This design point is a configuration of the plant, in which, with this perfect environmental situation, the heat transfer fluid reaches exactly the desired outflow temperature of 663.36 kelvin (see figure 12). The behavior of the temperature in the absorber tube results in a straight line, since the temperature rises evenly and strictly monotonously due to the constant solar irradiation and the constant pump flow.
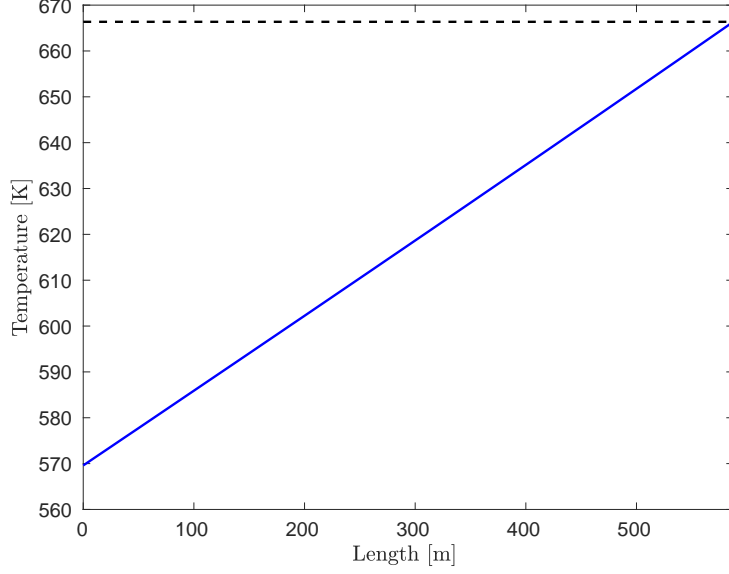
Figure 12: Design point of the test case for one single row.

Starting from there, overshadowing has to be considered, because that is where the need of control comes from. Thus Cherek's design point will be the initial setting all further simulations will start with. However, to be able to fully compare the simulations' results, they will all be restricted to a time horizon of simulated steps. Moreover the step size in time Δt has to be constant over all simulations.

From equation 22 and the data of table 7 we can deduce a value for Δt, that guarantees stability by fulfilling the Courant-Friedrichs-Lewy condition. With

$$\Delta x_{header} = \frac{200\,\text{m}}{48} = 4.1\bar{6}\,\text{m} \quad \text{and} \quad \Delta x_{absorber} = \frac{600\,\text{m}}{48} = 12.5\,\text{m} \tag{92}$$

and the velocity ν, which, by test runs, can be roughly estimated against the value of

$$\nu_{max} = 0.4\,\text{m\,s}^{-1}\,, \tag{93}$$

we get

$$\Delta t \leq \frac{\Delta x}{\nu_{max}} = \min\left(\frac{\Delta x_{header}}{\nu_{max}}, \frac{\Delta x_{absorber}}{\nu_{max}}\right) \approx \min\left(\frac{4\,\text{m}}{0.4\,\text{m\,s}^{-1}}, \frac{12.5\,\text{m}}{0.4\,\text{m\,s}^{-1}}\right) = 10\,\text{s.} \tag{94}$$

The smaller-equal-relationship applies, since ν_{max} is already estimated upwards. Thus the value $\Delta t = 10\,\text{s}$ can be used without causing any problems. As indicated in Algorithm 1 the variables $predicitveTime$ and β or $\frac{1}{\beta}$ respectively need to be set. Lastly the variable m determines how often the control is allowed to operate. As the irradiation depends on the time, in the test cases the weather cannot change faster than

every 10 seconds. So by setting $m = \Delta t$ the control is allowed to immediately react to every change in irradiation. All necessary parameters to execute the simulation code are summarized in table 9. The used code can be found in the appendix of this thesis.

Simulation parameters	
stepsize in time Δt	$10\,\mathrm{s}$
operational stepsize m	$10\,\mathrm{s}$
simulation time	$25\,000\,\mathrm{s}$
weight β	$10^9/3.7486$
predictive time	$15\,000\,\mathrm{s}$
steps for irradiation change	5000

Table 9: Simulation parameters.

The selection of these parameters is very important, so it makes sense to spend a lot of time on the correct choice. Apart from the already mentioned unwanted numerical effects, these can lead to instability or enormous computing times of up to 20 hours.

7.2. Control of a single collector row

In order to validate the control, a test case with shadows is necessary. Therefore the design point from Section 7.1 has been taken and for the collectors 1 and 2, as well as 27 - 32, a overshadowing is introduced. The test cases distinguish between two kinds of shadow. The first option is that the collectors are abruptly fully overshadowed. This scenario rather corresponds to broken mirrors. Still such a scenario needs to be observed, as mirrors cannot always be replaced right away, as special equipment is needed to do so. In the other case the shadow is introduced more slowly, representing the irradiation changes that inevitably occur while the weather changes over the day. Regardless, wether the shadow spreads fast or slow, the final situation of the power plant is depicted in Figure 13. Here no control has been used, so that the heat transfer fluid's outflow temperature decreases to a value of 649.67 kelvin that finally enter the heat exchanger.
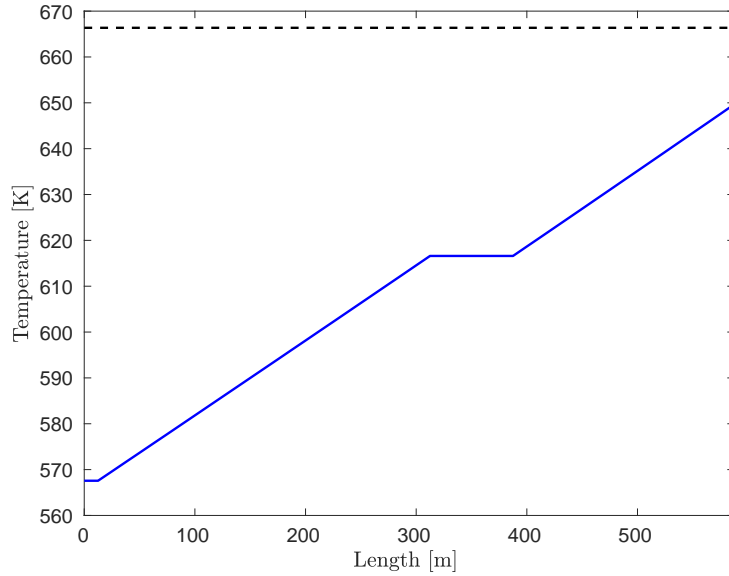
Figure 13: Design point of test case with shadows.

The simulations are performed on a Lenovo Thinkpad X230 with 4 GB RAM and an Intel(R) Core(TM) i7-3520M processor with CPU @ 2.90 GHz.

Control with simplifications of the source term

At first we will consider the results that can be obtained with the simplified control (compare Section 4.3.1). Using the above gathered parameters (see tables 7 - 9), a fast shadow introduction leads to the result shown in Figure 14. The behavior of the HTF's temperature is similar to the one in Figure 13. However, the gradient between the shaded areas is visibly higher, so that a final temperature of 666.45 kelvin can be reached in the absorber tube. The temperature finally flowing into the heat exchanger is at 666.96 kelvin. The reason why the outflow temperature is higher than the temperature at the end of the absorber tube, although there is no temperature increase or decrease in the header tube, is the limited simulation time. The value is still derived from the previous hotter HTF. With a longer simulation time, the outflow temperature drops to the above mentioned 666.45 kelvin. In the process of the simulation the highest, in the absorber tube reached, temperature is about 671 kelvin. As the highest temperature for Therminol VP1 Oil is a value of 673.21 kelvin, so the control came pretty close to the worst case, where the oil evaporates. Thus overall the control can handle broken mirrors, but too many at the same time might result in a too big drop in temperature, that should rather be handeled differently. The scenario simulating 6.94 hours took 90.64 seconds.

44
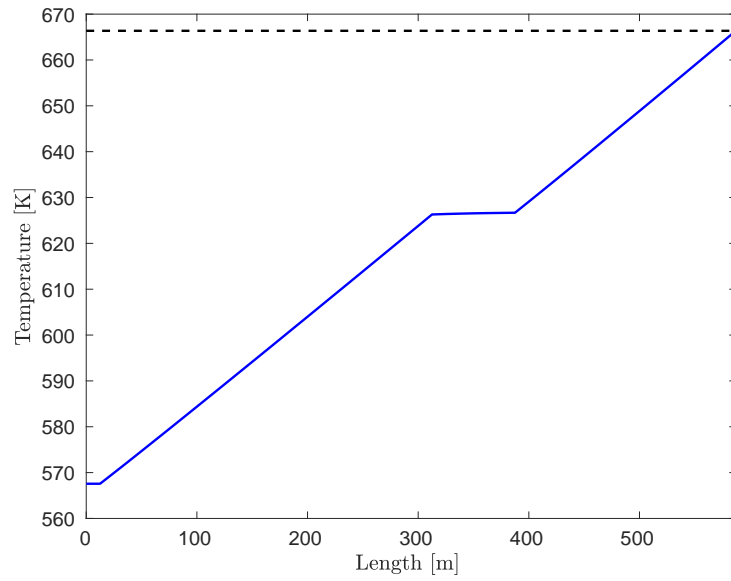
Figure 14: Result of simplified control with fast shadow introduction.

When it comes to a slowly spreading shadow, the simulation of the simplified control leads to the same result as for fast shadow introduction. However, as the shadow only appears gradually, the control is able to react better, so that the temperature does not rise above 667.5 kelvin during the simulation. The fact that the control has to react more often to changed irradiation also has an effect on the computation time. The simulation now takes 92.83 seconds.
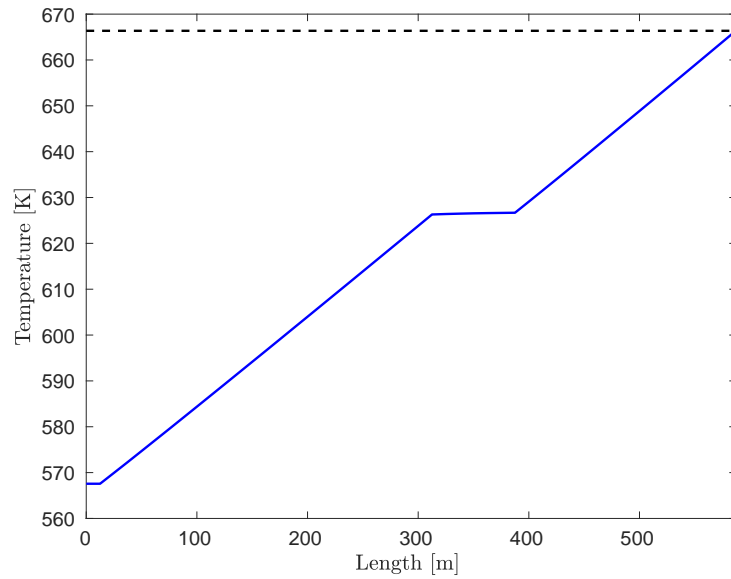
Figure 15: Result of simplified control with slow shadow introduction.

Control with less simplification

Figure 16 demonstrates, that the control with less simplification shows the same behavior as the simpliefied control. However this control is more accurate. Thus the HTF enters the heat exchanger with the desired temperature of 666.36 kelvin. In the 6.94 simulated hours, the highest temperature the HTF reached was 670.8 kelvin, significantly lower as for the simplified control. The simulation took 250 seconds, more than twice as much time as the simplified control needed. However, as the simulation still took only a hundredth of the simulated time, the control is nevertheless very efficient.
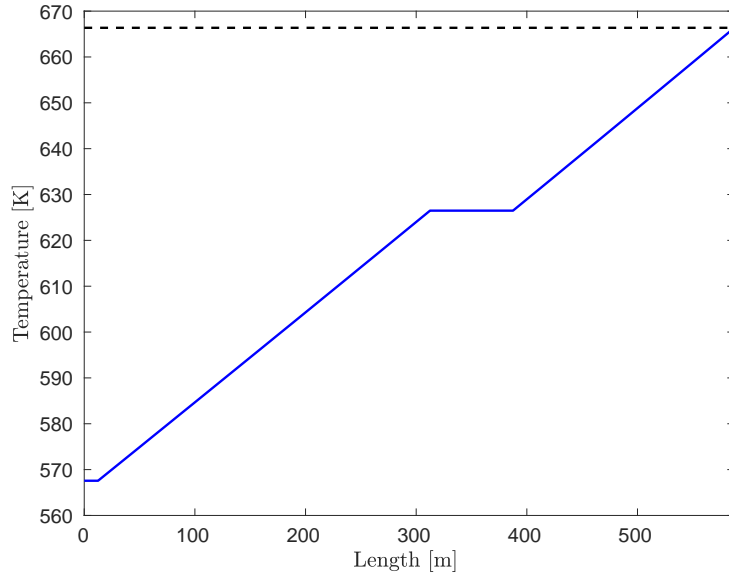
Figure 16: Result of control with fast shadow introduction.

As can be seen in Figure 17 the behavior of the less simplified control for slow shadow is the same as for fast shadow. In both cases the control manages to reach exactly the desired temperature of 666.36 kelvin, by setting a volumetric flow of $4.6005\,\mathrm{m^3\,s^{-1}}$. The highest temperature reached in the simulation is 666.93 kelvin, the lowest maximum temperature until now. The calculation time required for the simulation is 249 seconds, which is slightly less than for the simulation with fast shadow. This is contrary to the behavior of simplified control regarding fast and slow shadows. A possible reason for this would be that the control could settle down faster with slow shadows.

Assuming that a variation of 5 degrees is acceptable, both controls remain within the allowed range in all scenarios.
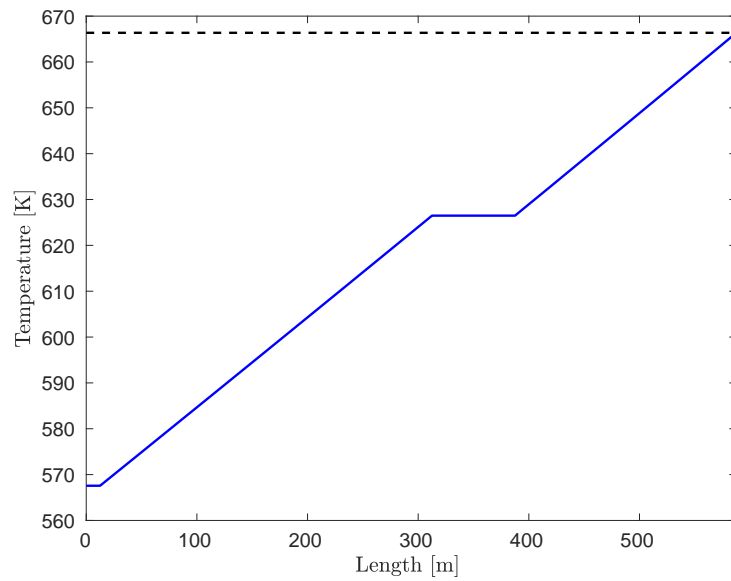
Figure 17: Result of control with slow shadow introduction.

Cherek's Control

Cherek's equivalent to this control, which only controls the volumetric flow, would be the valve control for a single tube, as it does not change the valve, but only regulates the pump flow. For $\Delta t = 0.5$ seconds Cherek's control leads to the result shown in Figure 18. For the validation of Cherek's control please refer to his thesis [4].
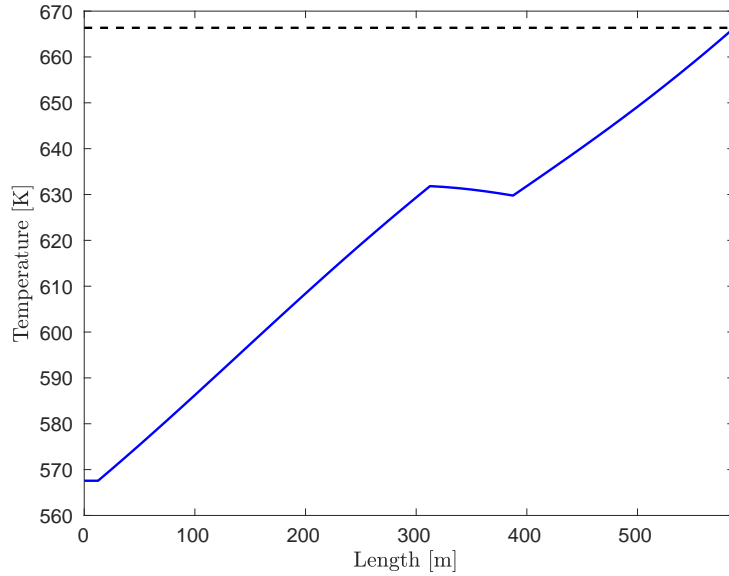
Figure 18: Result of Cherek's valve control for a single tube with fast shadow introduction and $\Delta t = 0.5$ seconds.

The simulation results in a similar behavior as the pump control. Such a behaviour is to be expected and exactly what is to be achieved. Instead of a horizontal straight line at the point where no irradiation occurs due to shadows, a temperature drop is to be observed. However, this is not disturbing, as it only shows that the achieved state is not a final state. With a longer simulation time the result settles and the completely shaded place is again recognizable as a horizontal straight line. When repeating the simulation with the actually used $\Delta t = 10$ seconds, the control leads to an CFL-error. If you take a closer look at the matlab code, which is part of the control, you will notice that always the initial value of the velocity is passed to the function. This means that the control cannot react to the current speed, i.e. it does not regulate the current situation at all. However, if the function is modified so that the correct value is passed to it, it can neither be executed for $\Delta t = 10$ seconds nor for $\Delta t = 0.5$ seconds. The control always results in an CFL-error. The same is true for the case with slow shadow (see Figure 19).

49
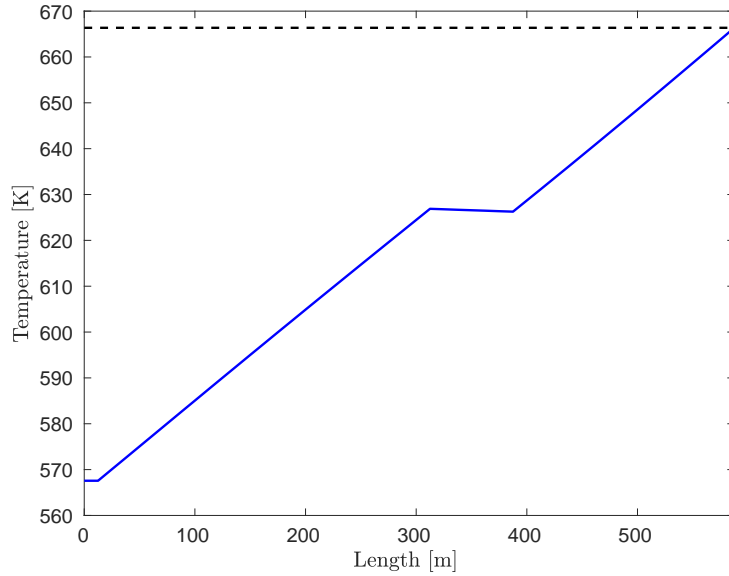
Figure 19: Result of Cherek's valve control for a single tube with slow shadow intro-
duction.

Nevertheless, since the controls discussed here are based on Cherek's theory and show
the expected behavior for various test runs, this suggests that Cherek's PI controller
may be faulty.

7.2.1. Mirror Control

Before the results of the simulations regarding the mirror control can be viewed, some
parameters have to be set again. The waiting time w is necessary to stabilize the
system after a mirror has been defocused or focused.

Parameters for mirror control	
waiting time w	5 s
upper degree boundary g	3 K
upper degree boundary for prediction $\tilde{g}$	5 K

Table 10: Simulation parameters for the mirror control.

The two upper degree boundaries determine the range above the desired temperature,
in which the control does not yet react. As the control uses a predicted temperature,
two boundaries are necessary, a smaller one for the actual temperature and a slightly
higher chosen boundary for the predicted temperature. See Algorithm 4 for their
function.

50

Now these parameters can be used to run the simulations. As with the pump control, the investigation of the mirror control will also begin with the simplified form.

Control with simplifications of the source term

The simulation takes 12.61 seconds and ends with a value of 667.58 kelvin both at the end of the absorber tube and in the heat exchanger. The mass flow is 4.5343 m^3 per second. The highest temperature reached in the meantime was 669.37 kelvin. It is noticeable that it was possible but obviously not necessary to defocus a mirror. Thus the result of the simplified mirror control can be compared well with that of the simplified pump control.

	simplified pump control	simplified mirror control
end-temperature of absorber tube [K]	666.45	667.58
maximal temperature in simulation [K]	671.00	669.37
temperature entering the heat exchanger [K]	666.96	667.58
mass flow [m^{3}s^{-1}]	4.81	4.53
computational time [s]	90.65	12.61

Table 11: Comparison of the results for the simulation with fast shadow inroduction.

Considering the different volume flow resulting from both controls, the pump control seems to approach the optimum from above, while the mirror control approaches from below. Since the result of the pump control shows that the temperature was significantly higher in the meantime, it is rather a jumpy behavior. This conclusion is only possible because the shadow is set as fast or sudden so that the situation to be regulated occurs immediately and then remains the same. Overall, the pump control manages to reach closer to the desired temperature than the mirror control in the given time. Nevertheless the mirror control is safer, because the maximum temperature is about 1 K lower. Furthermore the mirror control is much faster with about 13 instead of 91 seconds. With a longer simulation time, it can therefore be expected that the mirror control would deliver just as good or even better results in a shorter time. Although no mirror is defocused after 25000 seconds, the entire simulation process shows how mirrors are turned in and out. Thus it can be assumed that the use of the mirrors limits the erratic behavior.
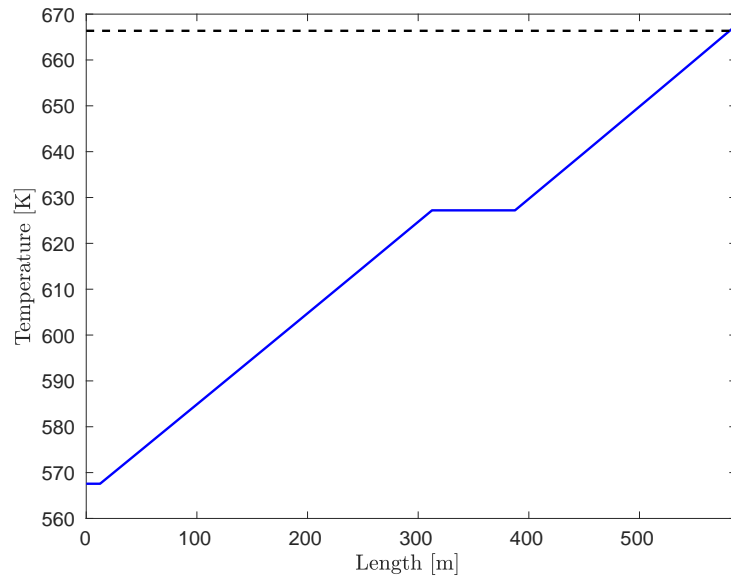
Figure 20: Result of simplified mirror control for a single tube with fast shadow introduction.

An adjustment of the simulation time does not only make sense in this case. The simulation time should also be varied if the mirror control parameters are changed. Figure 21 shows the result of the simulation with changed parameters $g = 1\,\mathrm{K}$ and $g = 3\,\mathrm{K}$. The simulation time of 25000 seconds is not sufficient to settle into a stable state. It is also possible that the state shown in Figure 20 is stable, but not a final state.
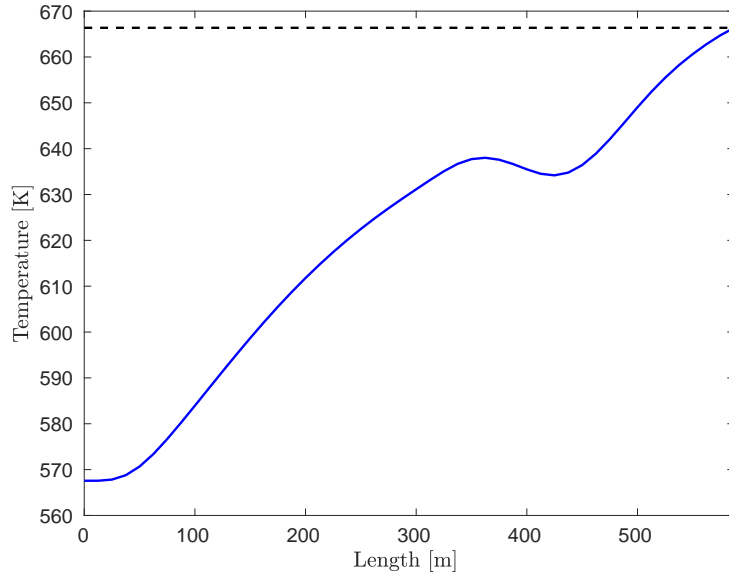
Figure 21: Result of simplified mirror control for a single tube with fast shadow intro-
duction. The parameters have been changed to $g = 1\,\mathrm{K}$ and $\tilde{g} = 3\,\mathrm{K}$.

A closer look at the cases investigated so far confirms this suspicion. Only the less simplified control was able to reach the final state in both cases in the given time. In addition to the importance of the appropriate choice of simulation time, this knowledge also underlines a much more important fact: In contrast to Cherek's static controls, the controls discussed in this thesis can be used dynamically. The critical temperature is never exceeded, even if the distance to the critical temperature of 673.21 kelvin varies depending on the control. Furthermore, states that do not correspond to the final state already represent good results. Therefore, the use of the controls can be considered efficient even if there is not enough time to reach the final state. Thus a dynamic use in practice is not only possible but reasonable.

If now the simulation time is increased up to the tenfold, the control with the parameters $g = 3\,\mathrm{K}$ and $g = 5\,\mathrm{K}$ always leads to the exact same result already shown in Figure 20. Performing the same simulations with the parameters $g = 1\,\mathrm{K}$ and $g = 3\,\mathrm{K}$, the reason becomes visible. At a certain point in time, the temperature of the HTF begins to oscillate endlessly between 662 and 667 kelvin, the so-called zigzagging effect occurs. This effect appears often in connection with the gradient method and is, since the control includes the gradient method, not surprising.

The zigzag effect is shown in Figure 22 using the example of the function $f(x, y) = \frac{1}{2}x^2 + 5y^2$. The minimum at the point $(0, 0)$ is not reached, instead the procedure oscillates back and forth. The x-value approaches steadily, but will not reach the minimal point. The y-value, on the other hand, does not approach but jumps up and down

between two values, provoking the zigzagging.
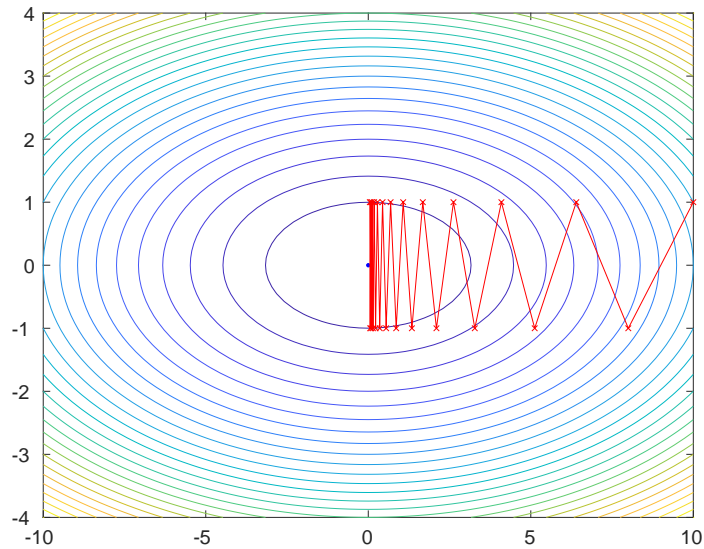
Figure 22: Zigzagging Effect of gradient method.
Contour plot of the function $f(x,y) = 0.5 \cdot x^2 + 5 \cdot y^2$ with minimum at point $(0,0)$. Gradient method performed with step size 0.2 and starting point $(x_0, y_0) = (10, 1)$. Twentyfive gradient steps shown in red.

To avoid this effect, the step size (here β) can be adjusted or also set dynamically. In the given situation of the solar thermal power plant, it is also possible to avoid this effect by setting the desired temperature value in a permissible interval (see Subsection "mirror defocus control").

Since the zigzag effect continues endlessly, it is not possible to find a suitable simulation time with final state. Within the set 25000 seconds the zigzag effect already occurs, therefore we will keep this simulation time also for the other simulation runs.

The simplified mirror control then leads to a result with slowly introduced shadow in 6.83 seconds, i.e. twice as fast as with fast shadow. The result is displayed in Figure 23.
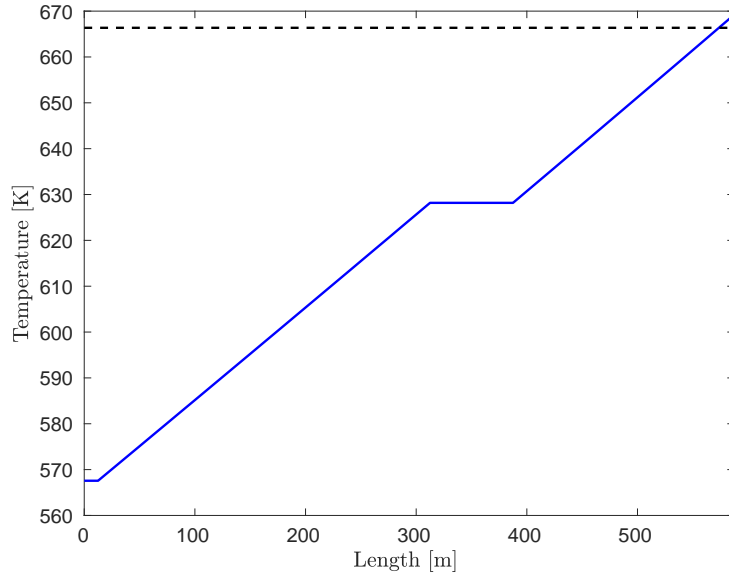
Figure 23: Result of simplified mirror control for a single tube with slow shadow intro-
duction.

The final temperature of both the absorber tube and the collector field is 669.24 kelvin,
about $2\,\mathrm{K}$ above the other result of this control. At the same time this is also the
maximum value. The oscillating behavior also occurs, which means that this behavior
is independent of the speed at which the shadows emerge. Nevertheless, it can be said
that the simplified mirror control can react better to fast introduced shadows than
to slow ones, because although the maximum value is lower, the oscillation is much
stronger.

Control with less simplification

Similar to before, in the case of mirror control we consider a less simplified form, where
the update calculation is simplified, but uses correctly calculated temperature values
(see Section 4.4). As with pump control, the less simplified control is better but slower
than the simplified form. This development is not surprising, since the calculations
with the actual values for density and specific heat capacity are more complex, but
more accurate. Compared to the pump control, this mirror control is worse but much
faster, which is also due to the oscillation.
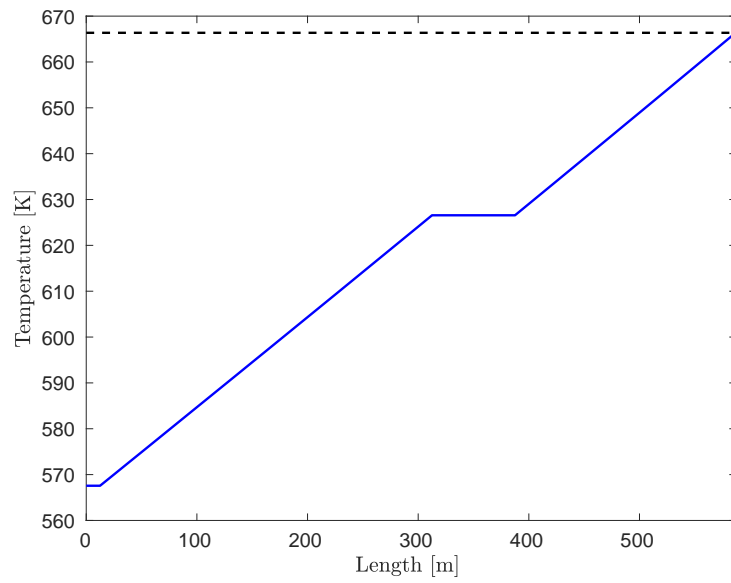
Figure 24: Result of the less simplified mirror control with fast shadow introduction.

With fast introduced shadows the temperature of the HTF rises to 669.36 kelvin in the meantime, before it begins to oscillate and ends after 25000 seconds at 666.49 kelvin. The calculation takes 30.49 seconds.
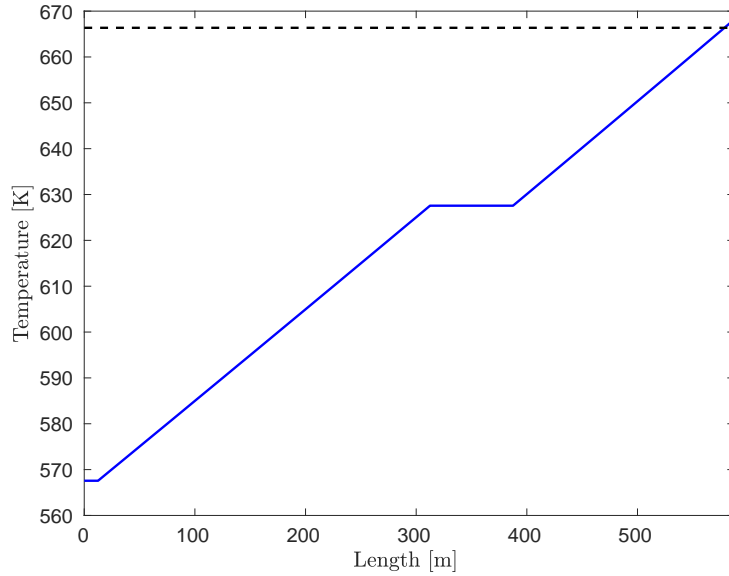
Figure 25: Result of the less simplified mirror control with slow shadow introduction.

When it comes to slow shadow introduction, the maximum temperature can be reduced to 668.19 kelvin. At the end of the simulation time, however, the oscillation is significantly higher with this value. At the same time, the fact that the two values are identical also shows that the control has stopped at the highest point of the oscillation and actually comes to better values. Nevertheless, with the previous results, it was not possible to determine at which point of the oscillation the simulation ended.

If the values determined so far are considered again, the following is noticeable:
Each of the controls seems to behave better when applied to slowly emerging shadows. This suggests that the controls cannot adequately handle the sudden shock of the fast shadow. A similar shock is likely to occur when the mirrors are suddenly defocused. So let's look at the less simplified mirror control again, but rather realize the rotation of the mirrors bit by bit, smeared out over the 5 seconds waited to let the effect settle.
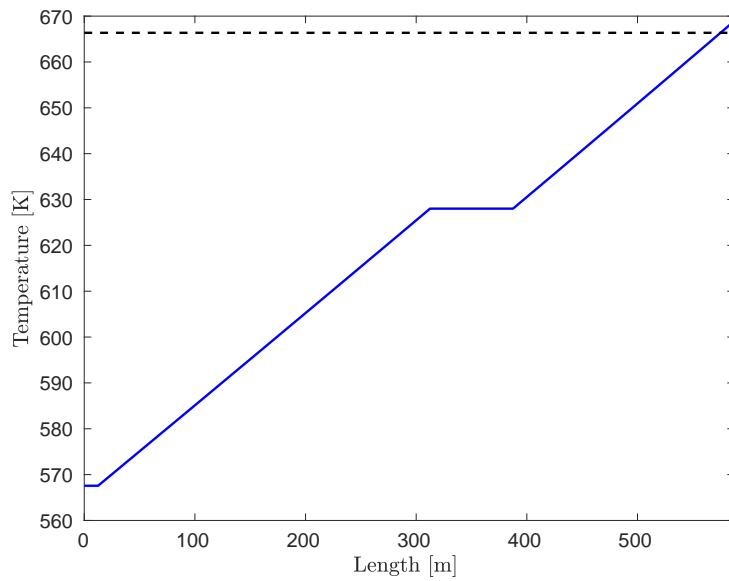
Figure 26: Result of the less simplified mirror control with slow shadow introduction and smeared out mirror defocusing.

Since the effect of turning the mirrors out and in now takes more time, control over the fast shadows can now react worse. This results in higher values (final temperature of 668.94 kelvin) and longer computing time. The exact values of the simulation can be found in the appendix.

In the more interesting case of slow shadows, the behavior is different. As expected, the results are better than for fast shadows, but surprisingly, the results are exactly the same as those of the original mirror control. Again, end and maximum values are 668.19 kelvin.
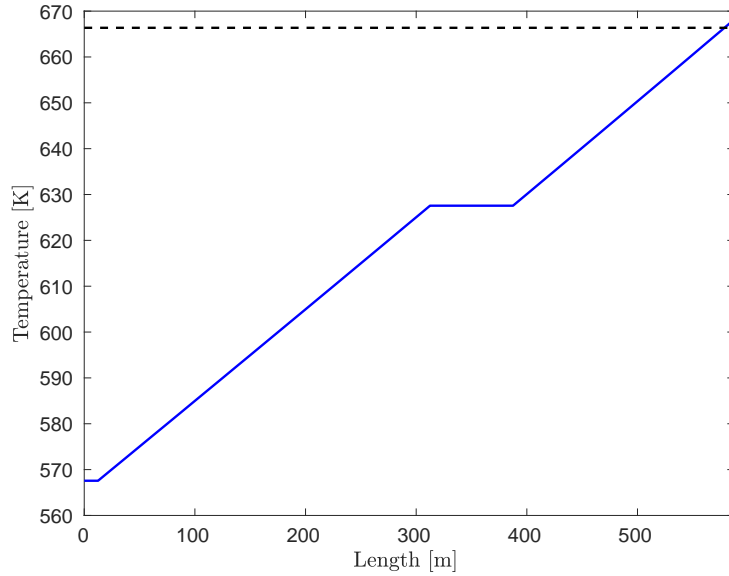
Figure 27: Result of the less simplified mirror control with slow shadow introduction and smeared out mirror defocusing.

This control, too, is not free of oscillation and is possibly capable of better results. The only difference is in computing time and rather unexpected: Although the movement of the mirrors is piece-wise and therefore the effect is slower, the simulation took about 2 seconds less time.

Control with calculated defocus number

As the last version of a mirror control, the original mirror control is adapted again. Since the smearing of mirrors seems to contribute little to the effectiveness, this tactic is discarded. As originally intended by Cherek, instead of defocusing 1 or 2 mirrors at a time, each control step now calculates how many mirrors have to be defocused (see eq. 6.1 in Section 6.1).

The results of the simulations with the calculated number of mirrors N_{defocus} show a clear jump to the other mirror controls. Now the strength of the mirror control is revealed. Both simulations reach exactly the desired value of 666.36 kelvin.
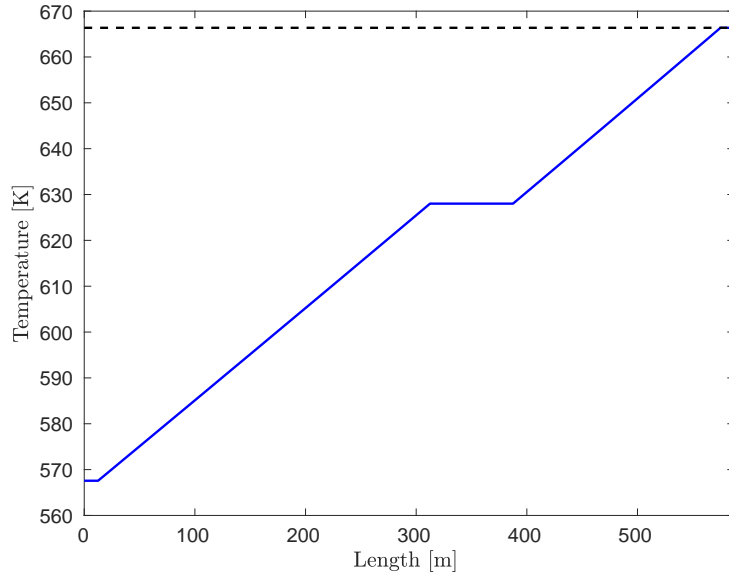
Figure 28: Result of the mirror control with fast shadow introduction and calculated N_{defocus}.

Moreover in the situation with fast emerging shadow the value of the maximum temperature of 667.51 kelvin is much lower than with pump control. On the other hand, the computing time is higher with about an additional 110 seconds. The circumstance, that this mirror control finally can exceed the values of the pump control is mainly due to the fact that there is no oscillation. This is the case, because this control determines a feasible interval, within the limits of which focusing or defocusing a mirror would be useless. The pump control is then used within these limits. The increased computational effort, which is connected with computing a new value for N_{defocus} and thus a new permissible interval in each control step, explains the need of additional 110 seconds.
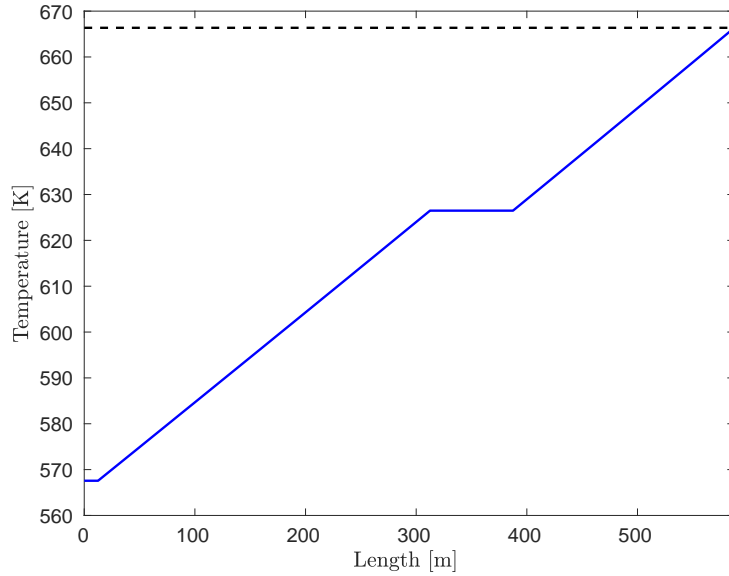
Figure 29: Result of the mirror control with slow shadow introduction and calculated N_{defocus}.

In the case of slow shadows, the maximum value does not deviate at all from the result of the pump control. So with 666.93 kelvin both controls are not even $1\,\text{K}$ above the desired temperature. However, the disadvantage of this mirror control is the higher computation time of 370.79 seconds. But as in networks it is no longer possible to control the pipes individually with the pump control, the accuracy of this control promises to pay off. Moreover, in both shadow simulations, the mirror control has been able to reach the final state before the given simulation time was over.

Cherek's Control

Finally, Cherek's mirror control is executed again in order to include it in the comparison of the mirror controls.

Cherek's mirror control is not able to process the shock of fast shadows. This can be seen clearly in Figure 30. The final temperature in the absorber tube is only 650.51 kelvin.
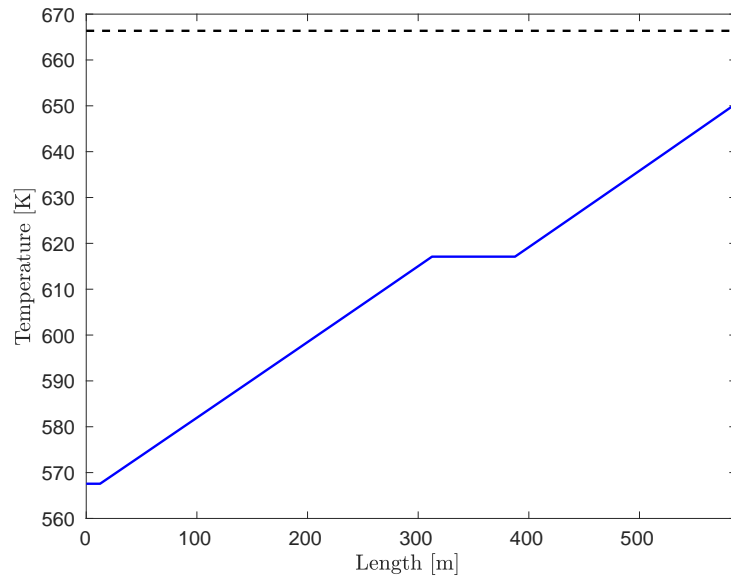
Figure 30: Result of Cherek's mirror control with fast shadow introduction.

Considering that without any control a value of 649.67 kelvin is reached, Cherek's control is therefore not efficient in this situation.

With slowly emerging shadows the control is at least able to generate an HTF temperature of 661.3 kelvin.
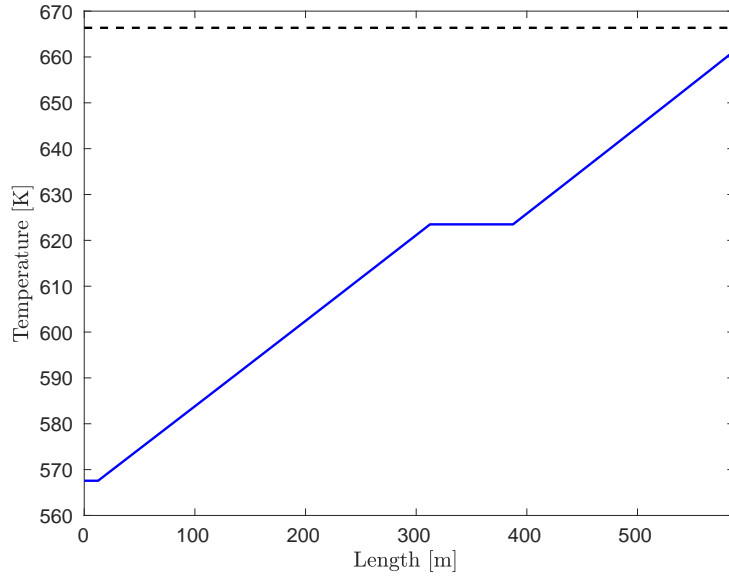
Figure 31: Result of Cherek's mirror control with slow shadow introduction.

It is noticeable that the maximum temperature in both cases corresponds exactly to the desired temperature. The control is therefore not sufficient to compensate for the temperature loss even in slow shadows.

Both simulations were completed in under 10 seconds. However, this time advantage is not sufficient to compensate for the large difference from the desired temperature, especially as the above controls achieve significantly better values.

Since Cherek's control is a static control, it is conceivable that a longer simulation time will lead to better values. Tests, however, contradict this.

Cherek's control includes a waiting time of 4000 seconds after adjusting a mirror, which is just about 1 hour. For a static control such a long waiting time is unproblematic, since also the simulation time can be adapted accordingly. According to Cherek this high value is necessary to guarantee stability. Since the step size of the time Δt is already increased from 0.5 seconds to 10 seconds in the simulations mentioned here, an adjustment of this value is also reasonable.

With a waiting time of 5 seconds, Cherek's control reaches values around 663 kelvin, which is much better than before (plot and values see appendix). This underlines the realization of the Sections 3.3 and 7.1, that a value of $\Delta t = 0.5$ seconds theoretically fulfills the CFL condition (22), but practically leads to unwanted numerical side effects. Furthermore, depending on the configuration, an oscillating behavior can also be observed in this control.

Accordingly, the mirror control discussed here with regular calculation of the value N_{defocus} seems to be the most efficient. Whether this is confirmed for networks as well

will be shown in Section 7.3.

7.2.2. Valve Control

As already mentioned in Section 7.2, the valve control does not make changes to the valve of a single pipe. Therefore, the application of this control is only interesting for networks of tubes and therefore only considered in Section 7.3.2.

7.3. Control of a Network

As already explained in Figure 1 in Section 2, solar thermal power plants are built as a network of several absorber tubes. Since the system is now a much more complex interaction, but pump control can only control the mass flow of the entire system, this control is no longer useful. The state of the art in practice already regulates with mirrors. Control without mirrors or valves would be retrograde, so the efficiency of mirror and valve control is examined directly.

In order to investigate the interaction of temperatures in a network of pipes and the effects of controls, the second test case maps a network of 4 pipes. Although the test case is artificial, it is still based on the power plant La Africana. Each pipe is shaded individually.
To force a clear difference, the first collector tube remains free of shadow. For the pipes 2 and 3 the cells $1 - 2$ and $9 - 14$ respectively cells $1 - 4$ and $12 - 18$ within the field are overshadowed until completely darkened.The last tube is more or less shortened by shading the first 16 cells.
If now a simulation is executed, that starts with full sunlight and optimal settings and is then exposed to the above shadows, the results shown in Figure 32 are obtained when omitting any control.
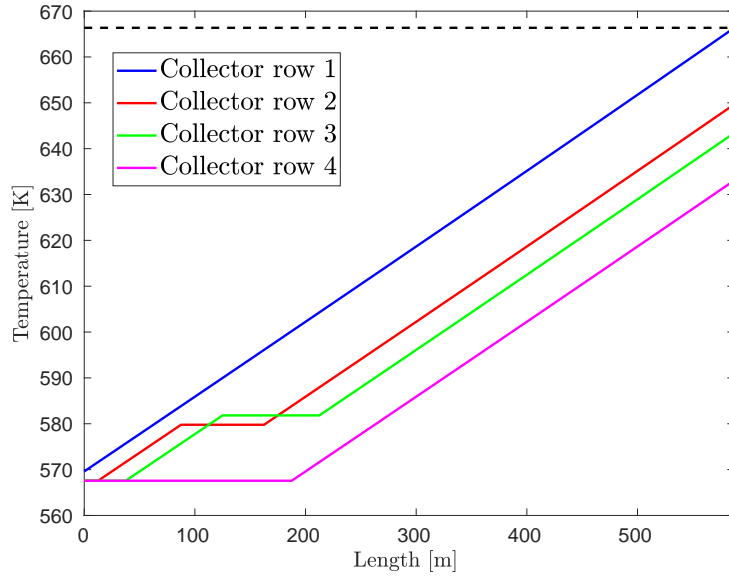
Figure 32: Results of the network test case without any control.

As the first collector row is not exposed to any shadow, the end temperature remains the optimal 666.36 kelvin. The other three pipes lead through the respective shadows to the end temperatures of 649.67, 643.44 and 633.08 kelvin. Due to the mixture of the different end temperatures, at the end of the collector field an outflow temperature of 648.34 kelvin finally flows into the heat exchanger.

7.3.1. Mirror Control

Since Cherek's static control can already serve as a basic setting, the associated results are used as a reference standard. Therefore, first consider the results obtained for each of the simulations when Cherek's mirror control is applied with the parameters determined in Section 7.1.

Both Simulations end ahead of schedule with an error. The error occurs, because Cherek's control does not have a boundary for defocused mirrors. Within the simulation the control tries to defocus more mirrors than available and hence the simulation is canceled. Furthermore a strong oscillation underlines again, that the control is not dynamically applicable.

When adjusting the waiting time to the 4000 seconds Cherek originally suggested, the following results are obtained (see Figure 33).
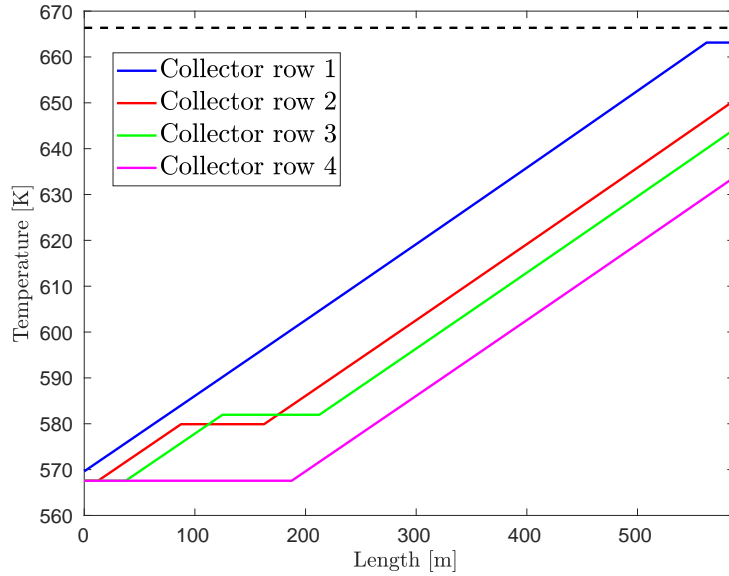
Figure 33: Results of a network with 4 tubes with Cherek's control for fast shadow introduction and a waiting time of 4000 seconds.

By defocusing 2 mirrors of the first absorber tube the HTF's temperature in that tube can be decreased to a value of 663.14 kelvin. The temperature is beneath the desired value, because the mirrors are of fixed length. Thus the temperature cannot be manipulated exactly only with mirrors. But the pump control regulates all tubes at the same time and is therefore dependent on all of them. At the other tubes, no mirror is defocused and the end temperatures range between 633.75 and 650.51 kelvin. The final mixture reaches a temperature of 648.06 kelvin.

Both simulations are executed in about 8.5 seconds, a very short computation time. Once again, it is evident that Cherek's control can react better to slow shadows.

In the same amount of time the simulation with slow emerging shadows leads to an outflow temperature of 668.11 kelvin, just $2\,\mathrm{K}$ above the desired temperature. The mass flow of the second simulation is with $16.61\,\mathrm{m^3/s}$ significantly below the mass flow of $22.64\,\mathrm{m^3/s}$ that is found in the first scenario. Hence the end temperatures in the absorber tubes are much higher, which results in several defocused mirrors and a mixing temperature of 668.11 kelvin. The last absorber tube heats the HTF up to a temperature of 654.65 kelvin. The first three tubes therefore reach values between 662.95 and 685.22 kelvin. To prevent the HTF from evaporating, in each of the other tubes, 5, 3 and 2 mirrors are defocused.
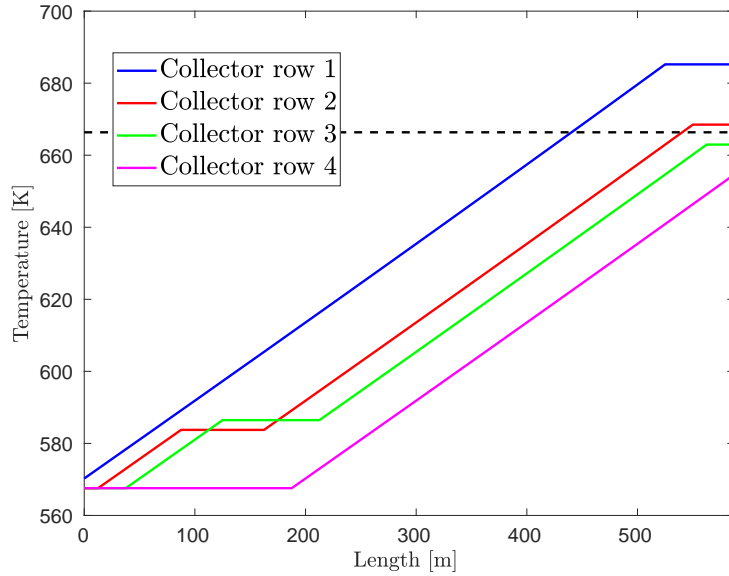
Figure 34: Results of a network with 4 tubes with Cherek's control for slow shadow introduction and a waiting time of 4000 seconds.

As the analysis in Section 7.2 already showed the clear superiority of the mirror control with calculated N_{defocus} over the other controls, those will be ignored here.

Control with calculated defocus number

The control seems to be responding well. The final result, however, shows that the system is not so good at dealing with the constant de-focusing of mirrors. This circumstance is due to the fact that the update of the volume flow is now determined by all pipes at the same time and thus cannot adequately absorb the shock in every pipe. If, for example, the heat in the first three pipes is already high enough, while the temperature in the last pipe is still far below the desired temperature, the first pipes will increase the volume flow and the last will want to reduce it. Therefore, a certain oscillation now occurs during this control as well. The increased complexity also leads to an exponentially growing computing time. Since the simulations with only 4 pipes are already so complex, one might think that a practical use would no longer be meaningful. However, it must be once again pointed out that, unlike Cherek's control, this one can be applied dynamically. While the computing time in Cherek's simulations thus represents the total calculation time necessary before those results can be applied to regulate the plant, the computing time in this control consists of several regulating steps that have already been successfully implemented. A direct comparison of the required times is therefore no longer possible. Still the found temperatures are a good measurement for comparison.

67

While the mixed temperature of Cherek's control reached the heat exchanger with 648.06 K, an even slightly worse result than in the situation without any control (compare Figure 32), the control with calculated N_{defocus} manages to reach an outflow temperature of 662.87 kelvin, when the shadow is directly introduced. As can be seen in Figure 35, collector row number 4 has the biggest difference to the desired temperature, as it only reaches 652.19 kelvin. The other three collector rows reach a temperature within the intervall of 665.5 K and 667 K. Calculating this simulation took about 1332.05 seconds.
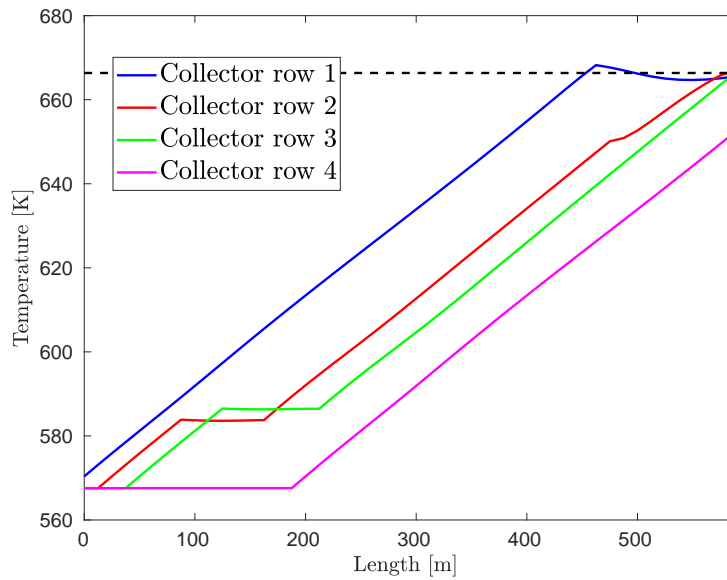
Figure 35: Results of a network with 4 tubes for the mirror control with calculated defocus number and fast shadow introduction.

The result of this control for slowly emerging shadow is similar to the one with fast shadow. Again oscillation keeps the control from reaching a final state. But when it comes to networks, the difference between handling fast and slow shadow becomes negligible for this control.
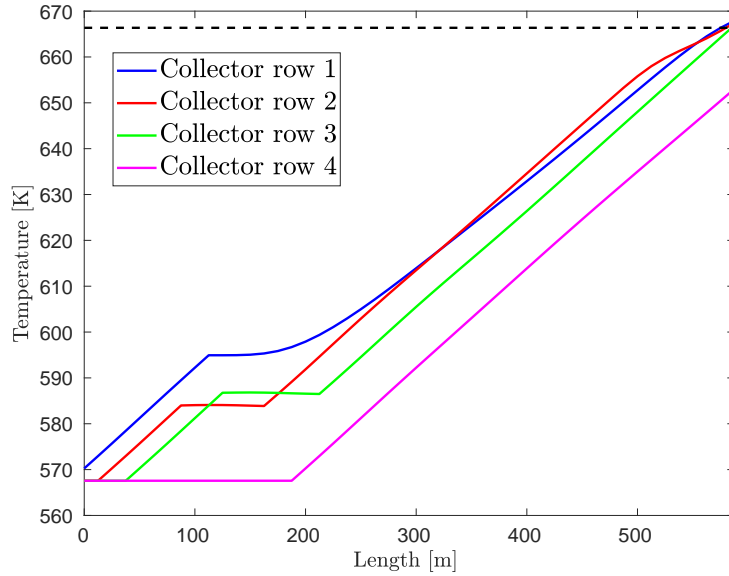
Figure 36: Results of a network with 4 tubes for the mirror control with calculated defocus number and slow shadow introduction.

Cherek's control was able to improve from a mixed temperature of 648.06 K to a value of 668.11 K.

The control with calculated defocus number N_{defocus} however has had a value of about 667 kelvin but again did not stop. Instead, while trying to optimize all absorber tubes on their own, the state shown in Figure 36 came down to a mixing temperature of 662.97 K, about the same amount as for direct shadow. So the outflow temperature could not be improved, but still the simulation needed 30 seconds more computing time. Anyhow, when taking a closer look, there is a slight difference in temperatures: The worst absorber, collector row number 4, now provides a temperature of 653.01 kelvin, about 0.9 K more than before. Also the interval, in which the remaining end temperatures move, changes to the smaller range between 667 and 668 kelvin. Thus the temperatures of the collector rows $1 - 3$ are not closer to the perfect temperature than before, as the control can only react corresponding to the yet emerged shadow. Moreover the figure clearly shows, that the state, which has been reached in the simulation time of 25000 seconds, is not a final state. Due to the oscillation even a bigger simulation time does unfortunately also not lead to a final state. Since oscillation can be held responsible for these relatively poor results, it would be conceivable in further investigations to circumvent this by permissible intervals per absorber tube.

Striking is, that the control comes across a setting, at which the temperature at the heat exchanger is 666.36 kelvin, but does not stop there. This is due to the fact that the objective, we try to solve with the optimization problem, is to have a temperature

69

of 666.36 K at each absorber tube. Hence the mixed temperature would be 666.36 K as well.

In the setting that is discarded by the control however the mixing temperature originates from some absorber tubes having a significantly higher, others a significantly lower temperature. Thereby some tubes' temperature could lie dangerously close to the worst case. If such a setting should be allowed, the control has to implement a stop-mechanism, by always also measuring the temperature at the heat exchanger. Yet controlling only with the information of the heat exchanger would encourage such a behavior, no longer avoiding the worst case, the HTF evaporating in some absorber tubes.

This control determines in each step the interval within which the control with mirrors would be exaggerated. Therefore, it is also interesting to see what happens when it is no longer possible to regulate within these bounds. The result for fast shadow introduction can be seen in Figure 37. Although the outflow temperature of 662.55 kelvin is about the same value as for the original defocus control, the absorber temperatures are all very close to the desired temperature. Collector row number 4 is with an amount of 661.19 kelvin still the worst, but nevertheless shows an improvement of 7 kelvin. Furthermore the computation of the simulation took only about half as long as the original control. As such a combination would be reasonable for practice. The constricted control leads to a convenient result, which the original control then adjusts to the optimum by small increments.
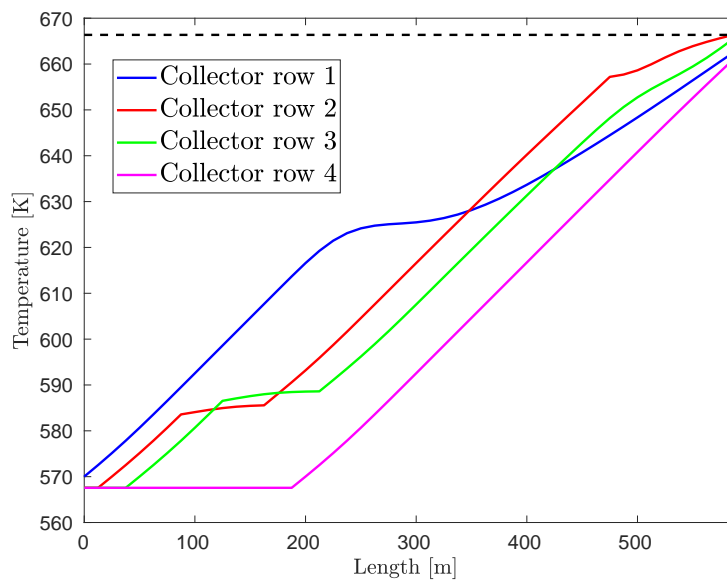
Figure 37: Results of a network with 4 tubes with mirror control with calculated defocus number, limited pump control and fast shadow introduction.

An alternative approach takes a closer look at the interaction between the pump flows of the individual pipes. One pipe, whose temperature is clearly too low, is prevented from making great improvements by the influence of the others. It is therefore conceivable that better results will be achieved if this is no longer possible. A too high temperature is therefore only controlled by defocusing the mirrors during the next variation. An additional change of the pump flow is no longer permitted. However, tests unfortunately show that oscillation cannot be contained with this strategy and that only the results shown in Figure 35 and 37 can be achieved.

In conclusion, it can be said that the dynamically used mirror control with calculated defocus number and limited effective interval delivers the best results. With an acceptable computing time, it is possible to reach the desired temperature up to about 4 kelvin without running the risk of the HTF evaporating. The discrepancy with Cherek's result is precisely due to this circumstance. The control avoids producing too high values. A mixed application in practice, with which Cherek's setting serves as the first working basis, which is further refined dynamically, is conceivable, as are small changes in the implementation in order to attenuate the oscillation or even eliminate it altogether.

7.3.2. Valve Control

Since the control of a solar thermal power plant with the help of mirrors and volumetric flow is already state-of-the-art, we are now going one step further. The analysis of mirror control for networks has already shown that the pump flow is regulated in general and cannot be adjusted according to the needs of the individual pipe. This is exactly where we come in and use the valves, that already exist at the inputs of the absorber pipes, for additional control. These valves are set to a fixed value once a year. Instead, we now use them to decouple the pipes from each other and to control the mass flow of the respective pipes separately (see Section 6.2). The test case as it is described in Figure 32 is still used for the following analysis of the valve control.

First of all, Cherek's valve control is applied to the test case, as this is again to serve as a reference value. As we already noticed in Section 7.2, Cherek's valve control cannot be performed for $\Delta t = 10$, nor for the actual velocity. A simulation that always uses the initial velocity and a Δt of $0.5\,\mathrm{s}$, with a simulation time of 25000 seconds, leads to the result shown in Figure 38. It can be clearly seen here that, with the help of the valves and the control of the pump flow, the exact desired temperature of 666.36 kelvin is reached in all absorber pipes and thus also for the mixing temperature. This optimal result can be achieved regardless of the speed at which the shadow is introduced in about 40 seconds. The control is so precise that the end temperatures do not deviate from the desired temperature even once during the simulation. Of course, optimal conditions are assumed in the test cases, at least regarding the control system. In practice, neither the valves nor the pump flow can be set to sufficient decimal places.
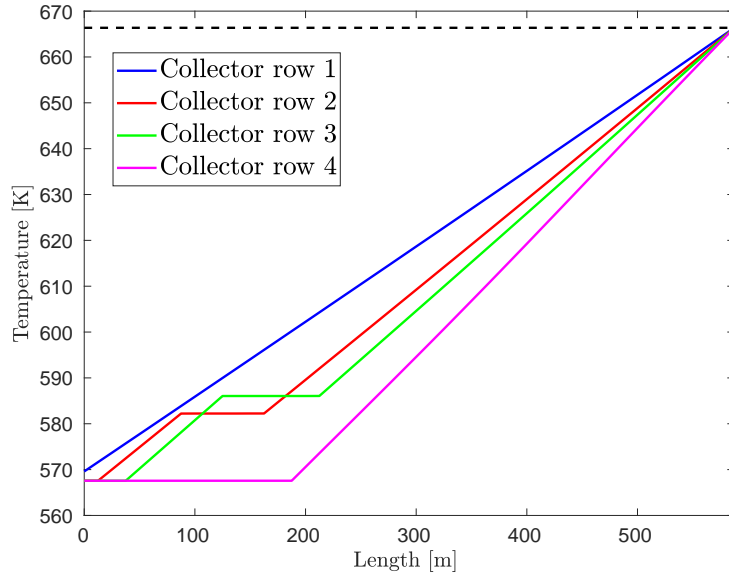
Figure 38: Results of a network with 4 tubes with Cherek's valve control and fast shadow introduction. In this simulation the stepsize in time is $\Delta t = 0.5\,\mathrm{s}$.

The following simulations will again be performed with $\Delta t = 10$ and a simulation time of 25000 seconds. Furthermore, analogously to the mirror control, the control's range of action can be regulated by the parameters g and $\tilde{g}$. The initial setting of those parameters will be $g = 3$ and $\tilde{g} = 5$.

Control with simplifications of the source term

As the calculations with the simplified control are imprecise, it is not surprising that this control does not have the accuracy of Cherek's control. The mixing temperature of 667.42 kelvin is about $1\,\mathrm{K}$ above the desired temperature. The temperatures of the pipes 1, 2 and 4 are 666 kelvin, but in the decimal places they are above the desired temperature. Pipe 3 on the other hand is 669.61 kelvin, which is much higher, so that the mixing temperature is larger. Due to inaccurate calculations caused by simplification, the temperature at the end of the absorber tubes fluctuates. During simulation, the temperature fluctuates so much that one pipe comes dangerously close to evaporation by reaching 672 kelvin. The entire simulation process took about 160 seconds.
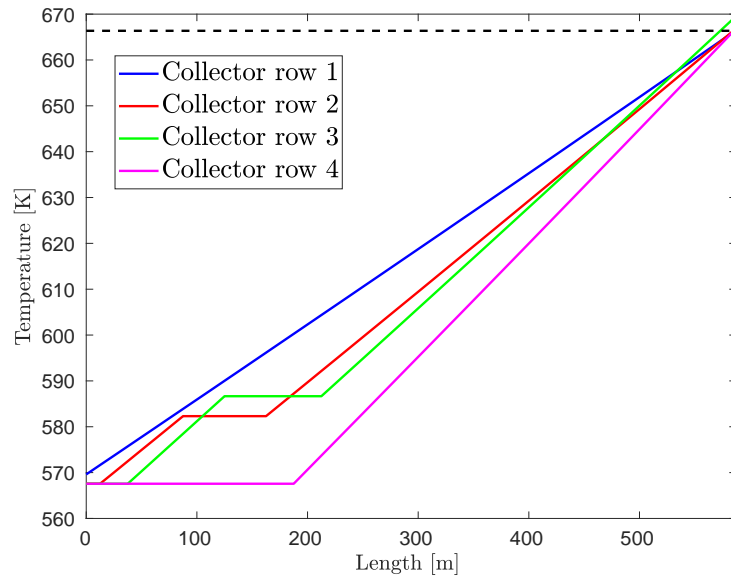
Figure 39: Results of a network with 4 tubes with simplified valve control and fast shadow introduction.

The simplified valve control behaves in the same way as the other controls before, when facing slower shadows. However, the result is only slightly better: The mixing temperature deviates by 0.2 kelvin, because the temperature of the third absorber tube is 0.5 kelvin colder than before. The fluctuation is also about $2\,\mathrm{K}$ lower. The calculation time of 60 seconds, on the contrary, is less than half of the time.
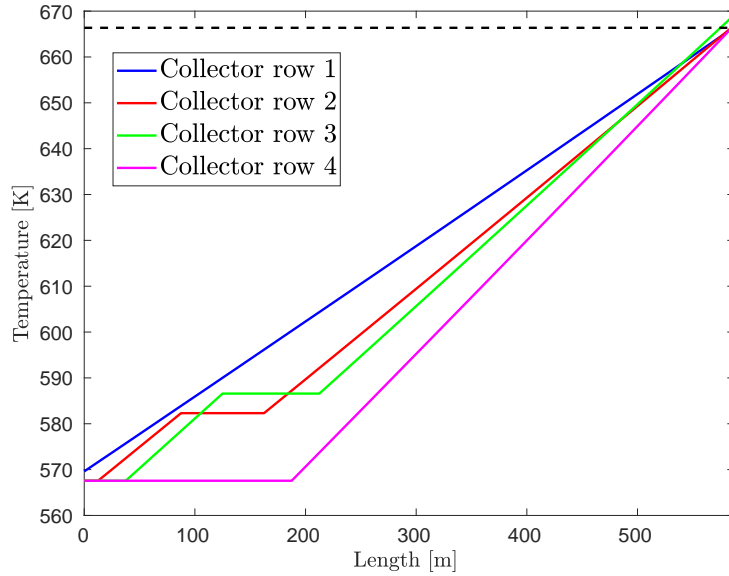
Figure 40: Results of a network with 4 tubes with simplified valve control and slow shadow introduction.

Since the simplified control obviously has strong weaknesses, we will analyze the less simplified control and its simulation results, as earlier with the mirror control.

Control with less simplification

Although the plot of the simulation result of the less simplified control for fast shadow hardly seems to differ from the results of the simplified control, the control is considerably better. The mixed temperature deviates only by $0.5\,\mathrm{K}$, but is also up to $0.6\,\mathrm{K}$ at the desired temperature. It is astonishing that the tubes 1, 2 and 4 reach the desired temperature, but tube 3 still deviates by about $2\,\mathrm{K}$. This circumstance is even more astonishing when one considers that the control has already been completed before the simulation time has elapsed. To be able to analyze this further, we include the valve position and the mass flow in the analysis and compare them with the values from Cherek. Despite the fact that, without further in-depth analysis of Cherek's control, it is inexplicable how it comes to the result shown in Figure 38, it is a valid and optimal configuration.

Now it becomes clear why the control could not be further improved: While the valves of pipes 1, 2 and 4 are $60 - 90\%$ open, the valve of the third pipe is already fully open. Since the other values are already optimal, they are no longer changed.
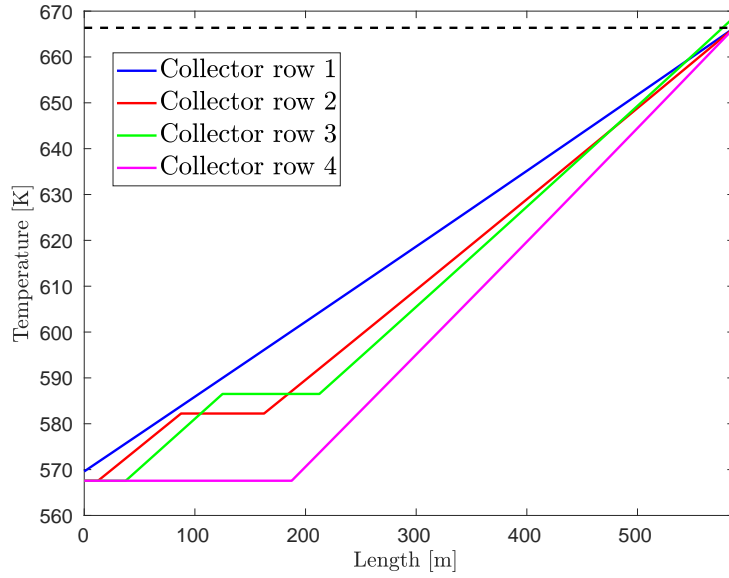
Figure 41: Results of a network with 4 tubes with less simplified valve control and fast shadow introduction.

Thus the question arises why the control does not try to adjust the volume flow for this pipe as well, since changes to the valve position are no longer possible. The comparison with the values of Cherek's control shows that these are already quite good. The valve positions here are all about $60 - 80\%$ and the mass flow with $18.11\,\mathrm{m^3/s}$ is only $0.17\,\mathrm{m^3/s}$ higher than the control discussed here. The fourth pipe could not be adjusted any further, because the parameter $g = 3$ specifies that it is only intervened from a deviation of $3\,\mathrm{K}$. We will now examine whether the setting $g = 0$ and $\tilde{g} = 0$ is sufficient to achieve the same result as Cherek's control.
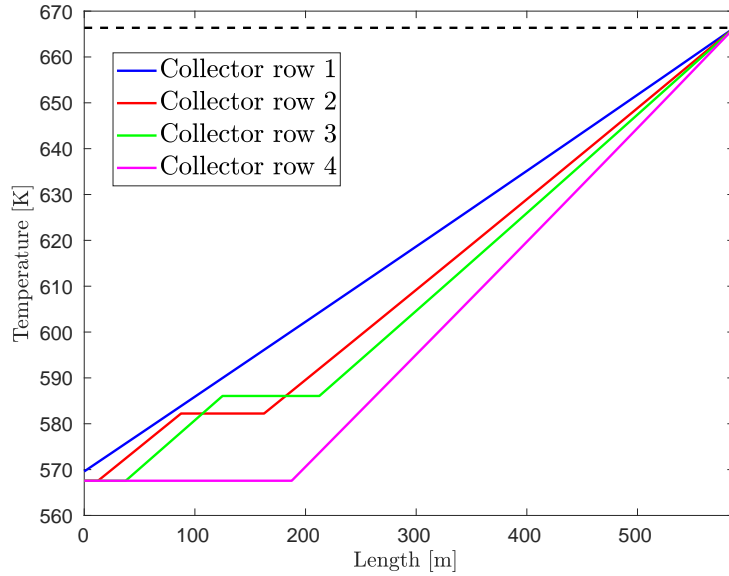
Figure 42: Results of a network with 4 tubes with less simplified valve control and fast
shadow introduction.
The control can react on every deviation since $g = 0$ and $\tilde{g} = 0$.

The Figure 42 proves, that with the new setting the valve control manages to reach an optimal state. All end temperatures of the collector rows and the temperature of the HTF entering the heat exchanger are exactly 666.36 kelvin. The simulation took 1179.93 seconds and the final setting was found before half the simulation time was over. Still, the aperture of the valves differ from the result of Cherek. This is probably because the control is approaching from a different configuration. There is therefore not only one optimum but several local optima. Which one is found depends on which configuration was previously applied by the control changes.

As all simulations for the less simplified control have been performed with direct shadow, the control configured with both parameters g and $\tilde{g}$ set to zero is finally also performed for slowly emerging shadow. We expect that a local optimum can be found again. It is interesting to see whether it is a different optimum and how the computing time behaves.
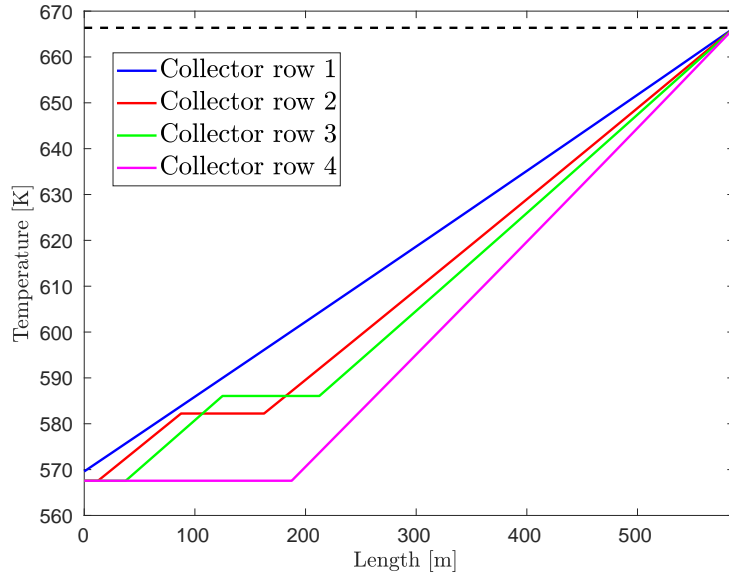
Figure 43: Results of a network with 4 tubes with less simplified valve control and slow
shadow introduction.
The control can react on every deviation since $g = 0$ and $\tilde{g} = 0$.

As expected, the valve control can also react better to slow shadows than to fast ones.
The control creates an optimum again, actually even the same optimum that was cre-
ated for fast shadows in the same time. However, there still seems to be a discrepancy
in the decimal places, because the mixing temperature is only 666.28 kelvin. But since
the settings are not exactly possible in practice anyway, this is basically still an opti-
mal value. Especially noticeable is the big difference in the fluctuation range during
the simulation. While with fast shadows the temperature of the HTF can reach 672.6
kelvin, the temperature is now only in the range of 665.5 to 666.7 kelvin.

7.3.3. General improvements

Since the control of a single tube is already very good, these improvements will relate
exclusively to simulation for networks.
As we just saw for valve control, the choice of the parameters g and $\tilde{g}$, which determine
the temperature difference that is accepted before the control reacts, is very important.
Figure 44 shows, that with the choice of $g = 0$ and $\tilde{g} = 0$ even the less simplified mirror
control can reach nearly optimal results.
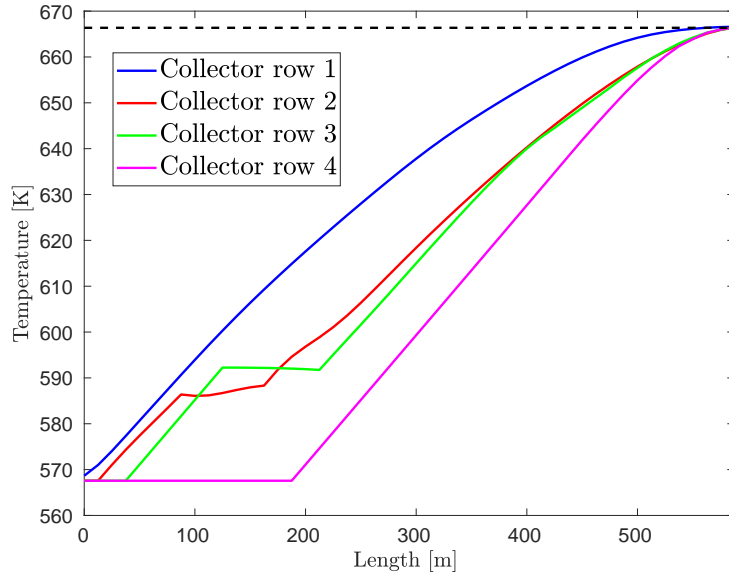
Figure 44: Results of a network with 4 tubes with less simplified mirror control and fast shadow introduction.
The control can react on every deviation since $g = 0$ and $\tilde{g} = 0$.

Nevertheless, it must be stressed once again that it is not practicable to intervene at every so small deviation or to avoid measurement inaccuracies and to implement the control perfectly. Therefore, with a view to improvements, other approaches should be explored. One such possibility is to make the calculations of the model more accurate by applying a second order upwind scheme instead of first order. It uses the values of the two previous cells to calculate the current value. In the following, this is done as an example for the less simplified mirror control.

The upwind scheme of the second order cannot be carried out with this composition of parameters, because the control tends to override. Therefore use $\Delta t = 0.5\,\mathrm{s}$. In order to still be able to compare with the results above, the simulation time must also be adjusted to execute as many steps as before. Therefore, the following applies to this simulation run:

$$\Delta t = 0.5\,\mathrm{s} \quad \text{and} \quad simulation\ time = 1250\,\mathrm{s} \tag{95}$$

The corresponding result is shown in Figure 45.
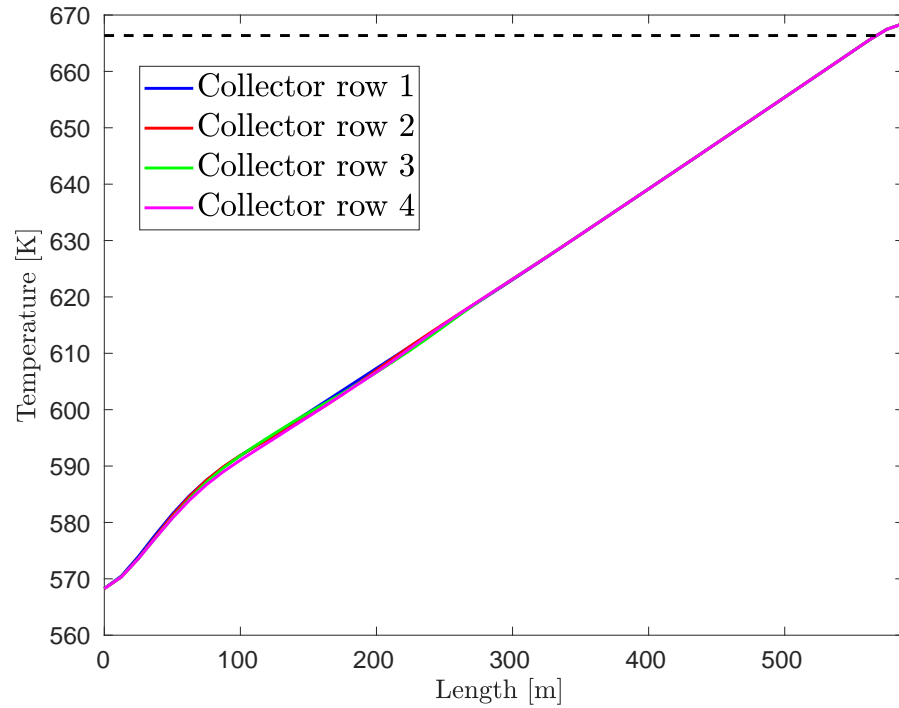
Figure 45: Results of a network with 4 tubes with less simplified mirror control and slow shadow introduction.
The control parameters are $g = 1$ and $\tilde{g} = 3$.
The temperature calculations are performed with an upwind scheme of second order and a simulation time of 1250 seconds.
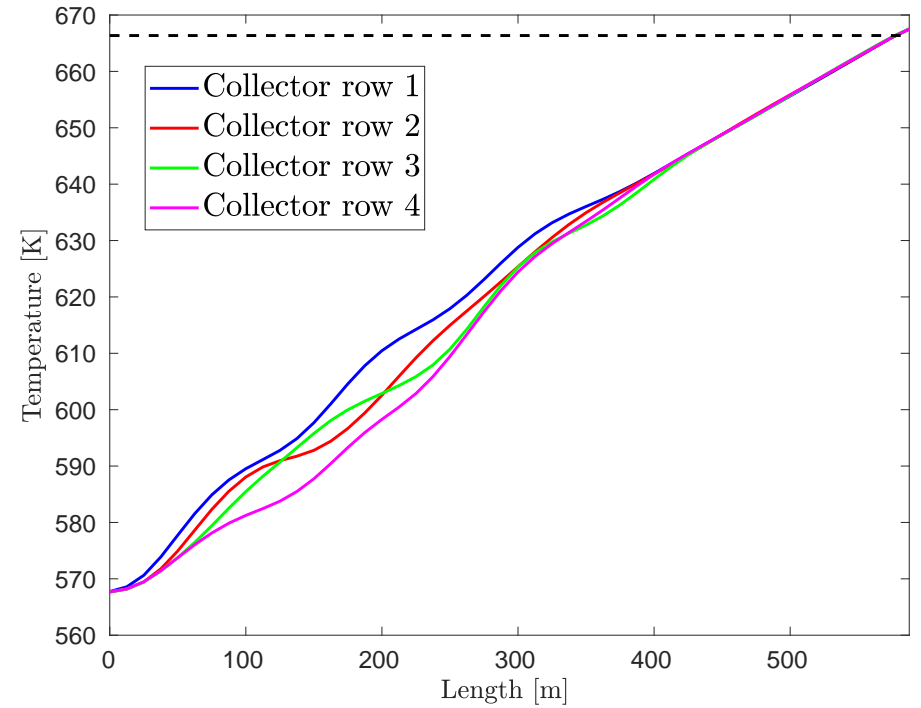
Figure 46: Results of a network with 4 tubes with less simplified mirror control and slow shadow introduction.
The control parameters are $g = 1$ and $\tilde{g} = 3$.
The temperature calculations are performed with an upwind scheme of second order and a simulation time of 5000 seconds.

However, this type of improvement should only be applied if sufficient computing power is available, since the hardly meaningful simulation run in Figure 45 already took about 670 seconds. This is due to the more precise calculations. Even a computing time of almost 11 hours is not yet sufficient to deliver meaningful results (see Figure 46). Compared to the about 390 seconds, which are needed by the same control with the upwind of first order to deliver useful results, this is a very clear difference. Apart from the enormously higher computation time, the increased accuracy of the second order upwind method makes the oscillation more clearly visible.

Depending on the desired ratio of accuracy and size of the calculation time, a further analysis of the settings of the parameters β, g and $\tilde{g}$ can also influence the results. The values selected in this thesis are already selected for accuracy.
Furthermore, the parameter m can be used to specify that the control must not react to every change of the weather conditions, but only to all $\frac{m}{\Delta t}$ steps.

Apart from the calculations within the model and the parameters mentioned above, the predictive control approach underlying all controls also offers an opportunity for improvement.
So far, the temperature is calculated 15000 seconds into the future, assuming that the weather conditions remain as they are at that time. In the following, we will analyze the influence of how far into the future the calculations reach. For this purpose we choose a predictive time horizon much smaller with *predictive time* = 5000 seconds. Instead of about 4 hours, the prediction only reaches 1.4 hours into the future.
The parameters are then no longer suitable for mirror control. For the better mirror control with N_{defocus} the result is shown in Figure 47. Compared to the simulation run with *predictive time* = 15000 seconds, this result is $2\,\text{K}$ better. However, this can also be due to oscillation. Yet, what is striking, is that the computing time of 141.32 seconds is almost only one tenth. Therefore, depending on the control selected, a shorter predictive time is sufficient to achieve good results. A too long predictive time can even lead to an overdrive.
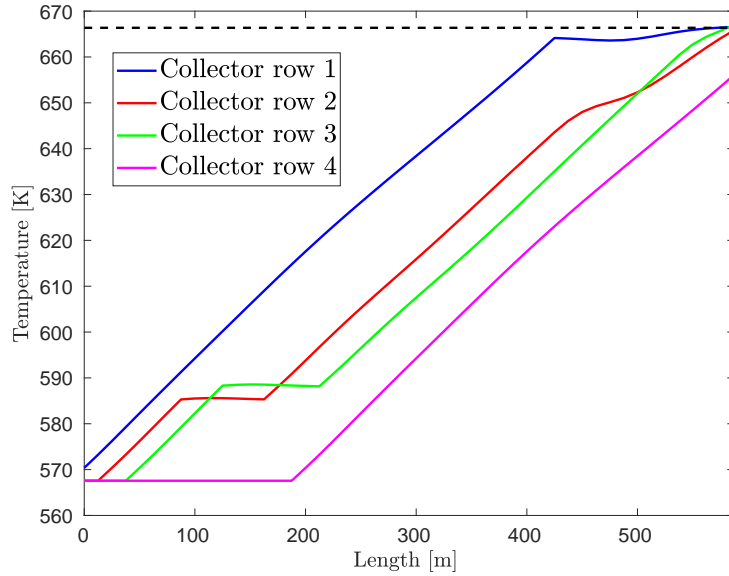
Figure 47: Results of a network with 4 tubes with mirror control with calculated defocus number and slow shadow introduction.

Finally, we consider the possibility of weather forecast. Some solar thermal systems already have cameras at the corners of the collector field that can detect the clouds outside the collector field. Based on the data they collect, it is then possible to make an approximate statement as to when the collector field will be overshadowed and how. A suspected side effect is that the use of weather forecasting avoids overdriving when the predictive time is too long.

Since the following analysis serves only the purpose of finding out how big the influence of this information is, we assume that the predicted weather course corresponds exactly with the actual one.

The mentioned laptop is no longer able to run the simulations with weather forecast. Therefore the following data has been created on the server of the Institute of Geometrical and Practical Mathematics (IGPM). There, 16 GB RAM and an Intel(R) Core(TM) i7-4790 processor with CPU @ 3.60 GHz are available.
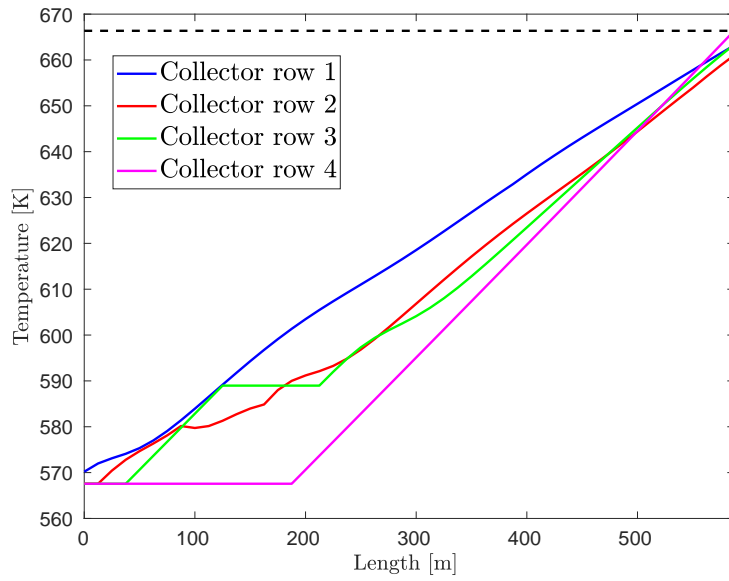
Figure 48: Results of a network with 4 tubes with mirror control, weather forecast and fast shadow introduction.
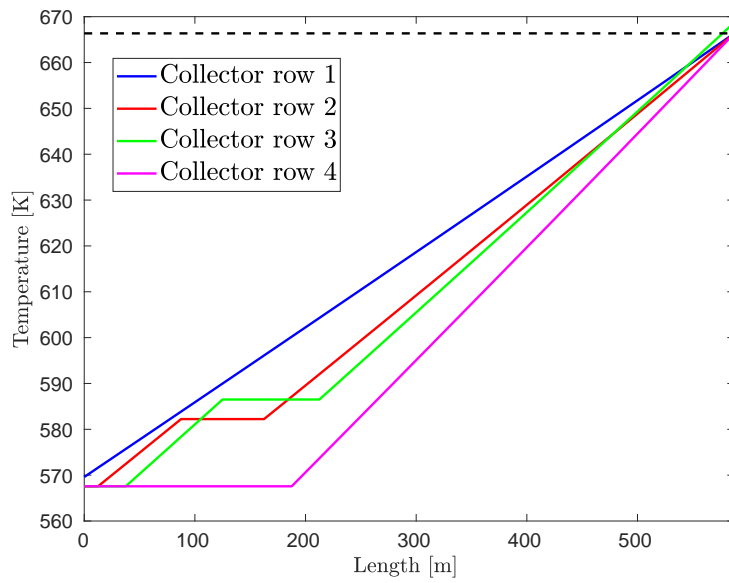
Figure 49: Results of a network with 4 tubes with valve control, weather forecast and slow shadow introduction.

Contrary to expectations, the use of the weather forecast does not bring any improvement. The results are the same and the calculation time is still higher. Nevertheless, this approach should not be rejected directly, as it could still bring an advantage over the exact test conditions here when used in combination with the real conditions.

In practice, different fluids are used, for example molten salt. However, since other fluids for control purposes are only changed parameters, the controllers discussed here can always be used provided the corresponding data such as density and specific heat capacity are available. This assertion is confirmed by a selection of simulations carried out in the appendix using molten salt, as these show the same behavior as has already been described in detail for oil. Only the control parameters have to be adjusted accordingly for the respective fluid (see Table A.6).

8. Conclusion

The objective of this thesis was to implement a state-of-the-art dynamic control for solar thermal power plants with parabolic troughs, based on Cherek's achievements in his Bachelor thesis. This control is the here considered mirror control. The dynamic application has been proved in Section 7.

Furthermore, the work aimed at developing an extended control with the help of valves, the valve control considered here. This control can also be used dynamically. In addition, both controls take the predictive approach into account in order to compensate for the delay in measurement, regulation and effect in the system. These controls, developed theoretically in Section 4 - 6, were then extensively tested and analyzed in several variations.

These tests are based on real data from the solar thermal power plant La Africana in Spain. Therefore, it can be summarized that the controls developed in this thesis are very efficient not only theoretically, but also in practical applications. The dynamic application makes it possible to regulate in real time. The predictive approach not only improves reaction time but also allows the control of every possible composition of light and shadow. Instead of only providing a guideline for specific cases, control can react to any weather situation when the appropriate information is given. Since a comparison with Cherek's data is not possible, we compare the mirror control with N_{defocus} and the valve control with each other instead. The comparison of the mass flows shows that the valve control generates about 20% more heated fluid. In addition, the mirror control does not reach the desired temperature. Therefore, the exact difference in produced power will be even greater. Moreover, the calculations could be carried out clearly beneath real time, so that the control can easily be maintained in practice. All in all, the control presented in this thesis is a dynamic, efficient improvement over the state-of-the-art control used so far.

Outlook

Since in practice it is not possible to adjust the valves as precisely as is necessary in the course of the simulations mentioned here, the next step is to realize the so-called sliding shutter valves. This would be possible via a kind of staircase function that represents the valve setting. Other small changes would be the use of an adaptive grid and the calculation of the mixing temperature using the Richmann formula. In general, it would be conceivable to revise the model or the implementation with regard to parallelization.

The type of application of this control depends ultimately on the maximum permitted computing time. The control is dynamic but if the calculation time is still considered too high, it is nevertheless very useful as a guideline for a look-up table. An excessive parameter study, concerning the parameters β and Δt might even find parameter settings, that are able to produce even better results, as wrong chosen parameters can result in a difference of several hours in computation time. Based on a different model, this type of control could possibly also provide correspondingly different results.

A. Appendix

The scope of a master thesis is not sufficient to execute and compare all simulations. Even this appendix can only represent a small part. It serves to provide results that were only mentioned in the thesis with the corresponding data and plots. In addition, the results are extended by the application case of molten salt, because molten salt as HTF was also part of the theoretical considerations.

In the following, the basic settings are summarized once again. Variations are always noted in the corresponding tables and figures.

Quantity	Value
Inner diameter of the absorber tube	$0.07\,\mathrm{m}$
Inner diameter of the header tube	$0.1\,\mathrm{m}$
Length of the header tube	$200\,\mathrm{m}$
Number of mirrors per collector row	48
Length of a mirror	$12.5\,\mathrm{m}$
Length of the absorber tube	$600\,\mathrm{m}$
Mirrors aperture	$5.45\,\mathrm{m}$
Global mirror efficiency	0.75
Global thermodynamic efficiency	0.7
Irradiation per area	$843.5\,\mathrm{W\,m^{-2}}$
Inflow temperature	$567.57\,\mathrm{K}$

Table A.1: Parameters for the matlab implementation of the test cases representing the power plant La Africana.

Due to the typical structure of a solar thermal power plant (see Figure 1) the following arrangement is given.

Test case	single row	network
number absorbers	1	4
number sections	3	12
number junctions	2	8

Table A.2: Structure of the two considered test cases.

Moreover, the following applies to the heat transfer fluid Therminol VP1:

Therminol VP1	
minimal temperature	$353.2\,\mathrm{K}$
maximal temperature	$673.2\,\mathrm{K}$
desired temperature	$666.36\,\mathrm{K}$

Table A.3: Temperature boundaries of Therminol VP1.

Further properties of Therminol VP1 are
Density:

$$\rho(T) = -0.90797\,(T - 273.15) + 0.00078116\,(T - 273.15)^2$$
$$- 2.367 \cdot 10^{-6}\,(T - 273.15)^3 + 1083.25$$

and

Specific heat capacity:

$$c_{\mathrm{v}}(T) = (0.002414\,(T - 273.15) + 5.9591 \cdot 10^{-6}\,(T - 273.15)^2$$
$$- 2.9879 \cdot 10^{-8}\,(T - 273.15)^3$$
$$+ 4.4172 \cdot 10^{-11}\,(T - 273.15)^4 + 1.498) \cdot 10^3\,,$$

illustrated below (also compare Figures 4a and 4b).
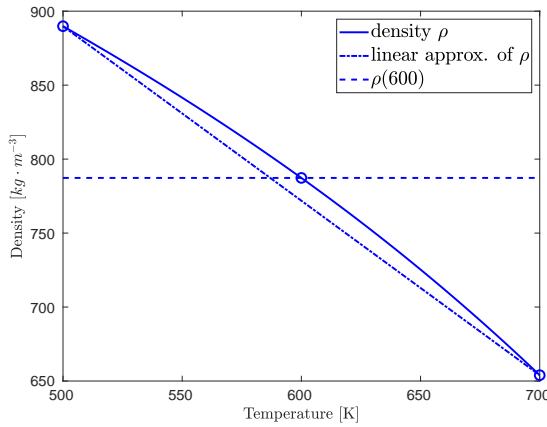
Figure A.1: Therminol VP1: Density in dependency of temperature.
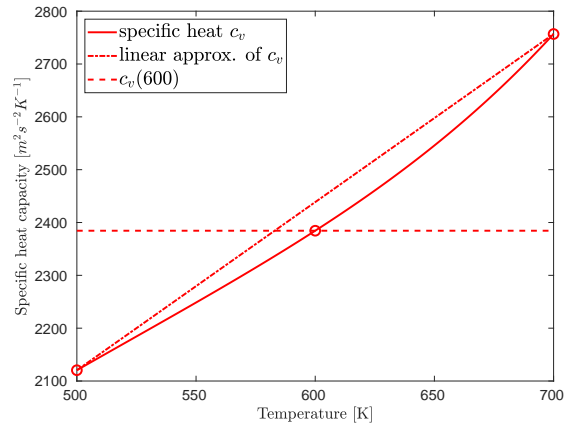
Figure A.2: Therminol VP1: Specific heat capacity.

On the other hand, the following holds for the temperature of molten salt

Molten Salt (NaNO$_3$-NaNO$_2$-KNO$_3$)	
minimal temperature	523.2 K
maximal temperature	710 K
desired temperature	703.15 K

Table A.4: Temperature boundaries for Molten Salt.

And the properties are for Molten Salt given via

Density:

$$\rho(T) = 2293.6 - 0.7497T$$

and

Specific heat capacity:

$$c_{\mathrm{v}}(T) = 5806 - 10.833T + 7.2413 \cdot 10^{-3}T^2 \ ,$$

again illustrated below (compare Figures 5a and 5b).
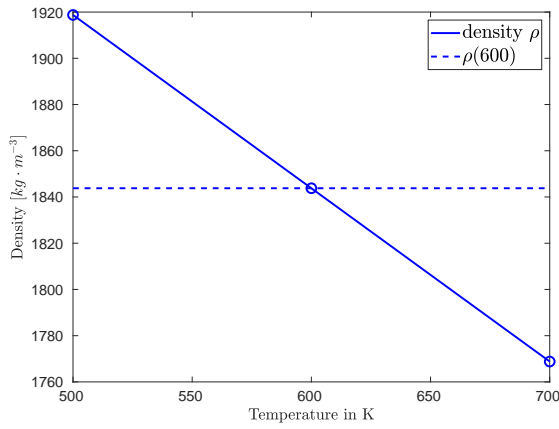
Figure A.3: Molten Salt: Density in dependency of temperature.
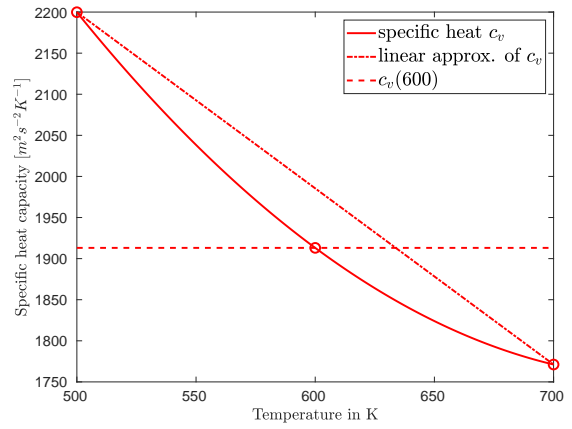
Figure A.4: Molten Salt: Specific heat capacity.

Unless otherwise stated, the following settings apply to all simulations:

Simulation parameters	
simulation time	$25\,000\,\mathrm{s}$
waiting time w	$5\,\mathrm{s}$
predictive time	$15\,000\,\mathrm{s}$
steps for irradiation change	5000

Table A.5: Simulation parameters.

In addition, depending on the heat transfer fluid used, it holds:

	Therminol VP1	**Molten Salt**
stepsize in time Δt	10 s	25 s *
operational stepsize	10 s	25 s
weight β	$10^9/3.7486$	$10^{11}/3.7486$

Table A.6: Additional parameters, depending on the fluid.

To enable a comparison of the computing times, all simulations were performed on a Lenovo Thinkpad X230 with 4 GB RAM and an Intel(R) Core(TM) i7-3520M processor with CPU @ 2.90 GHz.

However, since this device cannot handle the vast amount of calculations required to perform weather forecasting, those simulations were executed on the institute's server with 16 GB RAM and an Intel(R) Core(TM) i7-4790 processor with CPU @ 3.60 GHz.

---

*For molten salt and a single pipe a Δt of 80 s would be sufficient. In the case of a network, however, other velocities occur, so that a Δt of 25 s can be realized at most. This value is therefore used, in order to keep the settings consistent.

A.1. Single Tube - Therminol VP1

Simplified Pump Control
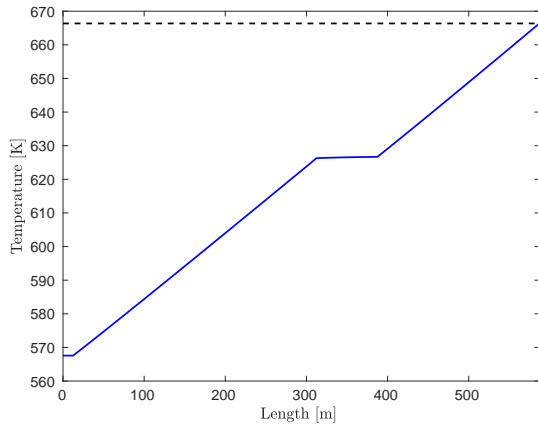

Figure A.1.1: Result of the simplified pump control with fast shadow introduction for a single tube.

Simplified Pump Control - Fast Shadow -	
end temp. absorber tube	666.45 K
temp. at heat exchanger	666.96 K
maximal temp.	671.02 K
mass flow	4.81 m^3s^{-1}
computational time	90.64 s
finished after	-

Table A.1.1: Data corresponding to the simulation of the simplified pump control with fast schadow introduction for a single tube.
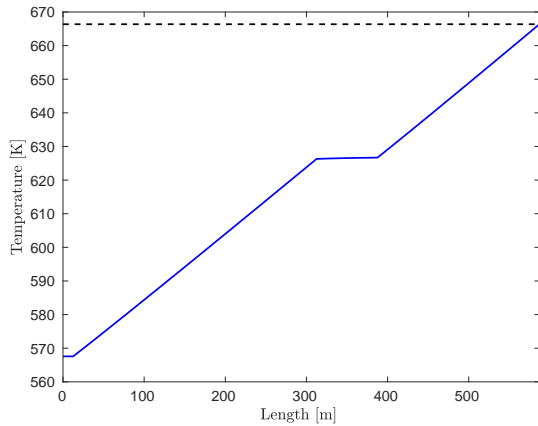

Figure A.1.2: Result of the simplified pump control with slow shadow introduction for a single tube.

Simplified Pump Control - Slow Shadow -	
end temp. absorber tube	666.45 K
temp. at heat exchanger	666.96 K
maximal temp.	667.5 K
mass flow	4.81 m^3s^{-1}
computational time	92.83 s
finished after	-

Table A.1.2: Data corresponding to the simulation of the simplified pump control with slow schadow introduction for a single tube.
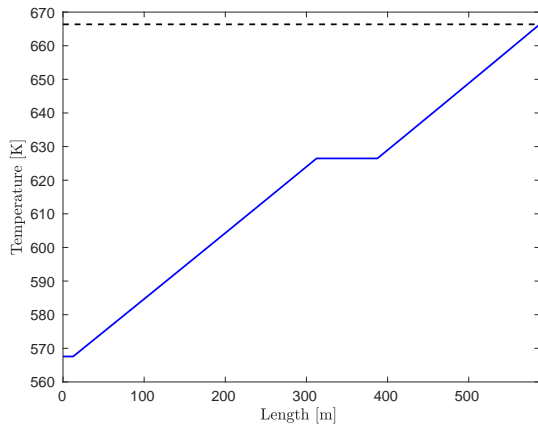
Pump Control

Figure A.3: Result of the pump control with fast shadow introduction for a single tube.

Pump Control - Fast Shadow -	
end temp. absorber tube	666.36 K
temp. at heat exchanger	666.36 K
maximal temp.	670.84 K
mass flow	4.60 $m^3 s^{-1}$
computational time	250.01 s
finished after	-

Table A.3: Data corresponding to the simulation of the pump control with fast schadow introduction for a single tube.
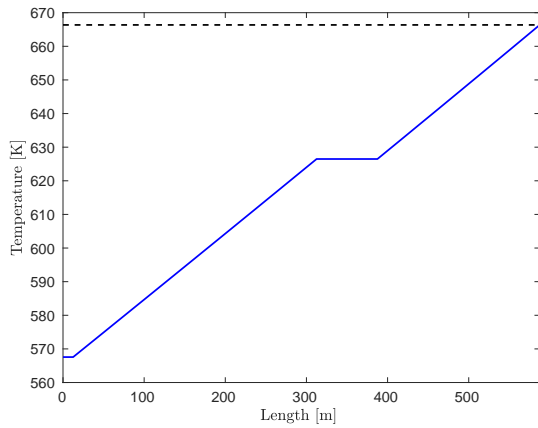
Figure A.4: Result of the pump control with slow shadow introduction for a single tube.

Pump Control - Slow Shadow -	
end temp. absorber tube	666.36 K
temp. at heat exchanger	666.36 K
maximal temp.	666.93 K
mass flow	4.60 $m^3 s^{-1}$
computational time	249.06 s
finished after	-

Table A.4: Data corresponding to the simulation of the pump control with slow schadow introduction for a single tube.

Simplified Mirror Control
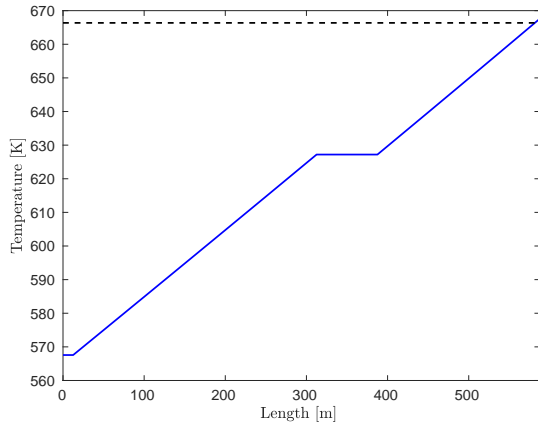
Figure A.5: Result of the simplified mirror control with fast shadow introduction for a single tube.

Simplified Mirror Control - Fast Shadow -	
g	3
$\tilde{g}$	5
end temp. absorber tube	667.58 K
temp. at heat exchanger	667.58 K
maximal temp.	669.37 K
mass flow	4.53 $m^3 s^{-1}$
computational time	12.61 s
finished after	-
defocused mirrors	-

Table A.5: Data corresponding to the simulation of the simplified mirror control with fast schadow introduction for a single tube.
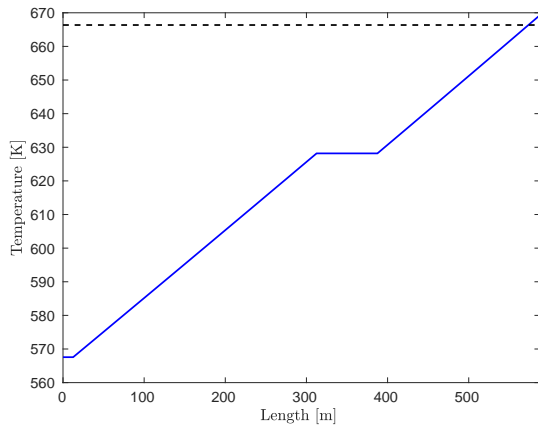

Figure A.6: Result of the simplified mirror control with slow shadow introduction for a single tube.

Simplified Mirror Control - Slow Shadow -	
g	3
$\tilde{g}$	5
end temp. absorber tube	669.24 K
temp. at heat exchanger	669.24 K
maximal temp.	669.24 K
mass flow	4.45 $m^3 s^{-1}$
computational time	6.83 s
finished after	-
defocused mirrors	-

Table A.6: Data corresponding to the simulation of the simplified mirror control with slow schadow introduction for a single tube.
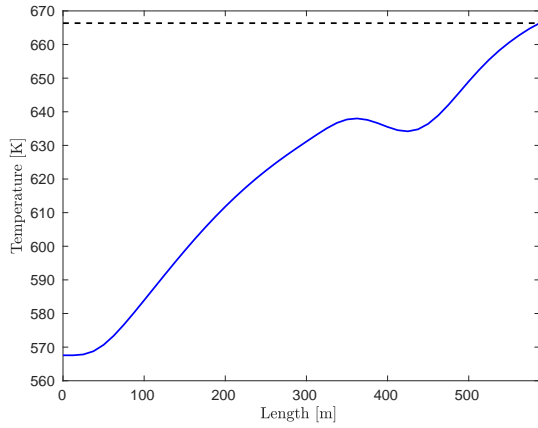
Figure A.7: Result of the simplified mirror control with fast shadow introduction for a single tube.

Simplified Mirror Control - Fast Shadow -	
g	1
$\tilde{g}$	3
end temp. absorber tube	666.37 K
temp. at heat exchanger	666.86 K
maximal temp.	669.18 K
mass flow	0.44 $m^3 s^{-1}$
computational time	32.23 s
finished after	-
defocused mirrors	48

Table A.7: Data corresponding to the simulation of the simplified mirror control with fast schadow introduction for a single tube.
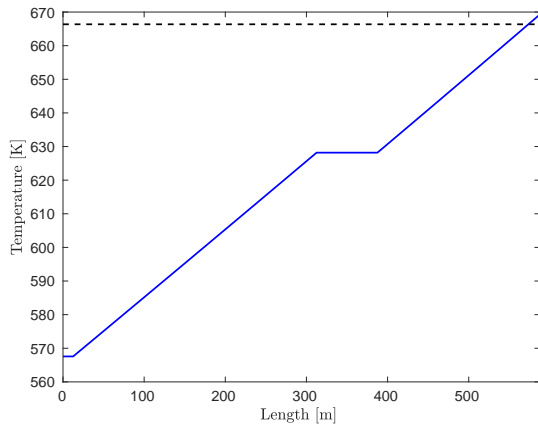

Figure A.8: Result of the simplified mirror control with slow shadow introduction for a single tube.

Simplified Mirror Control - Slow Shadow -	
g	1
$\tilde{g}$	3
end temp. absorber tube	666.98 K
temp. at heat exchanger	666.47 K
maximal temp.	667.46 K
mass flow	4.43 $m^3 s^{-1}$
computational time	5.88 s
finished after	-
defocused mirrors	1

Table A.8: Data corresponding to the simulation of the simplified mirror control with slow schadow introduction for a single tube.
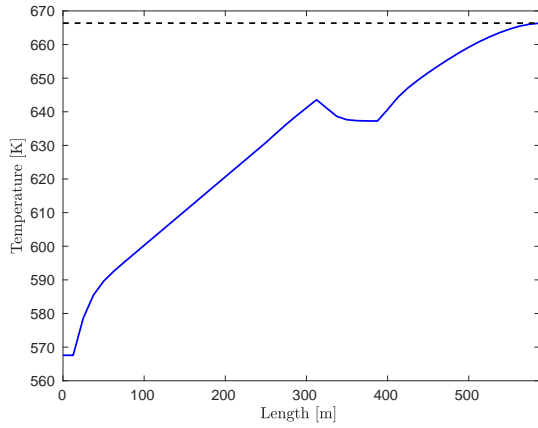
Figure A.9: Result of the simplified mirror control with fast shadow introduction for a single tube.

Simplified Mirror Control - Fast Shadow -	
g	0
$\tilde{g}$	0
end temp. absorber tube	666.35 K
temp. at heat exchanger	666.3 K
maximal temp.	666.53 K
mass flow	0.11 $m^3 s^{-1}$
computational time	46.86 s
finished after	-
defocused mirrors	27

Table A.9: Data corresponding to the simulation of the simplified mirror control with fast schadow introduction for a single tube.
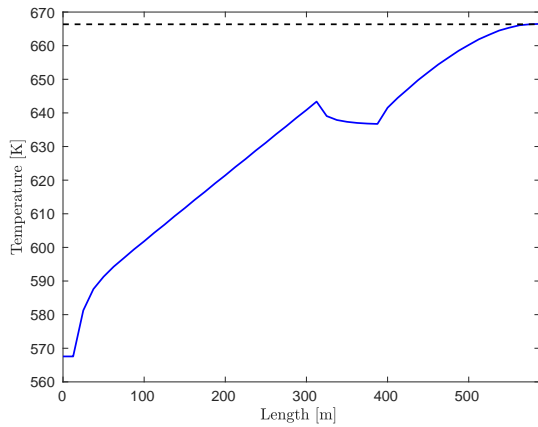
Figure A.10: Result of the simplified mirror control with slow shadow introduction for a single tube.

Simplified Mirror Control - Slow Shadow -	
g	0
$\tilde{g}$	0
end temp. absorber tube	666.48 K
temp. at heat exchanger	666.32 K
maximal temp.	666.53 K
mass flow	0.22 $m^3 s^{-1}$
computational time	47.98 s
finished after	-
defocused mirrors	48

Table A.10: Data corresponding to the simulation of the simplified mirror control with slow schadow introduction for a single tube.
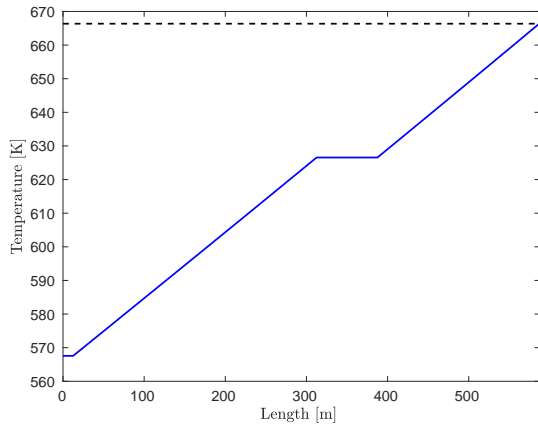
Mirror Control

Figure A.11: Result of the mirror control with fast shadow introduction for a single tube.

Mirror Control - Fast Shadow -	
g	3
$\tilde{g}$	5
end temp. absorber tube	666.49 K
temp. at heat exchanger	666.49 K
maximal temp.	669.36 K
mass flow	4.59 $m^3 s^{-1}$
computational time	30.49 s
finished after	-
defocused mirrors	-

Table A.11: Data corresponding to the simulation of the mirror control with fast schadow introduction for a single tube.


Figure A.12: Result of the mirror control with slow shadow introduction for a single tube.

Mirror Control - Slow Shadow -	
g	3
$\tilde{g}$	5
end temp. absorber tube	668.19 K
temp. at heat exchanger	668.19 K
maximal temp.	668.19 K
mass flow	4.50 $m^3 s^{-1}$
computational time	38.25 s
finished after	-
defocused mirrors	-

Table A.12: Data corresponding to the simulation of the mirror control with slow schadow introduction for a single tube.
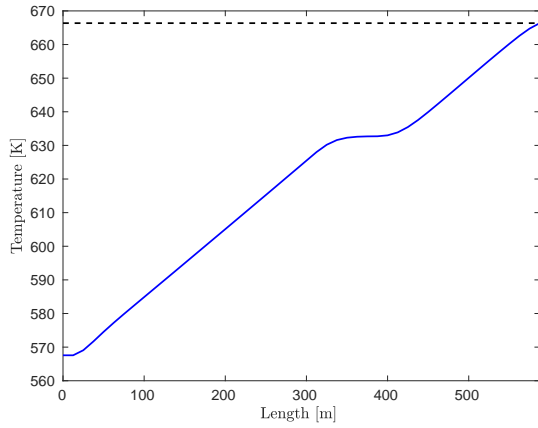
Figure A.13: Result of the mirror control with fast shadow introduction for a single tube.

Mirror Control - Fast Shadow -	
g	1
$\tilde{g}$	3
end temp. absorber tube	666.36 K
temp. at heat exchanger	666.61 K
maximal temp.	668.13 K
mass flow	0.15 $m^3 s^{-1}$
computational time	95.22 s
finished after	-
defocused mirrors	48

Table A.13: Data corresponding to the simulation of the mirror control with fast schadow introduction for a single tube.
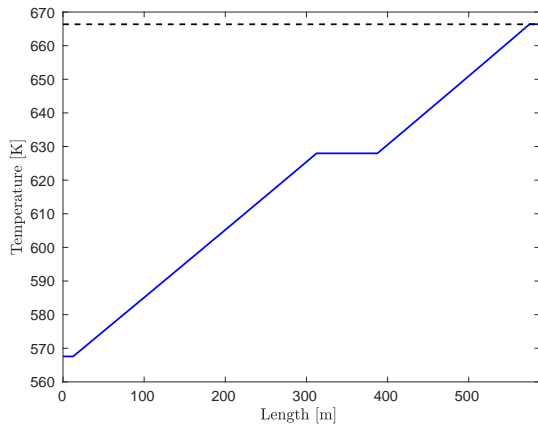
Figure A.14: Result of the mirror control with slow shadow introduction for a single tube.

Mirror Control - Slow Shadow -	
g	1
$\tilde{g}$	3
end temp. absorber tube	666.39 K
temp. at heat exchanger	666.38 K
maximal temp.	667.45 K
mass flow	4.49 $m^3 s^{-1}$
computational time	38.96 s
finished after	-
defocused mirrors	1

Table A.14: Data corresponding to the simulation of the mirror control with slow schadow introduction for a single tube.
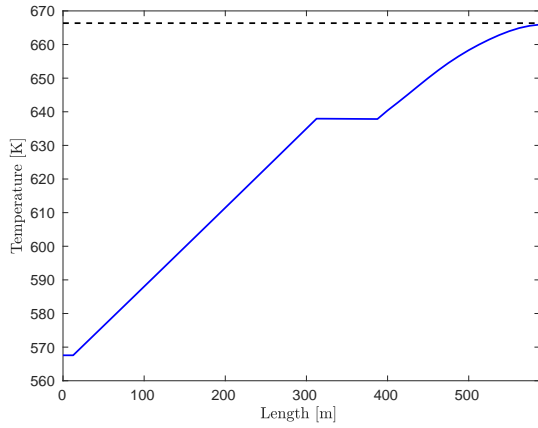
Figure A.15: Result of the mirror control with fast shadow introduction for a single tube.

Mirror Control - Fast Shadow -	
g	0
$\tilde{g}$	0
end temp. absorber tube	665.93 K
temp. at heat exchanger	666.32 K
maximal temp.	666.53 K
mass flow	3.85 m^3s^{-1}
computational time	162.37 s
finished after	-
defocused mirrors	-

Table A.15: Data corresponding to the simulation of the mirror control with fast schadow introduction for a single tube.
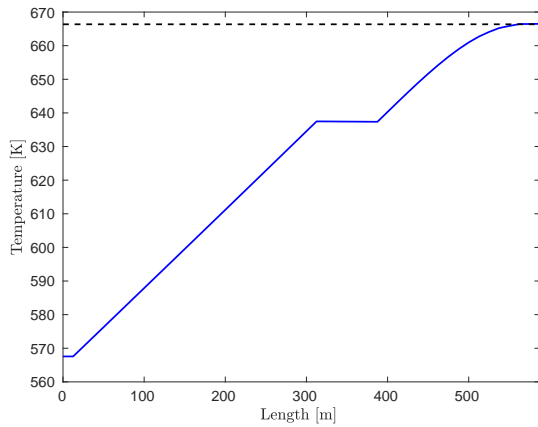
Figure A.16: Result of the mirror control with slow shadow introduction for a single tube.

Mirror Control - Slow Shadow -	
g	0
$\tilde{g}$	0
end temp. absorber tube	666.49 K
temp. at heat exchanger	666.32 K
maximal temp.	666.53 K
mass flow	3.87 m^3s^{-1}
computational time	170.67 s
finished after	-
defocused mirrors	6

Table A.16: Data corresponding to the simulation of the mirror control with slow schadow introduction for a single tube.

96

## Mirror Control with slowly moving mirrors
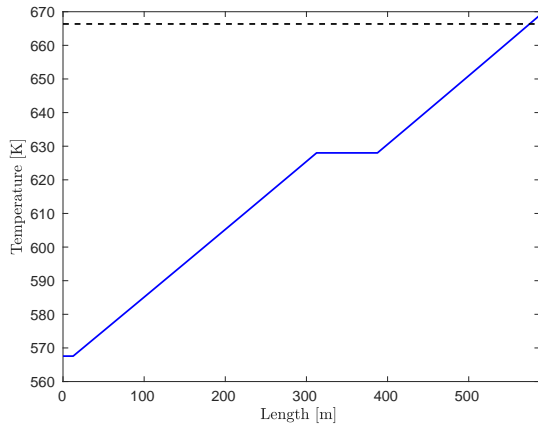
Figure A.17: Result of the mirror control with slowly defocused mirrors and fast shadow introduction for a single tube.

Mirror Control with slow Mirrors - Fast Shadow -	
g	3
$\tilde{g}$	5
end temp. absorber tube	668.94 K
temp. at heat exchanger	668.94 K
maximal temp.	669.47 K
mass flow	4.46 $m^3 s^{-1}$
computational time	31.78 s
finished after	-
defocused mirrors	-

Table A.17: Data corresponding to the simulation of the mirror control with slowly defocused mirrors and fast schadow introduction for a single tube.
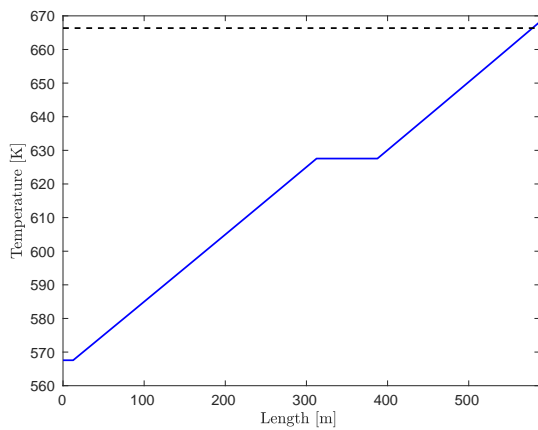

Figure A.18: Result of the mirror control with slowly defocused mirrors and slow shadow introduction for a single tube.

Mirror Control with slow Mirrors - Slow Shadow -	
g	3
$\tilde{g}$	5
end temp. absorber tube	668.19 K
temp. at heat exchanger	668.19 K
maximal temp.	668.19 K
mass flow	4.50 $m^3 s^{-1}$
computational time	36.46 s
finished after	-
defocused mirrors	-

Table A.18: Data corresponding to the simulation of the mirror control with slowly defocused mirrors and slow schadow introduction for a single tube.
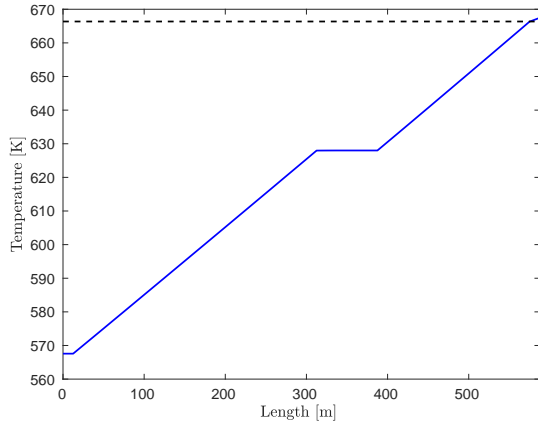
Figure A.19: Result of the mirror control with slowly defocused mirrors and fast shadow introduction for a single tube.

Mirror Control with slow Mirrors - Fast Shadow -	
g	1
$\tilde{g}$	3
end temp. absorber tube	667.45 K
temp. at heat exchanger	666.88 K
maximal temp.	667.63 K
mass flow	4.52 $m^3 s^{-1}$
computational time	51.35 s
finished after	-
defocused mirrors	1

Table A.19: Data corresponding to the simulation of the mirror control with slowly defocused mirrors and fast schadow introduction for a single tube.
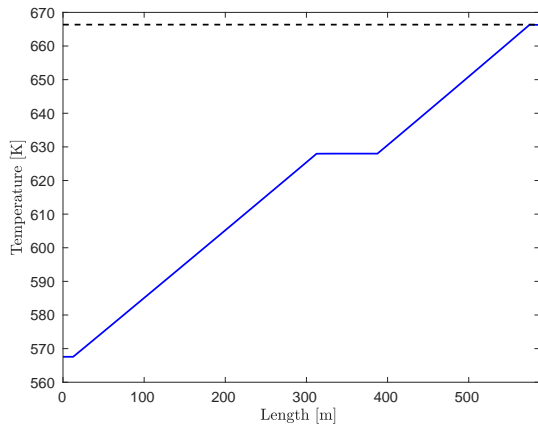

Figure A.20: Result of the mirror control with slowly defocused mirrors and slow shadow introduction for a single tube.

Mirror Control with slow Mirrors - Slow Shadow -	
g	1
$\tilde{g}$	3
end temp. absorber tube	666.29 K
temp. at heat exchanger	666.87 K
maximal temp.	667.47 K
mass flow	4.56 $m^3 s^{-1}$
computational time	42.05 s
finished after	-
defocused mirrors	-

Table A.20: Data corresponding to the simulation of the mirror control with slowly defocused mirrors and slow schadow introduction for a single tube.
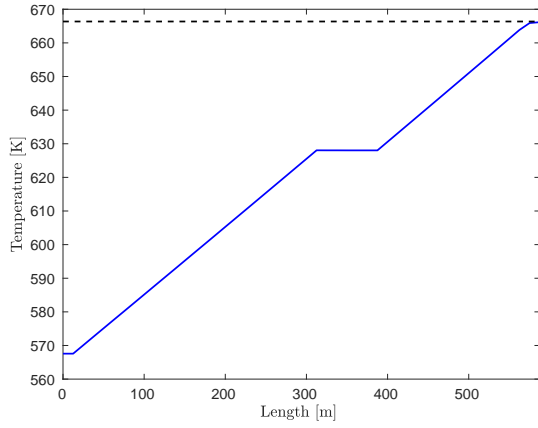
Figure A.21: Result of the mirror control with slowly defocused mirrors and fast shadow introduction for a single tube.

Mirror Control with slow Mirrors - Fast Shadow -	
g	0
$\tilde{g}$	0
end temp. absorber tube	666.16 K
temp. at heat exchanger	666.16 K
maximal temp.	666.58 K
mass flow	4.46 m^3s^{-1}
computational time	164.52 s
finished after	-
defocused mirrors	-

Table A.21: Data corresponding to the simulation of the mirror control with slowly defocused mirrors and fast schadow introduction for a single tube.
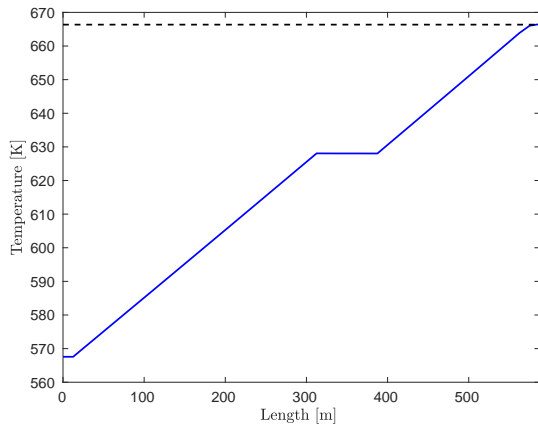
Figure A.22: Result of the mirror control with slowly defocused mirrors and slow shadow introduction for a single tube.

Mirror Control with slow Mirrors - Slow Shadow -	
g	0
$\tilde{g}$	0
end temp. absorber tube	666.52 K
temp. at heat exchanger	666.19 K
maximal temp.	666.53 K
mass flow	4.45 m^3s^{-1}
computational time	165.67 s
finished after	-
defocused mirrors	2

Table A.22: Data corresponding to the simulation of the mirror control with slowly defocused mirrors and slow schadow introduction for a single tube.

Mirror Control with calculated defocus number
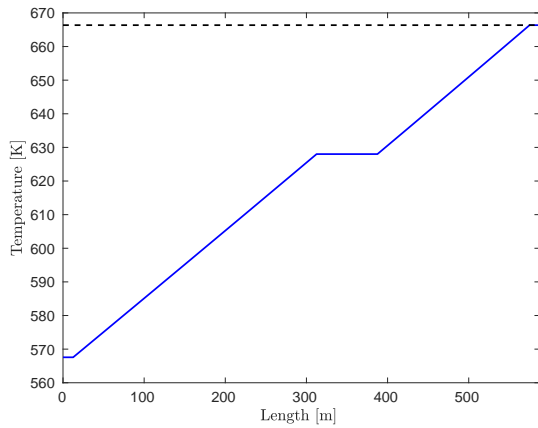
Figure A.23: Result of the mirror control with calculated defocus number and fast shadow introduction for a single tube.

Mirror Control with $N_{\mathbf{defocus}}$ - Fast Shadow -	
end temp. absorber tube	666.36 K
temp. at heat exchanger	666.36 K
maximal temp.	667.51 K
mass flow	4.49 $m^3 s^{-1}$
computational time	362.34 s
finished after	19150 s
defocused mirrors	1

Table A.23: Data corresponding to the simulation of the mirror control with calculated defocus number and fast schadow introduction for a single tube.
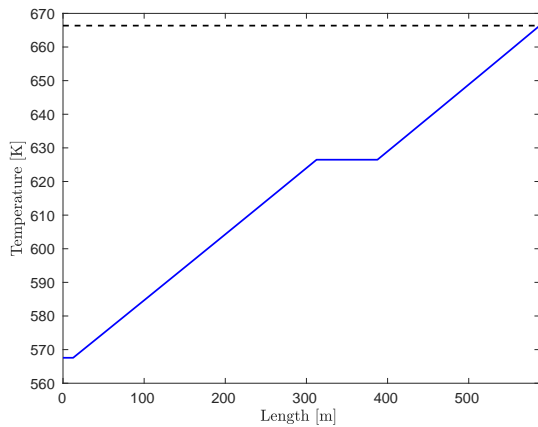
Figure A.24: Result of the mirror control with calculated defocus number and slow shadow introduction for a single tube.

Mirror Control with $N_{\mathbf{defocus}}$ - Slow Shadow -	
end temp. absorber tube	666.36 K
temp. at heat exchanger	666.36 K
maximal temp.	666.93 K
mass flow	4.60 $m^3 s^{-1}$
computational time	370.79 s
finished after	24070
defocused mirrors	-

Table A.24: Data corresponding to the simulation of the mirror control with calculated defocus number and slow schadow introduction for a single tube.

Cherek's Mirror Control
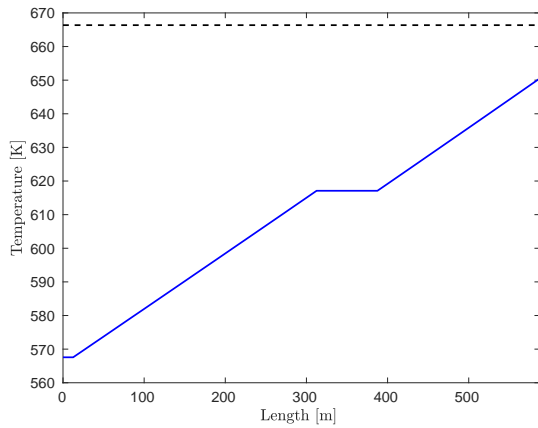
Figure A.25: Result of Cherek's mirror control with fast shadow introduction for a single tube.

Cherek's Mirror Control - Fast Shadow -	
end temp. absorber tube	663.41 K
temp. at heat exchanger	663.26 K
maximal temp.	666.36 K
mass flow	2.95 $m^3 s^{-1}$
computational time	9.01 s
finished after	-
defocused mirrors	12

Table A.25: Data corresponding to the simulation of Cherek's mirror control with fast schadow introduction for a single tube.
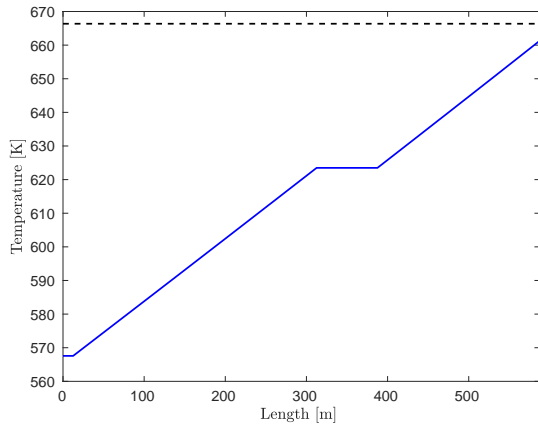
Figure A.26: Result of Cherek's mirror control with fast shadow introduction for a single tube.

Cherek's Mirror Control - Slow Shadow -	
end temp. absorber tube	663.23 K
temp. at heat exchanger	663.22 K
maximal temp.	666.36 K
mass flow	3.13 $m^3 s^{-1}$
computational time	5.22 s
finished after	-
defocused mirrors	-

Table A.26: Data corresponding to the simulation of Cherek's mirror control with slow schadow introduction for a single tube.

A.2. Single Tube - Molten Salt

Design Point
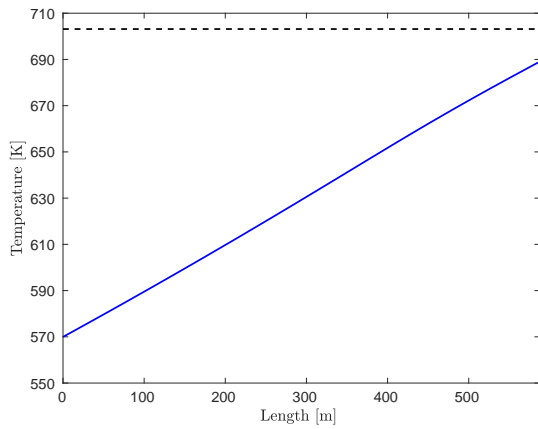
Figure A.27: Design point for a single tube and molten salt.

Design point - without Shadow -	
inflow temp.	569.97 K
end temp. absorber tube	689.05 K
temp. at heat exchanger	676.4 K
mass flow	6.03 $m^3 s^{-1}$

**Table A.27:** Data corresponding to the design point for a single tube and molten salt.
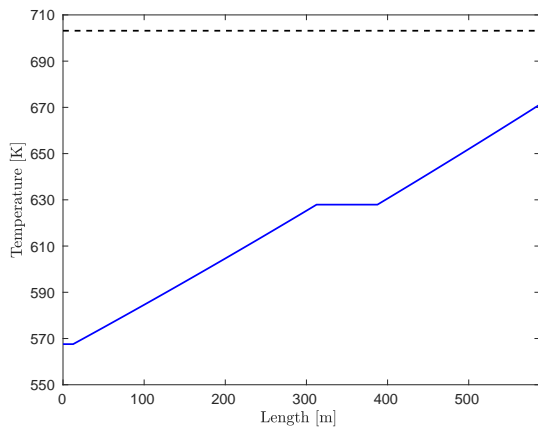
Figure A.28: Design point for a single tube and molten salt with shadow.

Design point - with Shadow -	
inflow temp.	567.57 K
end temp. absorber tube	671.19 K
temp. at heat exchanger	672.97 K
mass flow	6.04 $m^3 s^{-1}$

Table A.28: Data corresponding to the design point for a single tube and molten salt with shadow.

Pump Control
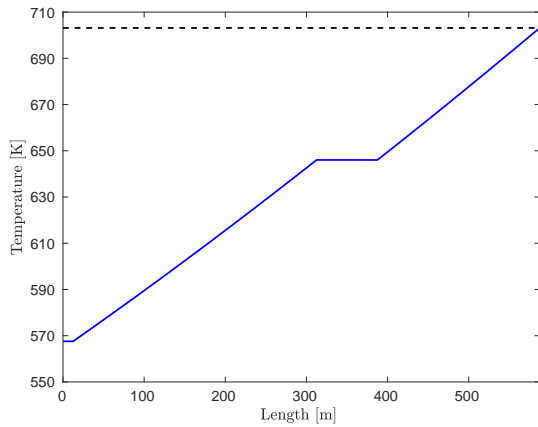
Figure A.29: Result of the simulation of pump control with slow shadow introduction for a single tube.

Pump Control - Slow Shadow -	
end temp. absorber tube	703.15 K
temp. at heat exchanger	700.08 K
maximal temp.	703.15 K
mass flow	4.65 m^3s^{-1}
computational time	42.64 s
finished after	-

Table A.29: Data corresponding to the simulation of pump control with slow shadow introduction for a single tube.
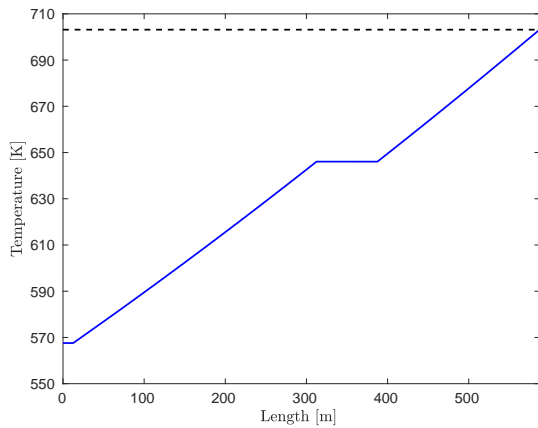
Mirror Control

Figure A.30: Result of the mirror control with slow shadow introduction for a single tube.

Mirror Control - Slow Shadow -	
g	3
$\tilde{g}$	5
end temp. absorber tube	703.21 K
temp. at heat exchanger	700.12 K
maximal temp.	703.21 K
mass flow	4.65 m^3s^{-1}
computational time	52.26 s
finished after	-
defocused mirrors	-

Table A.30: Data corresponding to the simulation of the mirror control with slow schadow introduction for a single tube.

## Mirror Control with calculated defocus number
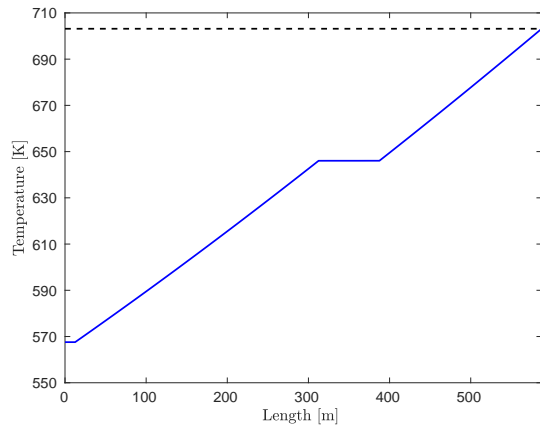
Figure A.31: Result of the mirror control with calculated defocus number and slow shadow introduction for a single tube.

Mirror Control with $N_{\mathbf{defocus}}$ - Slow Shadow -	
end temp. absorber tube	703.17 K
temp. at heat exchanger	700.12 K
maximal temp.	703.18 K
mass flow	4.66 $m^3 s^{-1}$
computational time	44.61 s
finished after	-
defocused mirrors	-

Table A.31: Data corresponding to the simulation of the mirror control with calculated defocus number and slow schadow introduction for a single tube.

A.3. Network - Therminol VP1

Design Point
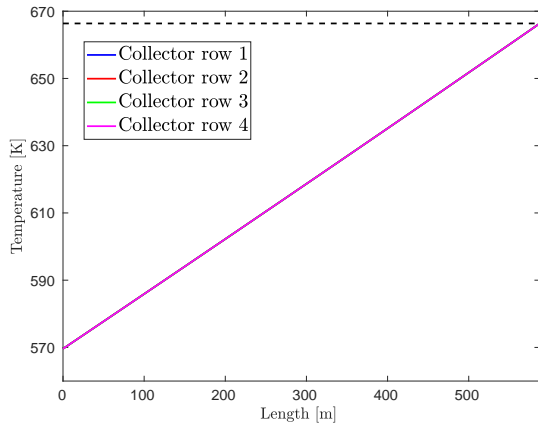
Figure A.32: Design point for a network of 4 tubes.

Design point - without Shadow -	
inflow temp.	569.6 K
end temp. absorber tube 1	666.36 K
end temp. absorber tube 2	666.36 K
end temp. absorber tube 3	666.36 K
end temp. absorber tube 4	666.36 K
temp. at heat exchanger	666.36 K
mass flow	$22.09 \ m^3 s^{-1}$

Table A.32: Data corresponding to the design point for a network of 4 tubes.
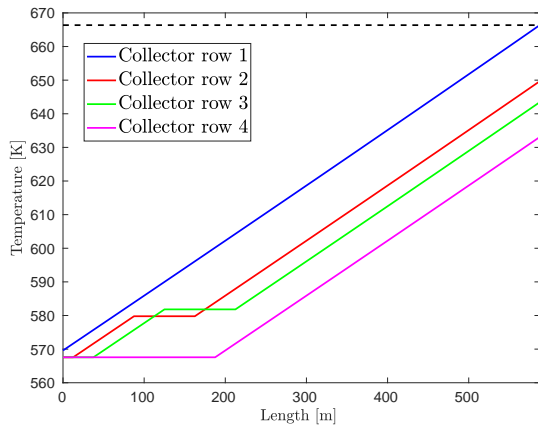
Figure A.33: Design point for a network of 4 tubes with shadow.

Design point - with Shadow -	
inflow temp.	567.57 K
end temp. absorber tube 1	666.36 K
end temp. absorber tube 2	649.67 K
end temp. absorber tube 3	643.44 K
end temp. absorber tube 4	633.08 K
temp. at heat exchanger	648.34 K
mass flow	$22.85 \ m^3 s^{-1}$

Table A.33: Data corresponding to the design point for a network of 4 tubes with shadow.
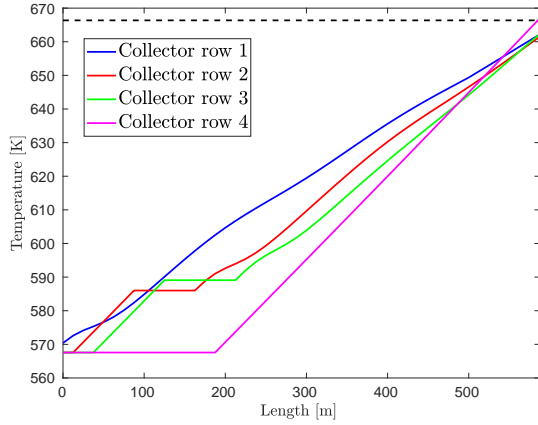
Figure A.34: Result of the simplified mirror control with fast shadow introduction for a network of 4 tubes.

Simplified Mirror Control - Fast Shadow -	
g	3
$\tilde{g}$	5
end temp. absorber tube 1	662.18 K
end temp. absorber tube 2	661.48 K
end temp. absorber tube 3	662.29 K
end temp. absorber tube 4	666.94 K
temp. at heat exchanger	667.42 K
mass flow	14.60 m^3s^{-1}
computational time	151.22 s
finished after	-
defocused mirrors in row 1	7
defocused mirrors in row 2	0
defocused mirrors in row 3	0
defocused mirrors in row 4	0

Table A.34: Data corresponding to the simulation of the simplified mirror control with fast schadow introduction for a network of 4 tubes.
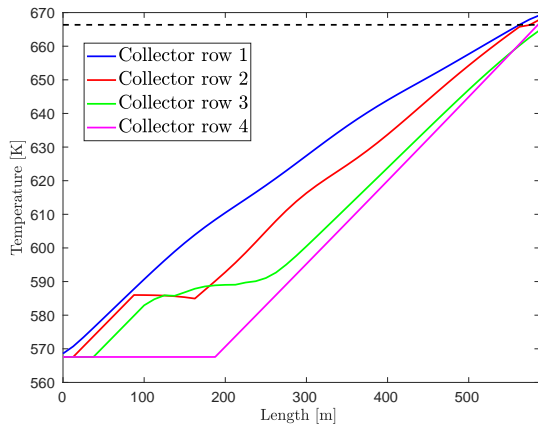

Figure A.35: Result of the simplified mirror control with slow shadow introduction for a network of 4 tubes.

Simplified Mirror Control - Slow Shadow -	
g	3
$\tilde{g}$	5
end temp. absorber tube 1	669.23 K
end temp. absorber tube 2	667.98 K
end temp. absorber tube 3	664.78 K
end temp. absorber tube 4	666.93 K
temp. at heat exchanger	666.81 K
mass flow	14.62 m^3s^{-1}
computational time	123.56 s
finished after	-
defocused mirrors in row 1	48
defocused mirrors in row 2	2
defocused mirrors in row 3	26
defocused mirrors in row 4	0

Table A.35: Data corresponding to the simulation of the simplified mirror control with slow schadow introduction for a network of 4 tubes.
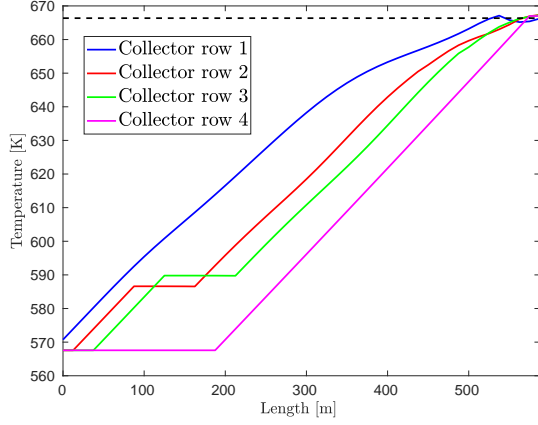
Figure A.36: Result of the simplified mirror control with fast shadow introduction for a network of 4 tubes.

Simplified Mirror Control - Fast Shadow -	
g	1
$\tilde{g}$	3
end temp. absorber tube 1	666.23 K
end temp. absorber tube 2	667.33 K
end temp. absorber tube 3	667.25 K
end temp. absorber tube 4	666.99 K
temp. at heat exchanger	666.38 K
mass flow	14.17 m^3s^{-1}
computational time	158.05 s
finished after	-
defocused mirrors in row 1	1
defocused mirrors in row 2	12
defocused mirrors in row 3	8
defocused mirrors in row 4	1

Table A.36: Data corresponding to the simulation of the simplified mirror control with fast schadow introduction for a network of 4 tubes.
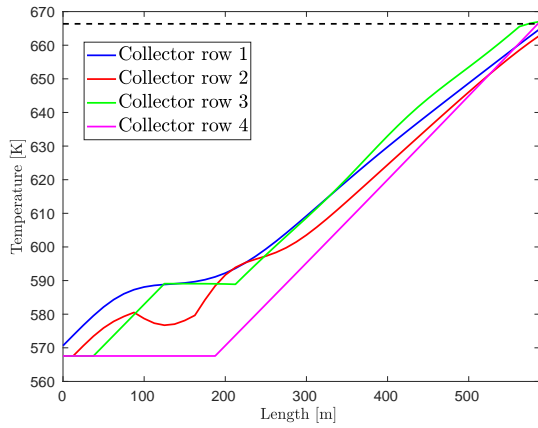

Figure A.37: Result of the simplified mirror control with slow shadow introduction for a network of 4 tubes.

Simplified Mirror Control - Slow Shadow -	
g	1
$\tilde{g}$	3
end temp. absorber tube 1	664.82 K
end temp. absorber tube 2	662.92 K
end temp. absorber tube 3	667.04 K
end temp. absorber tube 4	666.94 K
temp. at heat exchanger	665.79 K
mass flow	14.65 m^3s^{-1}
computational time	138.20 s
finished after	-
defocused mirrors in row 1	0
defocused mirrors in row 2	0
defocused mirrors in row 3	0
defocused mirrors in row 4	0

Table A.37: Data corresponding to the simulation of the simplified mirror control with slow schadow introduction for a network of 4 tubes.
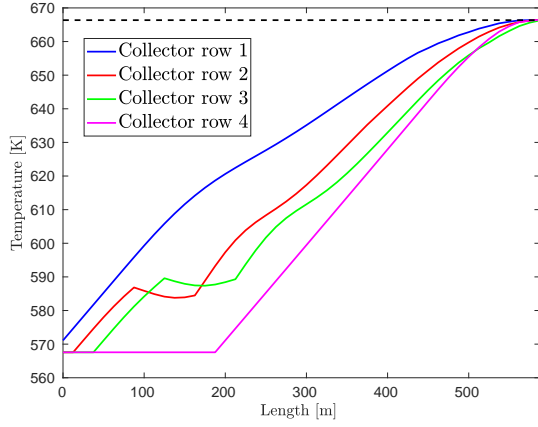
Figure A.38: Result of the simplified mirror control with fast shadow introduction for a network of 4 tubes.

Simplified Mirror Control - Fast Shadow -	
g	0
$\tilde{g}$	0
end temp. absorber tube 1	666.45 K
end temp. absorber tube 2	666.43 K
end temp. absorber tube 3	666.28 K
end temp. absorber tube 4	666.45 K
temp. at heat exchanger	666.33 K
mass flow	12.69 $m^3 s^{-1}$
computational time	246.37 s
finished after	-
defocused mirrors in row 1	14
defocused mirrors in row 2	18
defocused mirrors in row 3	5
defocused mirrors in row 4	4

Table A.38: Data corresponding to the simulation of the simplified mirror control with fast schadow introduction for a network of 4 tubes.
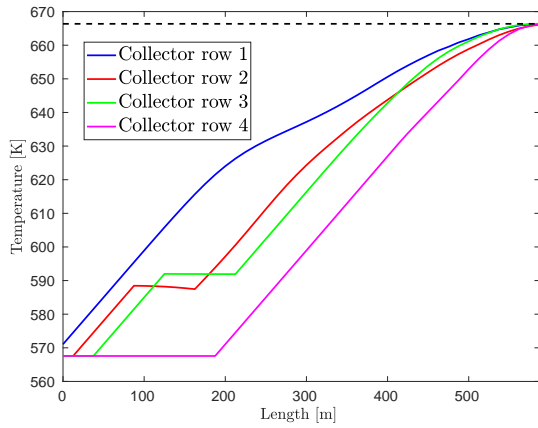

Figure A.39: Result of the simplified mirror control with slow shadow introduction for a network of 4 tubes.

Simplified Mirror Control - Slow Shadow -	
g	0
$\tilde{g}$	0
end temp. absorber tube 1	666.38 K
end temp. absorber tube 2	666.13 K
end temp. absorber tube 3	666.4 K
end temp. absorber tube 4	666.25 K
temp. at heat exchanger	666.34 K
mass flow	12.88 $m^3 s^{-1}$
computational time	249.77 s
finished after	-
defocused mirrors in row 1	12
defocused mirrors in row 2	6
defocused mirrors in row 3	14
defocused mirrors in row 4	8

Table A.39: Data corresponding to the simulation of the simplified mirror control with slow schadow introduction for a network of 4 tubes.
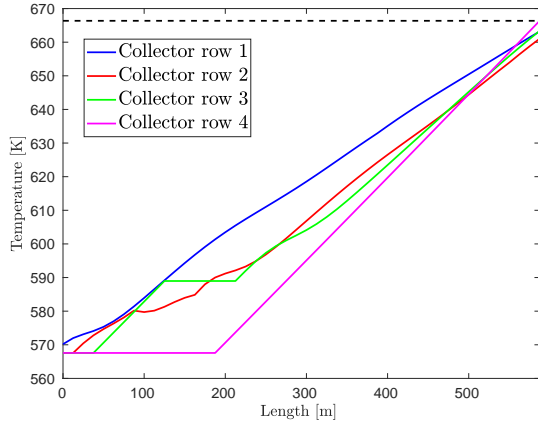
Mirror Control

Figure A.40: Result of the mirror control with fast shadow introduction for a network of 4 tubes.

Mirror Control - Fast Shadow -	
g	3
$\tilde{g}$	5
end temp. absorber tube 1	663.19 K
end temp. absorber tube 2	661.05 K
end temp. absorber tube 3	663.38 K
end temp. absorber tube 4	666.39 K
temp. at heat exchanger	667.96 K
mass flow	14.67 $m^3 s^{-1}$
computational time	423.76 s
finished after	-
defocused mirrors in row 1	16
defocused mirrors in row 2	3
defocused mirrors in row 3	0
defocused mirrors in row 4	0

Table A.40: Data corresponding to the simulation of the mirror control with fast schadow introduction for a network of 4 tubes.
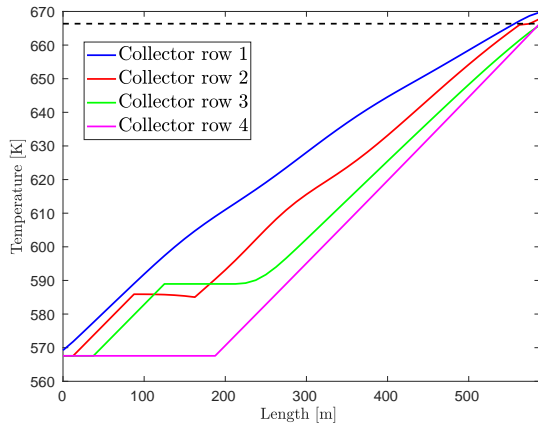

Figure A.41: Result of the mirror control with slow shadow introduction for a network of 4 tubes.

Mirror Control - Slow Shadow -	
g	3
$\tilde{g}$	5
end temp. absorber tube 1	669.75 K
end temp. absorber tube 2	667.81 K
end temp. absorber tube 3	665.94 K
end temp. absorber tube 4	666.38 K
temp. at heat exchanger	666.87 K
mass flow	14.70 $m^3 s^{-1}$
computational time	341.69 s
finished after	-
defocused mirrors in row 1	48
defocused mirrors in row 2	2
defocused mirrors in row 3	32
defocused mirrors in row 4	0

Table A.41: Data corresponding to the simulation of the mirror control with slow schadow introduction for a network of 4 tubes.
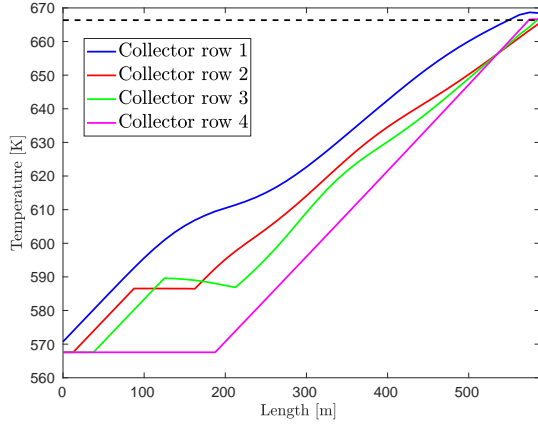
Figure A.42: Result of the mirror control with fast shadow introduction for a network of 4 tubes.

Mirror Control - Fast Shadow -	
g	1
$\tilde{g}$	3
end temp. absorber tube 1	668.46 K
end temp. absorber tube 2	665.55 K
end temp. absorber tube 3	667.07 K
end temp. absorber tube 4	666.62 K
temp. at heat exchanger	666.2 K
mass flow	14.23 $m^3 s^{-1}$
computational time	425.45 s
finished after	-
defocused mirrors in row 1	33
defocused mirrors in row 2	0
defocused mirrors in row 3	2
defocused mirrors in row 4	1

**Table A.42:** Data corresponding to the simulation of the mirror control with fast schadow introduction for a network of 4 tubes.
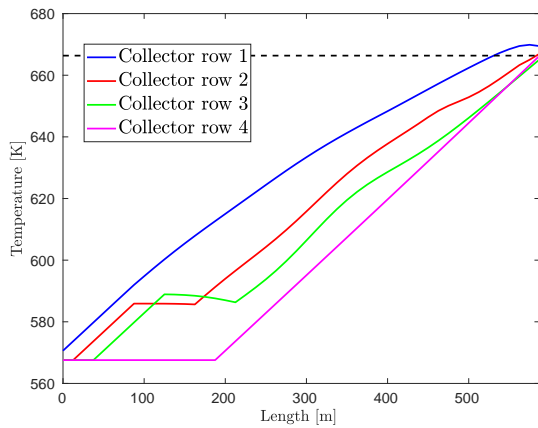
Figure A.43: Result of the mirror control with slow shadow introduction for a network of 4 tubes.

Mirror Control - Slow Shadow -	
g	1
$\tilde{g}$	3
end temp. absorber tube 1	669.45 K
end temp. absorber tube 2	667.02 K
end temp. absorber tube 3	665.16 K
end temp. absorber tube 4	666.39 K
temp. at heat exchanger	665.76 K
mass flow	14.73 $m^3 s^{-1}$
computational time	383.13 s
finished after	-
defocused mirrors in row 1	41
defocused mirrors in row 2	2
defocused mirrors in row 3	0
defocused mirrors in row 4	0

Table A.43: Data corresponding to the simulation of the mirror control with slow schadow introduction for a network of 4 tubes.
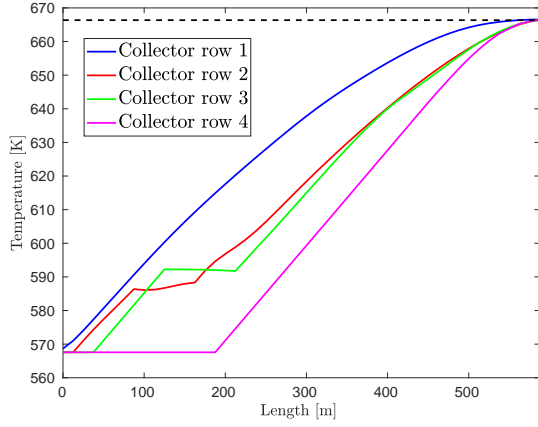
Figure A.44: Result of the mirror control with fast shadow introduction for a network of 4 tubes.

Mirror Control - Fast Shadow -	
g	0
$\tilde{g}$	0
end temp. absorber tube 1	666.59 K
end temp. absorber tube 2	666.48 K
end temp. absorber tube 3	666.33 K
end temp. absorber tube 4	666.44 K
temp. at heat exchanger	666.32 K
mass flow	12.74 $m^3 s^{-1}$
computational time	646.38 s
finished after	-
defocused mirrors in row 1	48
defocused mirrors in row 2	2
defocused mirrors in row 3	13
defocused mirrors in row 4	5

Table A.44: Data corresponding to the simulation of the mirror control with fast schadow introduction for a network of 4 tubes.
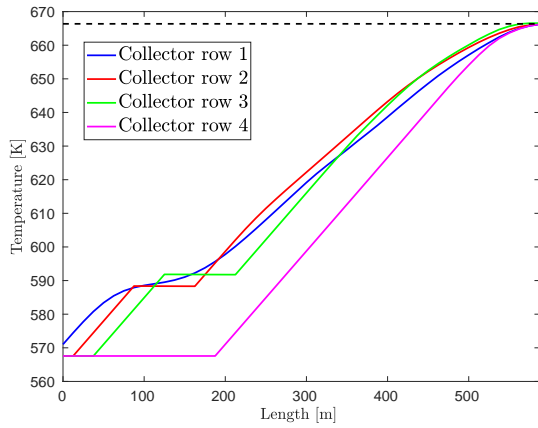

Figure A.45: Result of the mirror control with slow shadow introduction for a network of 4 tubes.

Mirror Control - Slow Shadow -	
g	0
$\tilde{g}$	0
end temp. absorber tube 1	666.22 K
end temp. absorber tube 2	666.4 K
end temp. absorber tube 3	666.56 K
end temp. absorber tube 4	666.22 K
temp. at heat exchanger	666.23 K
mass flow	12.95 $m^3 s^{-1}$
computational time	689.99 s
finished after	-
defocused mirrors in row 1	16
defocused mirrors in row 2	4
defocused mirrors in row 3	19
defocused mirrors in row 4	2

Table A.45: Data corresponding to the simulation of the mirror control with slow schadow introduction for a network of 4 tubes.

111

Mirror Control with slowly moving mirrors

Trying to simulate a network with slow moving mirrors leads to a CFL-error, when the parameters are set as mentioned above.

Mirror Control with calculated defocus number

Mirror Control with $N_{\textbf{defocus}}$ - Fast Shadow -	
end temp. absorber tube 1	665.51 K
end temp. absorber tube 2	666.95 K
end temp. absorber tube 3	666.24 K
end temp. absorber tube 4	652.19 K
temp. at heat exchanger	662.87 K
mass flow	15.99 $m^3 s^{-1}$
computational time	1332.05 s
finished after	-
defocused mirrors in row 1	10
defocused mirrors in row 2	9
defocused mirrors in row 3	0
defocused mirrors in row 4	0
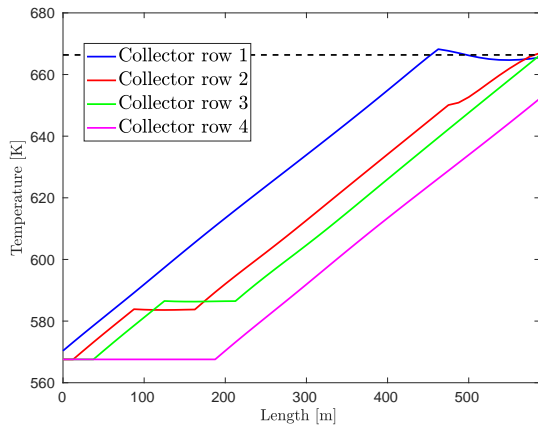
Figure A.46: Result of the mirror control with calculated defocus number and fast shadow introduction for a network of 4 tubes.

Table A.46: Data corresponding to the simulation of the mirror control with calculated defocus number and fast schadow introduction for a network of 4 tubes.
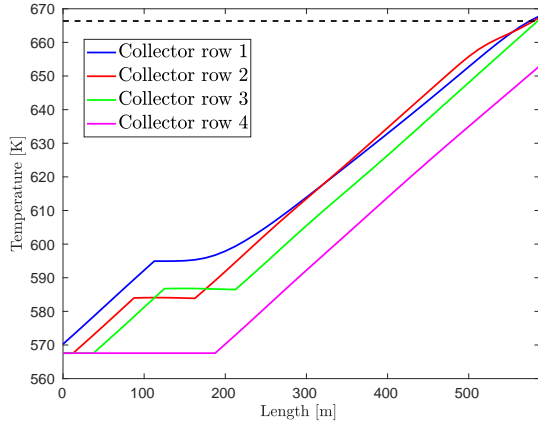
Figure A.47: Result of the mirror control with calculated defocus number and slow shadow introduction for a network of 4 tubes.

Mirror Control with $N_{\mathbf{defocus}}$ - Slow Shadow -	
end temp. absorber tube 1	667.89 K
end temp. absorber tube 2	667.42 K
end temp. absorber tube 3	666.87 K
end temp. absorber tube 4	653.01 K
temp. at heat exchanger	662.97 K
mass flow	16.84 $m^3 s^{-1}$
computational time	1359.07 s
finished after	-
defocused mirrors in row 1	38
defocused mirrors in row 2	1
defocused mirrors in row 3	0
defocused mirrors in row 4	0

Table A.47: Data corresponding to the simulation of the mirror control with calculated defocus number and slow schadow introduction for a network of 4 tubes.

## Mirror Control with calculated defocus number and limited pump control
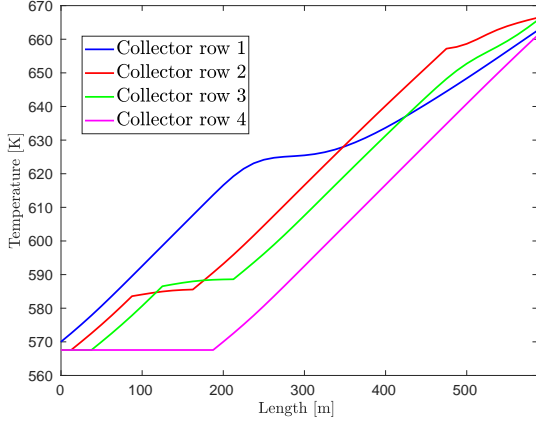
Figure A.48: Result of the mirror control with calculated defocus number, limited pump control and fast shadow introduction for a network of 4 tubes.

Mirror Control with $N_{\mathbf{defocus}}$ - Fast Shadow -	
end temp. absorber tube 1	662.64 K
end temp. absorber tube 2	666.41 K
end temp. absorber tube 3	665.68 K
end temp. absorber tube 4	661.19 K
temp. at heat exchanger	662.55 K
mass flow	18.59 $m^3 s^{-1}$
computational time	527.92 s
finished after	-
defocused mirrors in row 1	0
defocused mirrors in row 2	9
defocused mirrors in row 3	0
defocused mirrors in row 4	0

Table A.48: Data corresponding to the simulation of the mirror control with calculated defocus number, limited pump control and fast schadow introduction for a network of 4 tubes.
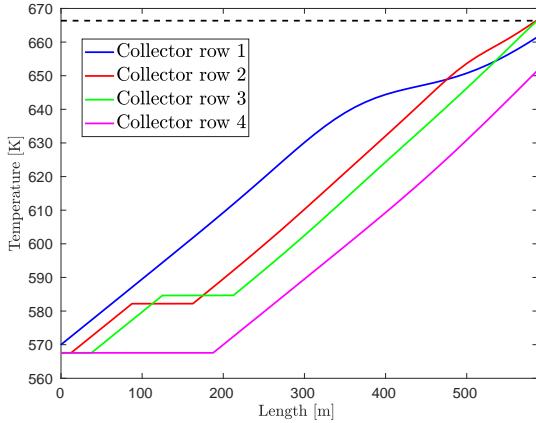

Figure A.49: Result of the mirror control with calculated defocus number, limited pump control and slow shadow introduction for a network of 4 tubes.

Mirror Control with $N_{\mathbf{defocus}}$ - Slow Shadow -	
end temp. absorber tube 1	661.57 K
end temp. absorber tube 2	666.66 K
end temp. absorber tube 3	666.49 K
end temp. absorber tube 4	651.63 K
temp. at heat exchanger	661.88 K
mass flow	18.61 $m^3 s^{-1}$
computational time	329.19 s
finished after	-
defocused mirrors in row 1	0
defocused mirrors in row 2	0
defocused mirrors in row 3	0
defocused mirrors in row 4	0

Table A.49: Data corresponding to the simulation of the mirror control with calculated defocus number, limited pump control and slow schadow introduction for a network of 4 tubes.

Mirror control with second order upwind scheme

Since the upwind scheme of second order cannot be used to create simulations with a clear result in reasonable time using the available resources, these are not listed here again.

Simplified Mirror Control with *predicitve time* 5000 **s**

For a simulation with the simplified Mirror Control and a *predictive time* of 5000 seconds the other parameters need to be adjusted differently. Thus the achieved results are not informative.

Mirror Control with *predicitve time* 5000 **s**

Same is true for Mirror Control.

Mirror Control with slow moving Mirrors and *predicitve time* 5000 **s**

Analogously to simulating a network with slowly movin mirrors, trying to simulate a network with a small predictive time and slowly moving mirrors also leads to a CFL-error, when the parameters are set as mentioned above.

Mirror Control with calculated defocus number and *predicitve time* 5000 **s**

The simulations with the mirror control with calculated defocus number and *predicitve time* 5000 s would again require adjusted parameters.
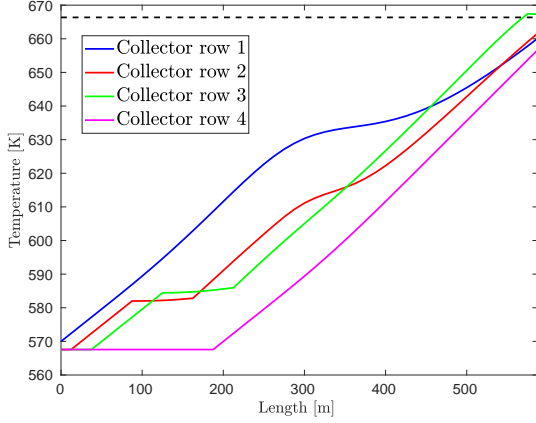
Figure A.50: Result of the mirror control with calculated defocus number, limited pump control and fast shadow introduction for a network of 4 tubes.

Mirror Control with $N_{\mathbf{defocus}}$ - Fast Shadow -	
end temp. absorber tube 1	660.13 K
end temp. absorber tube 2	661.62 K
end temp. absorber tube 3	667.27 K
end temp. absorber tube 4	656.73 K
temp. at heat exchanger	662.17 K
mass flow	18.75 $m^3 s^{-1}$
computational time	170.13 s
finished after	-
defocused mirrors in row 1	0
defocused mirrors in row 2	0
defocused mirrors in row 3	1
defocused mirrors in row 4	0

Table A.50: Data corresponding to the simulation of the mirror control with calculated defocus number, limited pump control and fast schadow introduction for a network of 4 tubes.
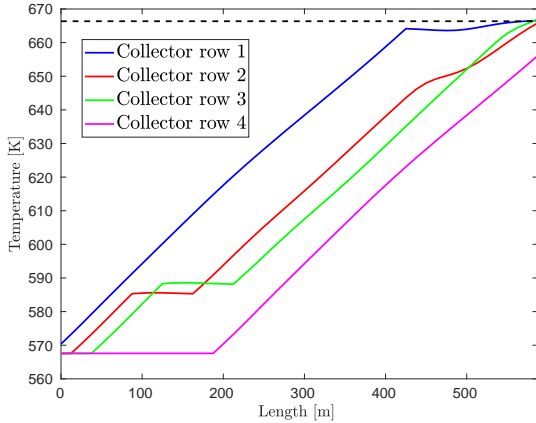

Figure A.51: Result of the mirror control with calculated defocus number, limited pump control and slow shadow introduction for a network of 4 tubes.

Mirror Control with $N_{\mathbf{defocus}}$ - Slow Shadow -	
end temp. absorber tube 1	666.55 K
end temp. absorber tube 2	665.85 K
end temp. absorber tube 3	666.98 K
end temp. absorber tube 4	656.11 K
temp. at heat exchanger	664.09 K
mass flow	15.55 $m^3 s^{-1}$
computational time	131.55 s
finished after	-
defocused mirrors in row 1	13
defocused mirrors in row 2	0
defocused mirrors in row 3	0
defocused mirrors in row 4	0

Table A.51: Data corresponding to the simulation of the mirror control with calculated defocus number, limited pump control and slow schadow introduction for a network of 4 tubes.

Mirror Control with weather forecast
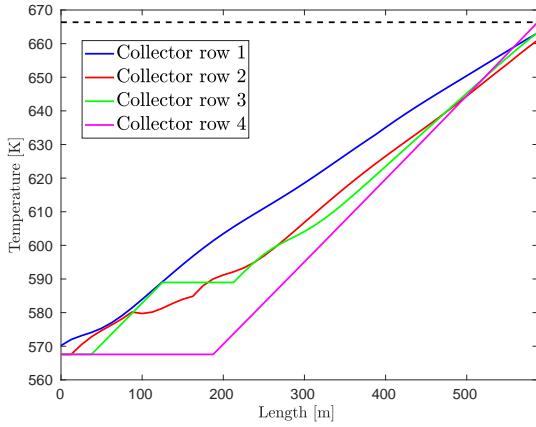
Figure A.52: Result of the mirror control with weather forecast and fast shadow introduction for a network of 4 tubes.

Mirror Control with weather forecast - Fast Shadow -	
g	3
$\tilde{g}$	5
end temp. absorber tube 1	663.19 K
end temp. absorber tube 2	661.05 K
end temp. absorber tube 3	663.38 K
end temp. absorber tube 4	666.39 K
temp. at heat exchanger	667.96 K
mass flow	14.67 m^3s^{-1}
computational time	708.78 s
finished after	-
defocused mirrors in row 1	16
defocused mirrors in row 2	3
defocused mirrors in row 3	0
defocused mirrors in row 4	0

Table A.52: Data corresponding to the simulation of the mirror control with weather forecast and fast schadow introduction for a network of 4 tubes.
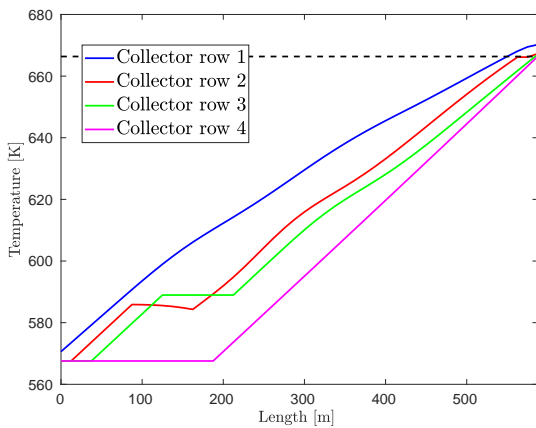

Figure A.53: Result of the mirror control with weather forecast and slow shadow introduction for a network of 4 tubes.

Mirror Control with weather forecast - Slow Shadow -	
g	3
$\tilde{g}$	5
end temp. absorber tube 1	670.21 K
end temp. absorber tube 2	667.27 K
end temp. absorber tube 3	667.08 K
end temp. absorber tube 4	666.38 K
temp. at heat exchanger	667.75 K
mass flow	14.68 m^3s^{-1}
computational time	587.5 s
finished after	-
defocused mirrors in row 1	48
defocused mirrors in row 2	2
defocused mirrors in row 3	0
defocused mirrors in row 4	0

Table A.53: Data corresponding to the simulation of the mirror control with weather forecast and slow schadow introduction for a network of 4 tubes.
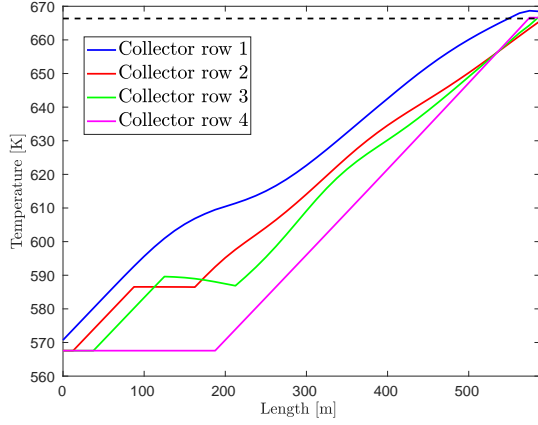
Figure A.54: Result of the mirror control with weather forecast and fast shadow introduction for a network of 4 tubes.

Mirror Control with weather forecast - Fast Shadow -	
g	1
$\tilde{g}$	3
end temp. absorber tube 1	668.46 K
end temp. absorber tube 2	665.55 K
end temp. absorber tube 3	667.07 K
end temp. absorber tube 4	666.62 K
temp. at heat exchanger	666.2 K
mass flow	14.23 $m^3 s^{-1}$
computational time	703.57 s
finished after	-
defocused mirrors in row 1	33
defocused mirrors in row 2	0
defocused mirrors in row 3	2
defocused mirrors in row 4	1

Table A.54: Data corresponding to the simulation of the mirror control with weather forecast and fast schadow introduction for a network of 4 tubes.
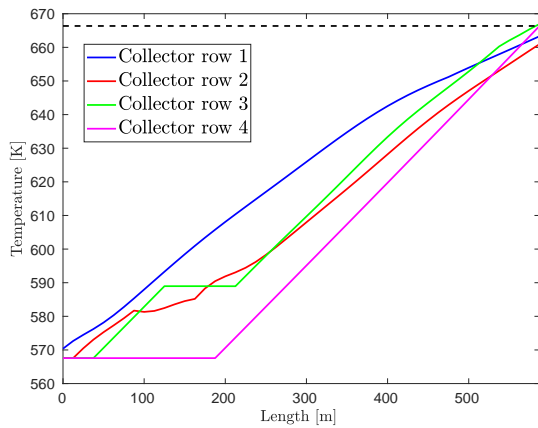

Figure A.55: Result of the mirror control with weather forecast and slow shadow introduction for a network of 4 tubes.

Mirror Control with weather forecast - Slow Shadow -	
g	1
$\tilde{g}$	3
end temp. absorber tube 1	663.33 K
end temp. absorber tube 2	660.99 K
end temp. absorber tube 3	666.98 K
end temp. absorber tube 4	666.42 K
temp. at heat exchanger	666.81 K
mass flow	14.7 $m^3 s^{-1}$
computational time	580.64 s
finished after	-
defocused mirrors in row 1	9
defocused mirrors in row 2	0
defocused mirrors in row 3	0
defocused mirrors in row 4	0

Table A.55: Data corresponding to the simulation of the mirror control with weather forecast and slow schadow introduction for a network of 4 tubes.
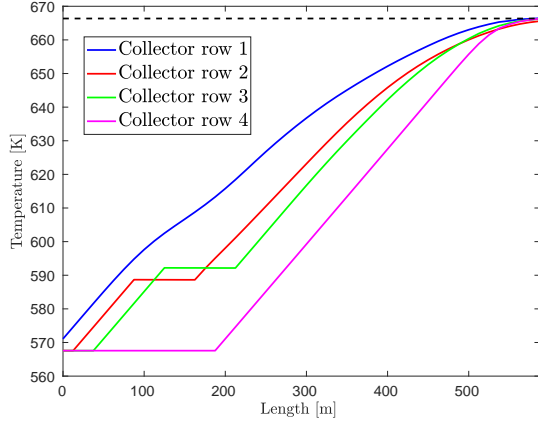
Figure A.56: Result of the mirror control with weather forecast and fast shadow introduction for a network of 4 tubes.

Mirror Control with weather forecast - Fast Shadow -	
g	0
$\tilde{g}$	0
end temp. absorber tube 1	666.45 K
end temp. absorber tube 2	665.58 K
end temp. absorber tube 3	666.28 K
end temp. absorber tube 4	666.32 K
temp. at heat exchanger	666.28 K
mass flow	12.77 $m^3 s^{-1}$
computational time	1090.42 s
finished after	-
defocused mirrors in row 1	6
defocused mirrors in row 2	0
defocused mirrors in row 3	1
defocused mirrors in row 4	2

Table A.56: Data corresponding to the simulation of the mirror control with weather forecast and fast schadow introduction for a network of 4 tubes.
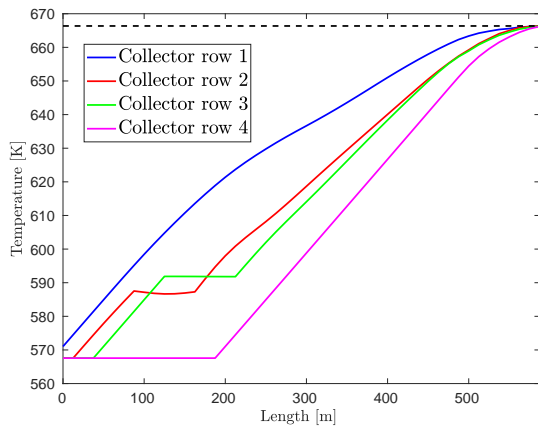

Figure A.57: Result of the mirror control with weather forecast and slow shadow introduction for a network of 4 tubes.

Mirror Control with weather forecast - Slow Shadow -	
g	0
$\tilde{g}$	0
end temp. absorber tube 1	666.32 K
end temp. absorber tube 2	666.42 K
end temp. absorber tube 3	666.33 K
end temp. absorber tube 4	666.21 K
temp. at heat exchanger	666.34 K
mass flow	12.94 $m^3 s^{-1}$
computational time	1101.74 s
finished after	-
defocused mirrors in row 1	3
defocused mirrors in row 2	10
defocused mirrors in row 3	7
defocused mirrors in row 4	2

Table A.57: Data corresponding to the simulation of the mirror control with weather forecast and slow schadow introduction for a network of 4 tubes.

# Mirror Control with calculated defocus number and weather forecast

Mirror Control with $N_{\mathbf{defocus}}$ and weather forecast - Fast Shadow -	
end temp. absorber tube 1	660.62 K
end temp. absorber tube 2	666.02 K
end temp. absorber tube 3	665.18 K
end temp. absorber tube 4	652.25 K
temp. at heat exchanger	661.41 K
mass flow	18.26 $m^3 s^{-1}$
computational time	2162.74 s
finished after	-
defocused mirrors in row 1	0
defocused mirrors in row 2	0
defocused mirrors in row 3	0
defocused mirrors in row 4	0
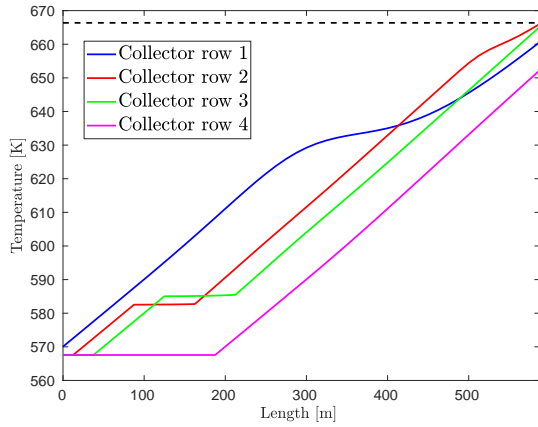
Figure A.58: Result of the mirror control with calculated defocus number, weather forecast and fast shadow introduction for a network of 4 tubes.

Table A.58: Data corresponding to the simulation of the mirror control with calculated defocus number, weather forecast and fast schadow introduction for a network of 4 tubes.
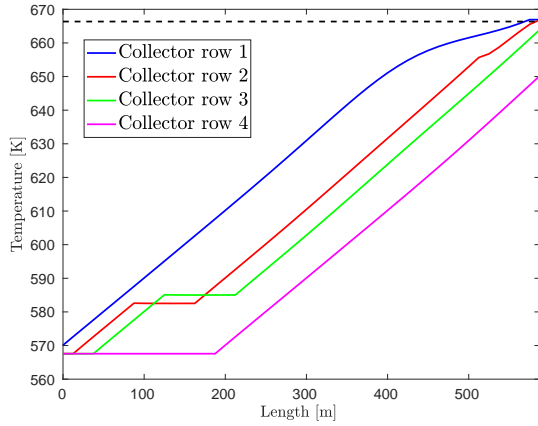
Figure A.59: Result of the mirror control with calculated defocus number, weather forecast and slow shadow introduction for a network of 4 tubes.

Mirror Control with $N_{\textbf{defocus}}$ and weather forecast - Slow Shadow -	
end temp. absorber tube 1	666.93 K
end temp. absorber tube 2	666.84 K
end temp. absorber tube 3	663.92 K
end temp. absorber tube 4	650.2 K
temp. at heat exchanger	662.12 K
mass flow	17.54 $m^3 s^{-1}$
computational time	2299.09 s
finished after	-
defocused mirrors in row 1	1
defocused mirrors in row 2	6
defocused mirrors in row 3	0
defocused mirrors in row 4	0

Table A.59: Data corresponding to the simulation of the mirror control with calculated defocus number, weather forecast and slow schadow introduction for a network of 4 tubes.

121
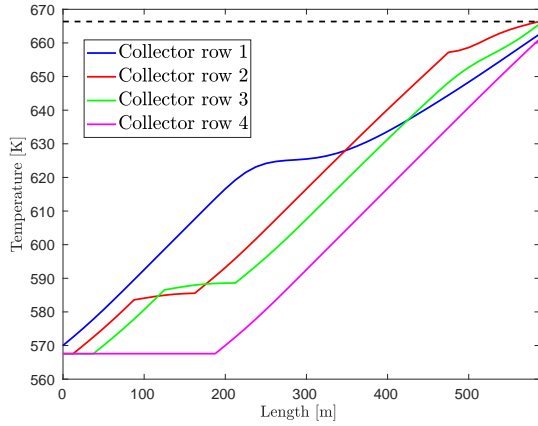
Figure A.60: Result of the mirror control with calculated defocus number, weather forecast, limited pump control and fast shadow introduction for a network of 4 tubes.

Mirror Control with $N_{\mathbf{defocus}}$ and weather forecast - Fast Shadow -	
end temp. absorber tube 1	662.64 K
end temp. absorber tube 2	666.41 K
end temp. absorber tube 3	665.68 K
end temp. absorber tube 4	661.19 K
temp. at heat exchanger	662.55 K
mass flow	18.59 $m^3 s^{-1}$
computational time	828.25 s
finished after	-
defocused mirrors in row 1	0
defocused mirrors in row 2	9
defocused mirrors in row 3	0
defocused mirrors in row 4	0

Table A.60: Data corresponding to the simulation of the mirror control with calculated defocus number, weather forecast, limited pump control and fast schadow introduction for a network of 4 tubes.
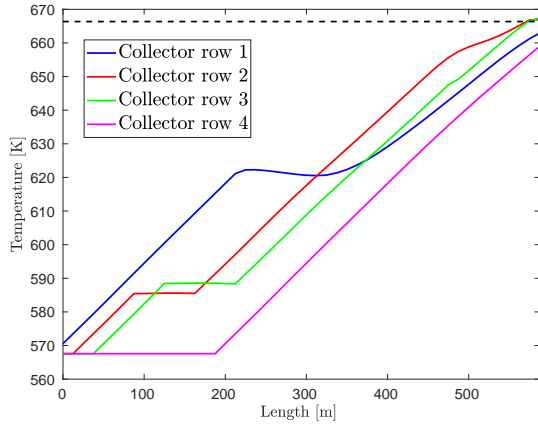
Figure A.61: Result of the mirror control with calculated defocus number, weather forecast, limited pump control and slow shadow introduction for a network of 4 tubes.

Mirror Control with $N_{\textbf{defocus}}$ and weather forecast - Slow Shadow -	
end temp. absorber tube 1	662.96 K
end temp. absorber tube 2	666.91 K
end temp. absorber tube 3	667.43 K
end temp. absorber tube 4	659.03 K
temp. at heat exchanger	665.35 K
mass flow	14.75 $m^3 s^{-1}$
computational time	558.07 s
finished after	-
defocused mirrors in row 1	21
defocused mirrors in row 2	1
defocused mirrors in row 3	9
defocused mirrors in row 4	0

Table A.61: Data corresponding to the simulation of the mirror control with calculated defocus number, weather forecast, limited pump control and slow schadow introduction for a network of 4 tubes.

Cherek's Mirror Control
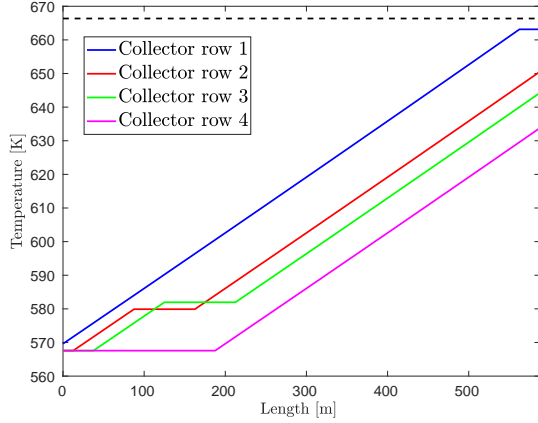
Figure A.62: Result of Cherek's mirror control with fast shadow introduction and a waiting time of 4000 seconds for a network of 4 tubes.

Cherek's Mirror Control - Fast Shadow -	
end temp. absorber tube 1	663.14 K
end temp. absorber tube 2	650.51 K
end temp. absorber tube 3	644.21 K
end temp. absorber tube 4	633.75 K
temp. at heat exchanger	648.06 K
mass flow	22.64 $m^3 s^{-1}$
computational time	7.83 s
finished after	-
defocused mirrors in row 1	2
defocused mirrors in row 2	0
defocused mirrors in row 3	0
defocused mirrors in row 4	0

Table A.62: Data corresponding to the simulation of Cherek's mirror control with fast schadow introduction and a waiting time of 4000 seconds for a network of 4 tubes.
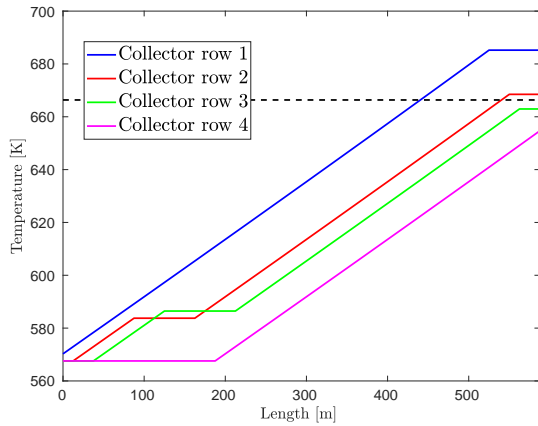

Figure A.63: Result of Cherek's mirror control with slow shadow introduction and a waiting time of 4000 seconds for a network of 4 tubes.

Cherek's Mirror Control - Slow Shadow -	
end temp. absorber tube 1	685.22 K
end temp. absorber tube 2	668.49 K
end temp. absorber tube 3	662.95 K
end temp. absorber tube 4	654.65 K
temp. at heat exchanger	668.11 K
mass flow	16.61 $m^3 s^{-1}$
computational time	7.87 s
finished after	-
defocused mirrors in row 1	5
defocused mirrors in row 2	3
defocused mirrors in row 3	2
defocused mirrors in row 4	0

Table A.63: Data corresponding to the simulation of Cherek's mirror control with slow schadow introduction and a waiting time of 4000 seconds for a network of 4 tubes.

Simplified Valve Control
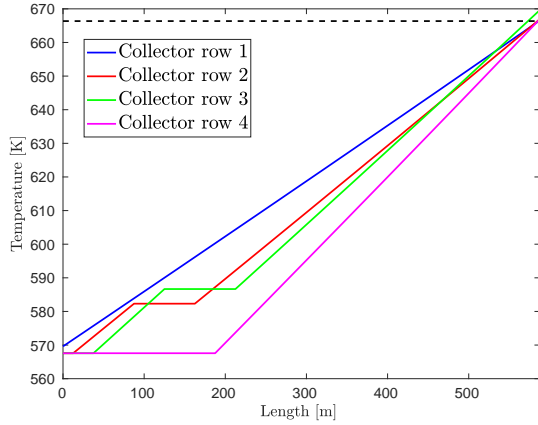
Figure A.64: Result of the simplified valve control with fast shadow introduction for a network of 4 tubes.

Simplified Valve Control - Fast Shadow -	
g	3
$\tilde{g}$	5
end temp. absorber tube 1	666.54 K
end temp. absorber tube 2	666.92 K
end temp. absorber tube 3	669.61 K
end temp. absorber tube 4	666.91 K
temp. at heat exchanger	667.42 K
mass flow	17.83 $m^3 s^{-1}$
computational time	157.54 s
finished after	-
valve position at row 1	0.64
valve position at row 2	0.84
valve position at row 3	1
valve position at row 4	0.89

Table A.64: Data corresponding to the simulation of the simplified valve control with fast schadow introduction for a network of 4 tubes.
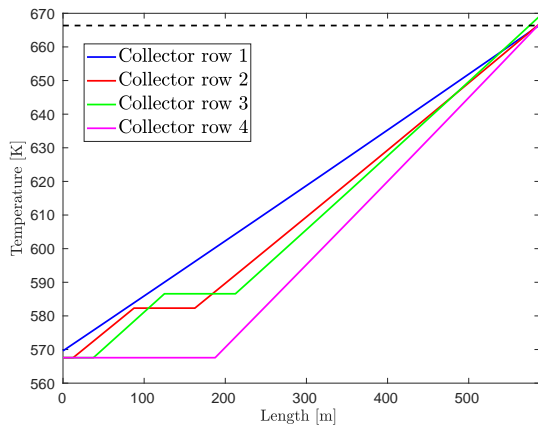

Figure A.65: Result of the simplified valve control with slow shadow introduction for a network of 4 tubes.

Simplified Valve Control - Slow Shadow -	
g	3
$\tilde{g}$	5
end temp. absorber tube 1	666.54 K
end temp. absorber tube 2	666.92 K
end temp. absorber tube 3	669.17 K
end temp. absorber tube 4	666.92 K
temp. at heat exchanger	667.21 K
mass flow	17.86 $m^3 s^{-1}$
computational time	60.20 s
finished after	-
valve position at row 1	0.64
valve position at row 2	0.84
valve position at row 3	1
valve position at row 4	0.88

Table A.65: Data corresponding to the simulation of the simplified valve control with slow schadow introduction for a network of 4 tubes.
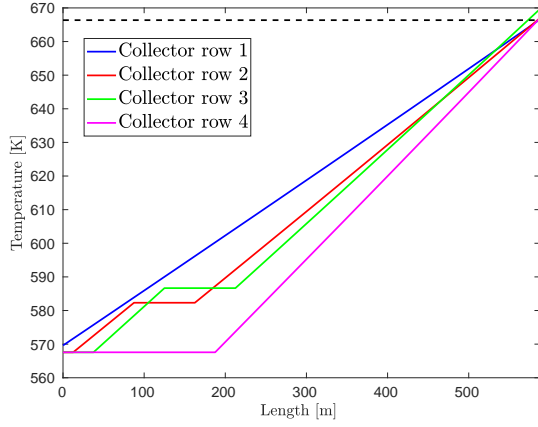
Figure A.66: Result of the simplified valve control with fast shadow introduction for a network of 4 tubes.

Simplified Valve Control - Fast Shadow -	
g	1
$\tilde{g}$	3
end temp. absorber tube 1	666.54 K
end temp. absorber tube 2	666.92 K
end temp. absorber tube 3	669.61 K
end temp. absorber tube 4	666.91 K
temp. at heat exchanger	667.42 K
mass flow	17.83 $m^3 s^{-1}$
computational time	225.1 s
finished after	-
valve position at row 1	0.64
valve position at row 2	0.84
valve position at row 3	1
valve position at row 4	0.89

Table A.66: Data corresponding to the simulation of the simplified valve control with fast schadow introduction for a network of 4 tubes.
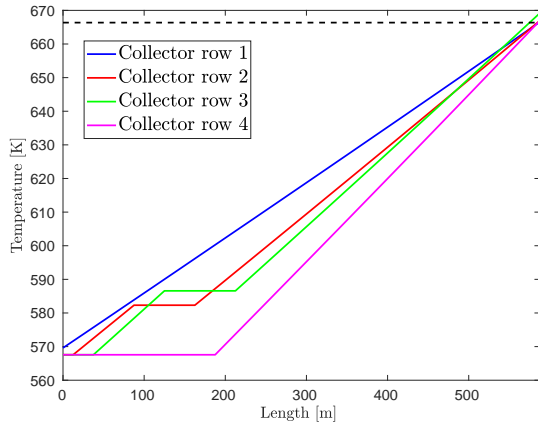

Figure A.67: Result of the simplified valve control with slow shadow introduction for a network of 4 tubes.

Simplified Valve Control - Slow Shadow -	
g	1
$\tilde{g}$	3
end temp. absorber tube 1	666.54 K
end temp. absorber tube 2	666.92 K
end temp. absorber tube 3	669.15 K
end temp. absorber tube 4	666.91 K
temp. at heat exchanger	667.09 K
mass flow	17.86 $m^3 s^{-1}$
computational time	117.49 s
finished after	-
valve position at row 1	0.64
valve position at row 2	0.84
valve position at row 3	1
valve position at row 4	0.88

Table A.67: Data corresponding to the simulation of the simplified valve control with slow schadow introduction for a network of 4 tubes.
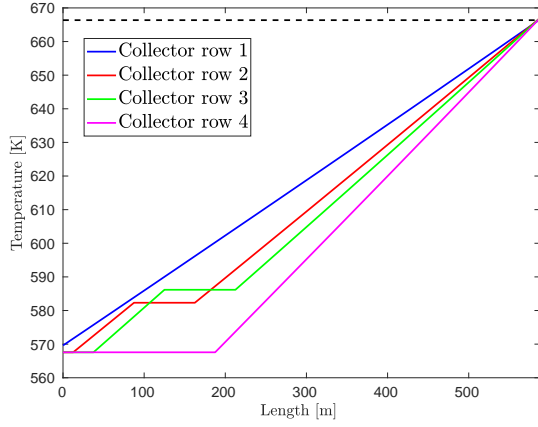
Figure A.68: Result of the simplified valve control with fast shadow introduction for a network of 4 tubes.

Simplified Valve Control - Fast Shadow -	
g	0
$\tilde{g}$	0
end temp. absorber tube 1	666.54 K
end temp. absorber tube 2	666.92 K
end temp. absorber tube 3	666.92 K
end temp. absorber tube 4	666.91 K
temp. at heat exchanger	666.8 K
mass flow	17.96 $m^3 s^{-1}$
computational time	511.13 s
finished after	-
valve position at row 1	0.63
valve position at row 2	0.83
valve position at row 3	1
valve position at row 4	0.86

Table A.68: Data corresponding to the simulation of the simplified valve control with fast schadow introduction for a network of 4 tubes.
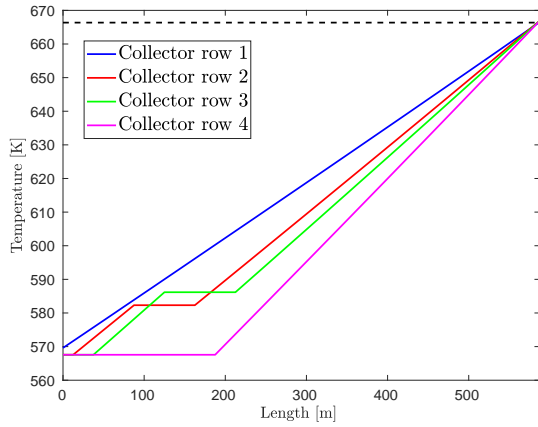

Figure A.69: Result of the simplified valve control with slow shadow introduction for a network of 4 tubes.

Simplified Valve Control - Slow Shadow -	
g	0
$\tilde{g}$	0
end temp. absorber tube 1	666.54 K
end temp. absorber tube 2	666.92 K
end temp. absorber tube 3	669.15 K
end temp. absorber tube 4	666.91 K
temp. at heat exchanger	666.56 K
mass flow	17.97 $m^3 s^{-1}$
computational time	508.69 s
finished after	-
valve position at row 1	0.63
valve position at row 2	0.83
valve position at row 3	1
valve position at row 4	0.86

Table A.69: Data corresponding to the simulation of the simplified valve control with slow schadow introduction for a network of 4 tubes.
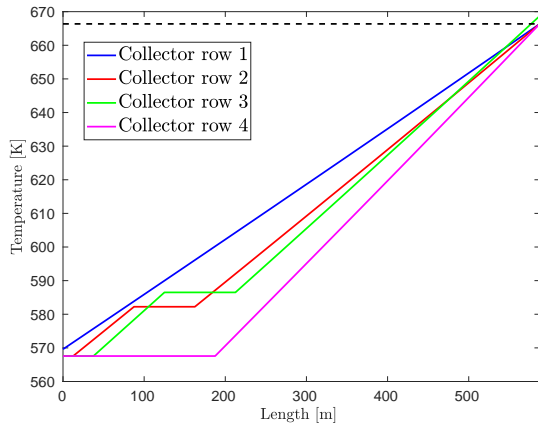
Valve Control

Figure A.70: Result of the valve control with fast shadow introduction for a network of 4 tubes.

Valve Control - Fast Shadow -	
g	3
$\tilde{g}$	5
end temp. absorber tube 1	666.36 K
end temp. absorber tube 2	666.36 K
end temp. absorber tube 3	668.72 K
end temp. absorber tube 4	666.36 K
temp. at heat exchanger	666.91 K
mass flow	17.94 $m^3 s^{-1}$
computational time	746.46 s
finished after	10990
valve position at row 1	0.63
valve position at row 2	0.84
valve position at row 3	1
valve position at row 4	0.89

Table A.70: Data corresponding to the simulation of the valve control with fast schadow introduction for a network of 4 tubes.
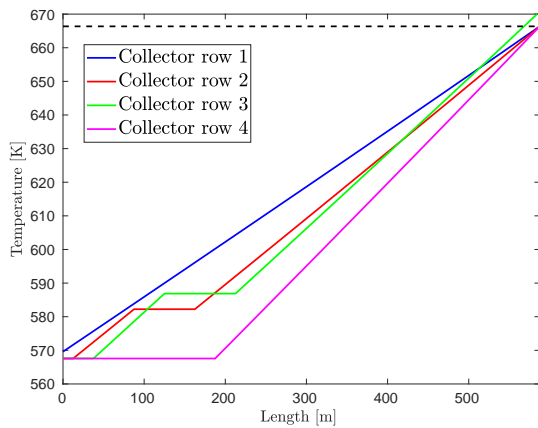

Figure A.71: Result of the valve control with slow shadow introduction for a network of 4 tubes.

Valve Control - Slow Shadow -	
g	3
$\tilde{g}$	5
end temp. absorber tube 1	666.36 K
end temp. absorber tube 2	666.36 K
end temp. absorber tube 3	670.75 K
end temp. absorber tube 4	666.36 K
temp. at heat exchanger	667.23 K
mass flow	17.85 $m^3 s^{-1}$
computational time	587.62 s
finished after	10990
valve position at row 1	0.64
valve position at row 2	0.85
valve position at row 3	1
valve position at row 4	0.90

Table A.71: Data corresponding to the simulation of the valve control with slow schadow introduction for a network of 4 tubes.
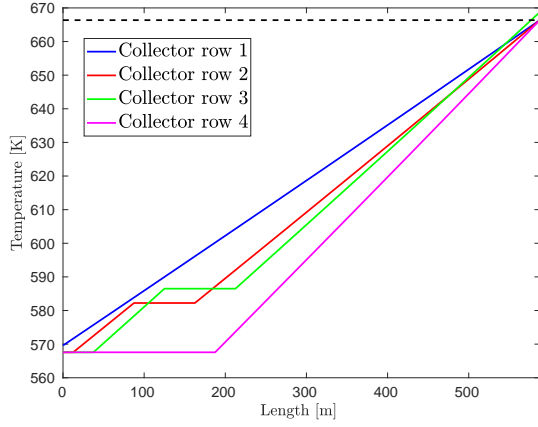
Figure A.72: Result of the valve control with fast shadow introduction for a network of 4 tubes.

Valve Control - Fast Shadow -	
g	1
$\tilde{g}$	3
end temp. absorber tube 1	666.36 K
end temp. absorber tube 2	666.36 K
end temp. absorber tube 3	668.72 K
end temp. absorber tube 4	666.36 K
temp. at heat exchanger	666.91 K
mass flow	17.94 m^3s^{-1}
computational time	981.07 s
finished after	10990
valve position at row 1	0.63
valve position at row 2	0.84
valve position at row 3	1
valve position at row 4	0.89

**Table A.72:** Data corresponding to the simulation of the valve control with fast schadow introduction for a network of 4 tubes.
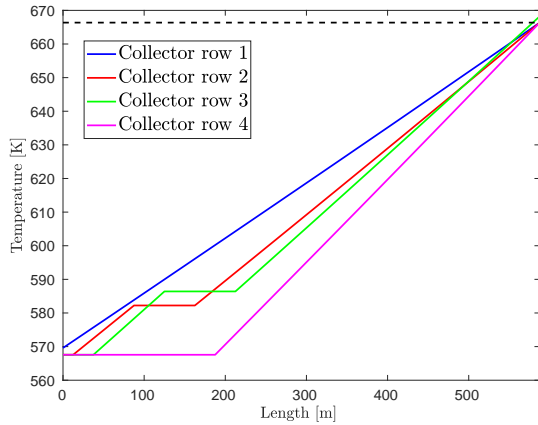
Figure A.73: Result of the valve control with slow shadow introduction for a network of 4 tubes.

Valve Control - Slow Shadow -	
g	1
$\tilde{g}$	3
end temp. absorber tube 1	666.36 K
end temp. absorber tube 2	666.36 K
end temp. absorber tube 3	668.23 K
end temp. absorber tube 4	666.36 K
temp. at heat exchanger	666.73 K
mass flow	17.97 m^3s^{-1}
computational time	609.74 s
finished after	10990
valve position at row 1	0.63
valve position at row 2	0.84
valve position at row 3	1
valve position at row 4	0.88

**Table A.73:** Data corresponding to the simulation of the valve control with slow schadow introduction for a network of 4 tubes.
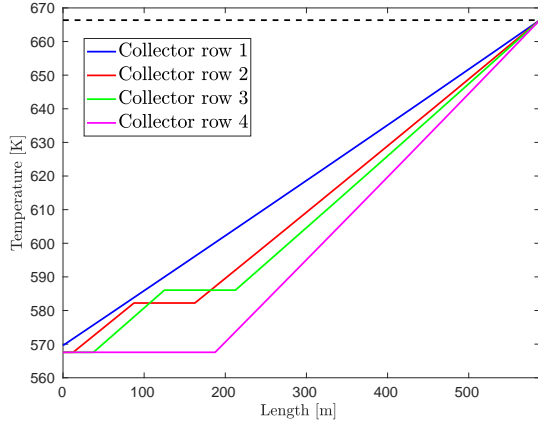
Figure A.74: Result of the valve control with fast shadow introduction for a network of 4 tubes.

Valve Control - Fast Shadow -	
g	0
$\tilde{g}$	0
end temp. absorber tube 1	666.36 K
end temp. absorber tube 2	666.36 K
end temp. absorber tube 3	666.36 K
end temp. absorber tube 4	666.36 K
temp. at heat exchanger	666.36 K
mass flow	18.06 $m^3 s^{-1}$
computational time	1266.32 s
finished after	10990
valve position at row 1	0.63
valve position at row 2	0.83
valve position at row 3	1
valve position at row 4	0.86

**Table A.74:** Data corresponding to the simulation of the valve control with fast schadow introduction for a network of 4 tubes.
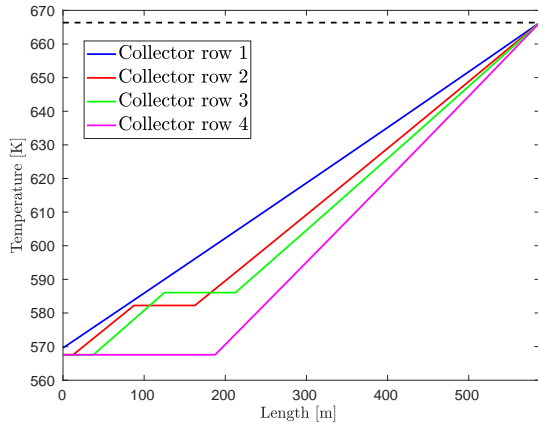
Figure A.75: Result of the valve control with slow shadow introduction for a network of 4 tubes.

Valve Control - Slow Shadow -	
g	0
$\tilde{g}$	0
end temp. absorber tube 1	666.36 K
end temp. absorber tube 2	666.36 K
end temp. absorber tube 3	666.36 K
end temp. absorber tube 4	666.36 K
temp. at heat exchanger	666.28 K
mass flow	18.06 $m^3 s^{-1}$
computational time	1395.27 s
finished after	10990
valve position at row 1	0.63
valve position at row 2	0.83
valve position at row 3	1
valve position at row 4	0.86

Table A.75: Data corresponding to the simulation of the valve control with slow schadow introduction for a network of 4 tubes.

Valve Control with second order upwind scheme

Since the upwind scheme of second order cannot be used to create simulations with a clear result in reasonable time using the available resources, these are not listed here again.

## Simplified Valve Control with *predicitve time* 5000 s

Simplified Valve Control - Fast Shadow -	
g	3
$\tilde{g}$	5
end temp. absorber tube 1	666.55 K
end temp. absorber tube 2	669.23 K
end temp. absorber tube 3	668.25 K
end temp. absorber tube 4	669.67 K
temp. at heat exchanger	668.26 K
mass flow	17.66 $m^3 s^{-1}$
computational time	77.07 s
finished after	-
valve position at row 1	0.64
valve position at row 2	0.83
valve position at row 3	1
valve position at row 4	0.85
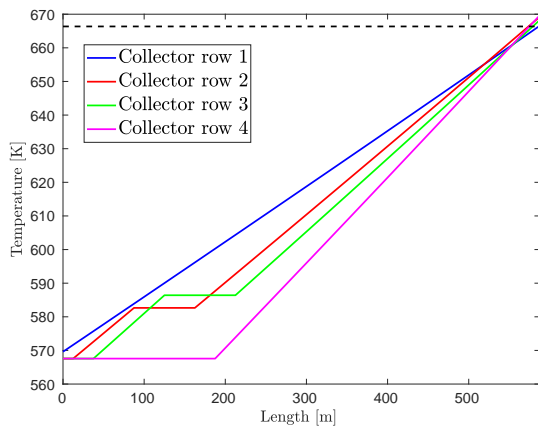
Figure A.76: Result of the simplified valve control with *predicitve time* 5000 s and fast shadow introduction for a network of 4 tubes.

Table A.76: Data corresponding to the simulation of the simplified valve control with *predicitve time* 5000 s and fast schadow introduction for a network of 4 tubes.
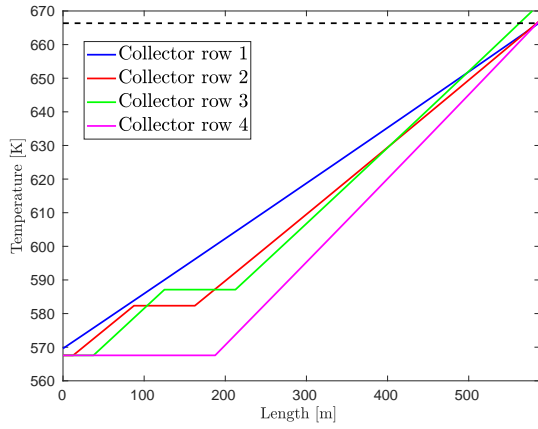
Figure A.77: Result of the simplified valve control with *predicitve time* 5000 s and slow shadow introduction for a network of 4 tubes.

Simplified Valve Control - Slow Shadow -	
g	3
$\tilde{g}$	5
end temp. absorber tube 1	666.55 K
end temp. absorber tube 2	667.1 K
end temp. absorber tube 3	672.12 K
end temp. absorber tube 4	667.14 K
temp. at heat exchanger	667.87 K
mass flow	17.7 $m^3 s^{-1}$
computational time	36.19 s
finished after	-
valve position at row 1	0.64
valve position at row 2	0.85
valve position at row 3	1
valve position at row 4	0.91

Table A.77: Data corresponding to the simulation of the simplified valve control with *predicitve time* 5000 s and slow schadow introduction for a network of 4 tubes.
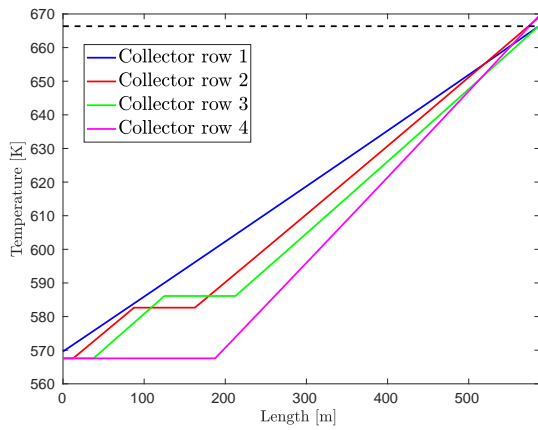
Figure A.78: Result of the simplified valve control with *predicitve time* 5000 s and fast shadow introduction for a network of 4 tubes.

Simplified Valve Control - Fast Shadow -	
g	1
$\tilde{g}$	3
end temp. absorber tube 1	666.55 K
end temp. absorber tube 2	669.23 K
end temp. absorber tube 3	666.65 K
end temp. absorber tube 4	669.67 K
temp. at heat exchanger	667.88 K
mass flow	17.74 $m^3 s^{-1}$
computational time	107.66 s
finished after	-
valve position at row 1	0.64
valve position at row 2	0.82
valve position at row 3	1
valve position at row 4	0.84

Table A.78: Data corresponding to the simulation of the simplified valve control with *predicitve time* 5000 s and fast schadow introduction for a network of 4 tubes.
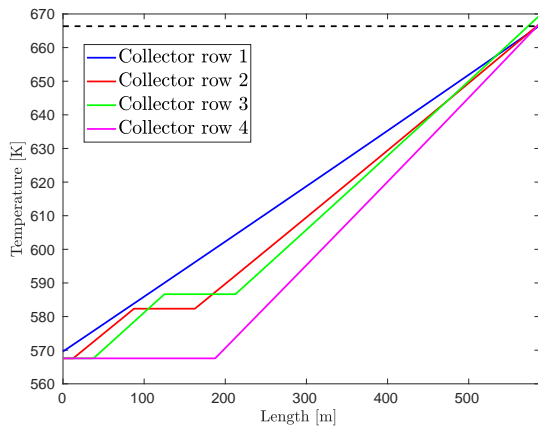
Figure A.79: Result of the simplified valve control with *predicitve time* 5000 s and slow shadow introduction for a network of 4 tubes.

Simplified Valve Control - Slow Shadow -	
g	1
$\tilde{g}$	3
end temp. absorber tube 1	666.55 K
end temp. absorber tube 2	667.1 K
end temp. absorber tube 3	669.59 K
end temp. absorber tube 4	667.14 K
temp. at heat exchanger	667.35 K
mass flow	17.82 $m^3 s^{-1}$
computational time	36.47 s
finished after	-
valve position at row 1	0.64
valve position at row 2	0.84
valve position at row 3	1
valve position at row 4	0.89

Table A.79: Data corresponding to the simulation of the simplified valve control with *predicitve time* 5000 s and slow schadow introduction for a network of 4 tubes.
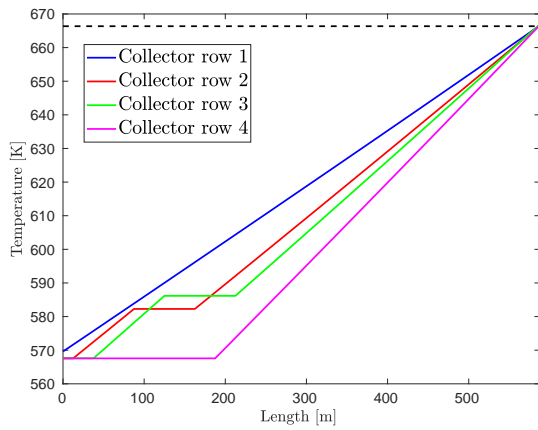
Figure A.80: Result of the simplified valve control with *predicitve time* 5000 s and fast shadow introduction for a network of 4 tubes.

Simplified Valve Control - Fast Shadow -	
g	0
$\tilde{g}$	0
end temp. absorber tube 1	666.55 K
end temp. absorber tube 2	666.63 K
end temp. absorber tube 3	666.92 K
end temp. absorber tube 4	666.67 K
temp. at heat exchanger	666.7 K
mass flow	17.99 $m^3 s^{-1}$
computational time	177.26 s
finished after	-
valve position at row 1	0.63
valve position at row 2	0.83
valve position at row 3	0.97
valve position at row 4	0.84

Table A.80: Data corresponding to the simulation of the simplified valve control with *predicitve time* 5000 s and fast schadow introduction for a network of 4 tubes.
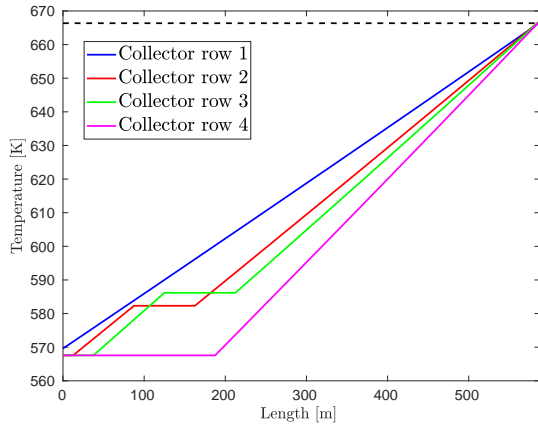
Figure A.81: Result of the simplified valve control with *predicitve time* 5000 s and slow shadow introduction for a network of 4 tubes.

Simplified Valve Control - Slow Shadow -	
g	0
$\tilde{g}$	0
end temp. absorber tube 1	666.55 K
end temp. absorber tube 2	666.98 K
end temp. absorber tube 3	666.99 K
end temp. absorber tube 4	666.95 K
temp. at heat exchanger	666.69 K
mass flow	17.96 m^3s^{-1}
computational time	173.45 s
finished after	-
valve position at row 1	0.63
valve position at row 2	0.83
valve position at row 3	1
valve position at row 4	0.86

Table A.81: Data corresponding to the simulation of the simplified valve control with *predicitve time* 5000 s and slow schadow introduction for a network of 4 tubes.

## Valve Control with *predicitve time* 5000 s
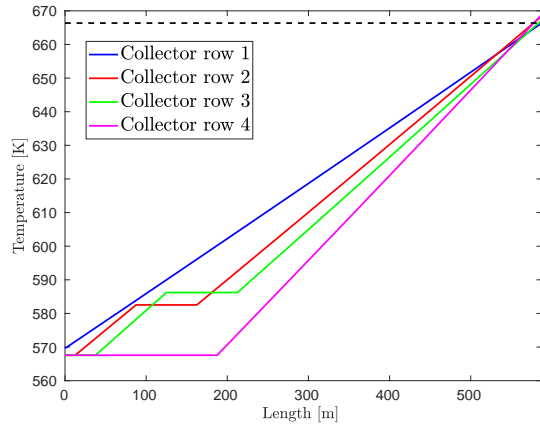
Figure A.82: Result of the valve control with *predicitve time* 5000 s and fast shadow introduction for a network of 4 tubes.

Valve Control - Fast Shadow -	
g	3
$\tilde{g}$	5
end temp. absorber tube 1	666.36 K
end temp. absorber tube 2	668.44 K
end temp. absorber tube 3	667.27 K
end temp. absorber tube 4	668.89 K
temp. at heat exchanger	667.61 K
mass flow	17.79 $m^3 s^{-1}$
computational time	128.63 s
finished after	-
valve position at row 1	0.64
valve position at row 2	0.82
valve position at row 3	1
valve position at row 4	0.85

Table A.82: Data corresponding to the simulation of the valve control with *predicitve time* 5000 s and fast schadow introduction for a network of 4 tubes.

Valve Control - Slow Shadow -	
g	3
$\tilde{g}$	5
end temp. absorber tube 1	666.36 K
end temp. absorber tube 2	666.56 K
end temp. absorber tube 3	668.98 K
end temp. absorber tube 4	666.55 K
temp. at heat exchanger	667.08 K
mass flow	17.91 $m^3 s^{-1}$
computational time	110.24 s
finished after	-
valve position at row 1	0.64
valve position at row 2	0.84
valve position at row 3	1
valve position at row 4	0.89
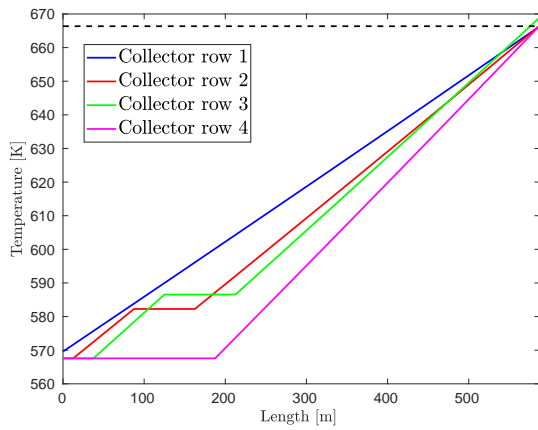
Figure A.83: Result of the valve control with *predicitve time* 5000 s and slow shadow introduction for a network of 4 tubes.

Table A.83: Data corresponding to the simulation of the valve control with *predicitve time* 5000 s and slow schadow introduction for a network of 4 tubes.

Valve Control - Fast Shadow -	
g	1
$\tilde{g}$	3
end temp. absorber tube 1	666.36 K
end temp. absorber tube 2	668.44 K
end temp. absorber tube 3	667.47 K
end temp. absorber tube 4	668.89 K
temp. at heat exchanger	667.66 K
mass flow	17.78 $m^3 s^{-1}$
computational time	366.55 s
finished after	-
valve position at row 1	0.64
valve position at row 2	0.83
valve position at row 3	1
valve position at row 4	0.85
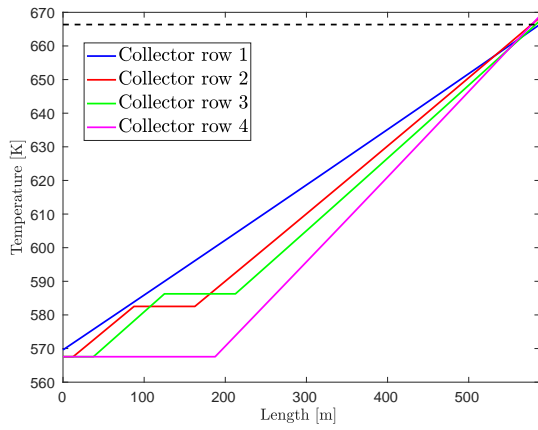
Figure A.84: Result of the valve control with *predicitve time* 5000 s and fast shadow introduction for a network of 4 tubes.

Table A.84: Data corresponding to the simulation of the valve control with *predicitve time* 5000 s and fast schadow introduction for a network of 4 tubes.

Valve Control - Slow Shadow -	
g	1
$\tilde{g}$	3
end temp. absorber tube 1	666.36 K
end temp. absorber tube 2	666.56 K
end temp. absorber tube 3	667.67 K
end temp. absorber tube 4	666.55 K
temp. at heat exchanger	666.65 K
mass flow	17.98 $m^3 s^{-1}$
computational time	123.68 s
finished after	-
valve position at row 1	0.63
valve position at row 2	0.83
valve position at row 3	1
valve position at row 4	0.87
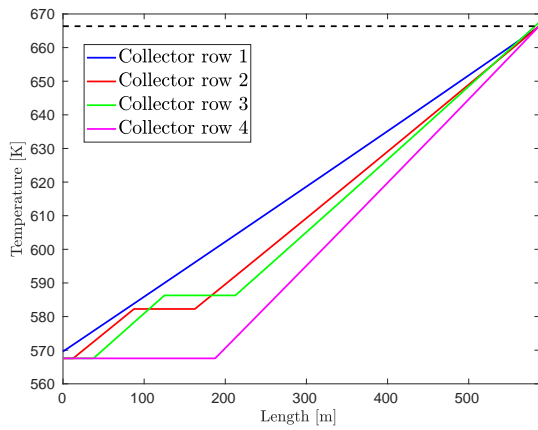
Figure A.85: Result of the valve control with *predicitve time* 5000 s and slow shadow introduction for a network of 4 tubes.

Table A.85: Data corresponding to the simulation of the valve control with *predicitve time* 5000 s and slow schadow introduction for a network of 4 tubes.
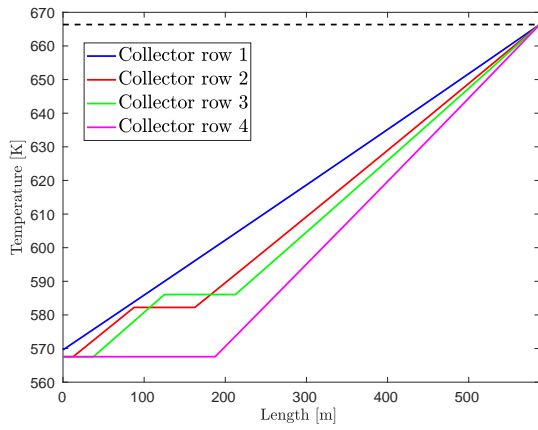
Figure A.86: Result of the valve control with *predicitve time* 5000 s and fast shadow introduction for a network of 4 tubes.

Valve Control - Fast Shadow -	
g	0
$\tilde{g}$	0
end temp. absorber tube 1	666.36 K
end temp. absorber tube 2	666.36 K
end temp. absorber tube 3	666.33 K
end temp. absorber tube 4	666.36 K
temp. at heat exchanger	666.35 K
mass flow	18.06 $m^3 s^{-1}$
computational time	473.65 s
finished after	17840
valve position at row 1	0.63
valve position at row 2	0.83
valve position at row 3	0.98
valve position at row 4	0.84

Table A.86: Data corresponding to the simulation of the valve control with *predicitve time* 5000 s and fast schadow introduction for a network of 4 tubes.
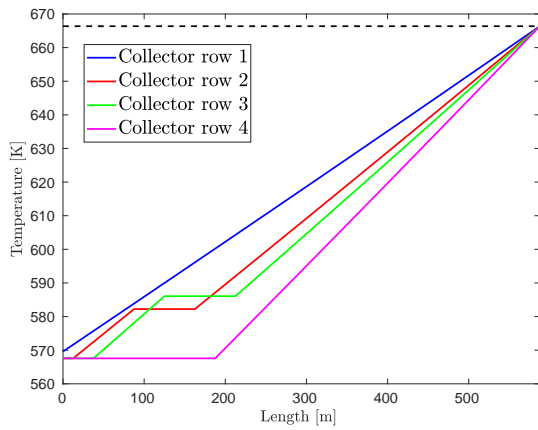
Figure A.87: Result of the valve control with *predicitve time* 5000 s and slow shadow introduction for a network of 4 tubes.

Valve Control - Slow Shadow -	
g	0
$\tilde{g}$	0
end temp. absorber tube 1	666.36 K
end temp. absorber tube 2	666.35 K
end temp. absorber tube 3	666.34 K
end temp. absorber tube 4	666.35 K
temp. at heat exchanger	666.28 K
mass flow	18.06 $m^3 s^{-1}$
computational time	459.68 s
finished after	17810
valve position at row 1	0.63
valve position at row 2	0.83
valve position at row 3	1
valve position at row 4	0.86

Table A.87: Data corresponding to the simulation of the valve control with *predicitve time* 5000 s and slow schadow introduction for a network of 4 tubes.

Valve Control with weather forecast
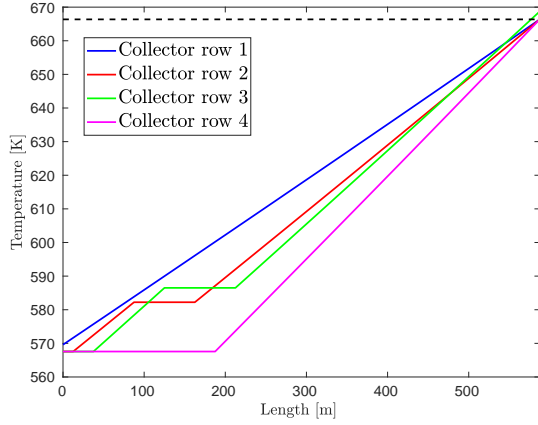
Figure A.88: Result of the valve control with weather forecast and fast shadow introduction for a network of 4 tubes.

Valve Control with weather forecast - Fast Shadow -	
g	3
$\tilde{g}$	5
end temp. absorber tube 1	666.36 K
end temp. absorber tube 2	666.36 K
end temp. absorber tube 3	668.72 K
end temp. absorber tube 4	666.36 K
temp. at heat exchanger	666.91 K
mass flow	17.94 $m^3 s^{-1}$
computational time	1156.79 s
finished after	10990 s
valve position at row 1	0.63
valve position at row 2	0.84
valve position at row 3	1
valve position at row 4	0.89

Table A.88: Data corresponding to the simulation of the valve control with weather forecast and fast schadow introduction for a network of 4 tubes.
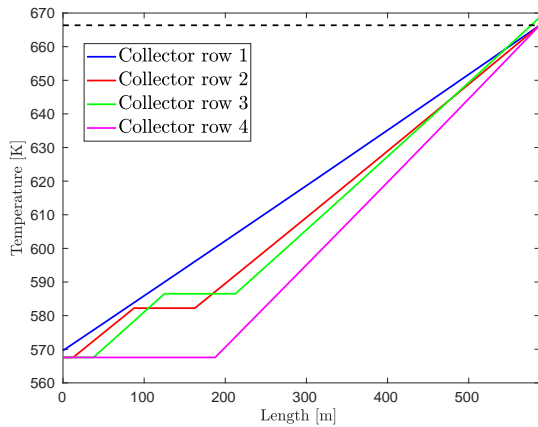

Figure A.89: Result of the valve control with weather forecast and slow shadow introduction for a network of 4 tubes.

Valve Control with weather forecast - Slow Shadow -	
g	3
$\tilde{g}$	5
end temp. absorber tube 1	666.36 K
end temp. absorber tube 2	666.36 K
end temp. absorber tube 3	668.73 K
end temp. absorber tube 4	666.36 K
temp. at heat exchanger	666.96 K
mass flow	17.94 $m^3 s^{-1}$
computational time	893.13 s
finished after	10990 s
valve position at row 1	0.63
valve position at row 2	0.84
valve position at row 3	1
valve position at row 4	0.89

Table A.89: Data corresponding to the simulation of the valve control with weather forecast and slow schadow introduction for a network of 4 tubes.
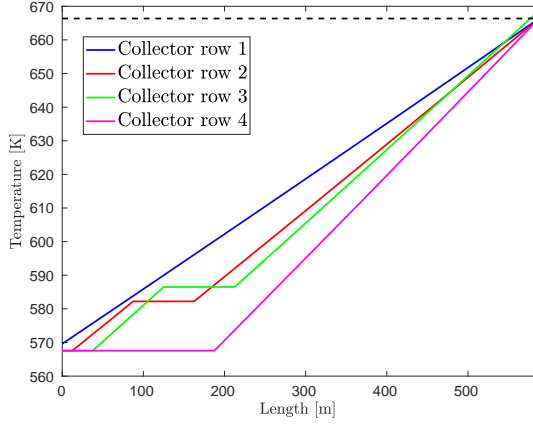
Figure A.90: Result of the valve control with weather forecast and fast shadow introduction for a network of 4 tubes.

Valve Control with weather forecast - Fast Shadow -	
g	1
$\tilde{g}$	3
end temp. absorber tube 1	666.36 K
end temp. absorber tube 2	666.36 K
end temp. absorber tube 3	668.72 K
end temp. absorber tube 4	666.36 K
temp. at heat exchanger	666.91 K
mass flow	17.94 $m^3 s^{-1}$
computational time	1527.44 s
finished after	10990 s
valve position at row 1	0.63
valve position at row 2	0.84
valve position at row 3	1
valve position at row 4	0.89

Table A.90: Data corresponding to the simulation of the valve control with weather forecast and fast schadow introduction for a network of 4 tubes.
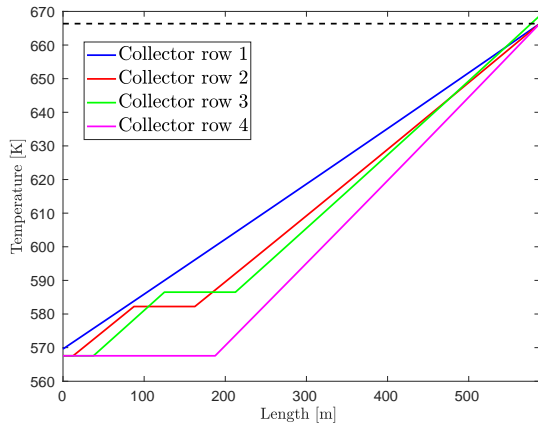

Figure A.91: Result of the valve control with weather forecast and slow shadow introduction for a network of 4 tubes.

Valve Control with weather forecast - Slow Shadow -	
g	1
$\tilde{g}$	3
end temp. absorber tube 1	666.36 K
end temp. absorber tube 2	666.36 K
end temp. absorber tube 3	668.72 K
end temp. absorber tube 4	666.36 K
temp. at heat exchanger	666.82 K
mass flow	17.94 $m^3 s^{-1}$
computational time	1007.65 s
finished after	10990 s
valve position at row 1	0.63
valve position at row 2	0.84
valve position at row 3	1
valve position at row 4	0.89

Table A.91: Data corresponding to the simulation of the valve control with weather forecast and slow schadow introduction for a network of 4 tubes.

144
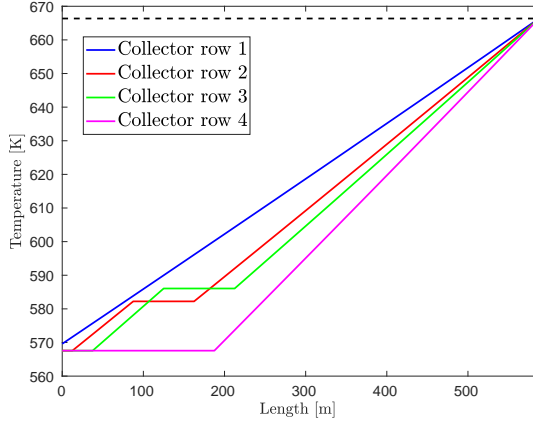
Figure A.92: Result of the valve control with weather forecast and fast shadow introduction for a network of 4 tubes.

Valve Control with weather forecast - Fast Shadow -	
g	0
$\tilde{g}$	0
end temp. absorber tube 1	666.36 K
end temp. absorber tube 2	666.36 K
end temp. absorber tube 3	666.36 K
end temp. absorber tube 4	666.36 K
temp. at heat exchanger	666.36 K
mass flow	18.06 $m^3 s^{-1}$
computational time	2266.78 s
finished after	10970 s
valve position at row 1	0.63
valve position at row 2	0.83
valve position at row 3	1
valve position at row 4	0.86

Table A.92: Data corresponding to the simulation of the valve control with weather forecast and fast schadow introduction for a network of 4 tubes.
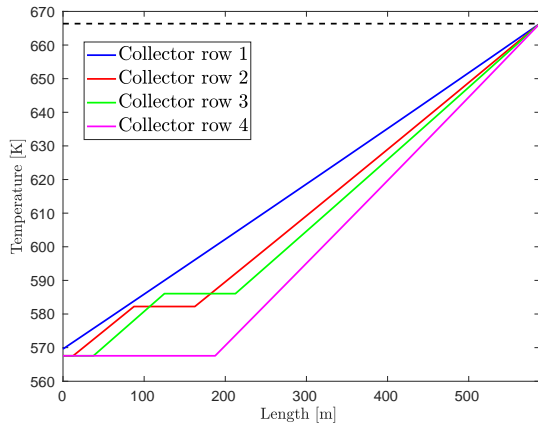

Figure A.93: Result of the valve control with weather forecast and slow shadow introduction for a network of 4 tubes.

Valve Control with weather forecast - Slow Shadow -	
g	0
$\tilde{g}$	0
end temp. absorber tube 1	666.36 K
end temp. absorber tube 2	666.36 K
end temp. absorber tube 3	666.36 K
end temp. absorber tube 4	666.36 K
temp. at heat exchanger	666.27 K
mass flow	18.06 $m^3 s^{-1}$
computational time	2276.94 s
finished after	10990 s
valve position at row 1	0.63
valve position at row 2	0.83
valve position at row 3	1
valve position at row 4	0.86

Table A.93: Data corresponding to the simulation of the valve control with weather forecast and slow schadow introduction for a network of 4 tubes.

Cherek's Valve Control

Cherek's Valve control cannot cope with the given situation. The simulation ends immediately with a CFL-error.
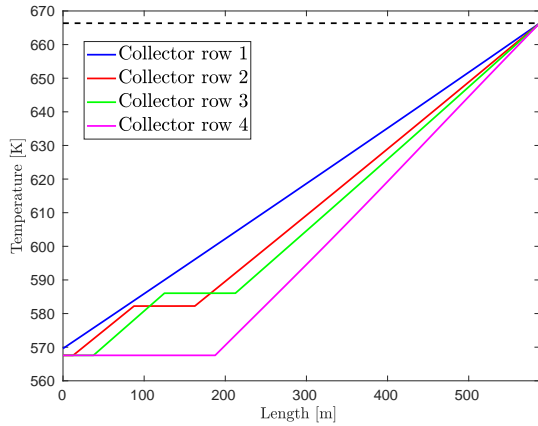
Figure A.94: Result of Cherek's valve control for fast shadow introduction and a network of 4 tubes, when using $\Delta t = 0.5$ s.

Cherek's Valve Control - Fast Shadow -	
end temp. absorber tube 1	666.36 K
end temp. absorber tube 2	666.36 K
end temp. absorber tube 3	666.36 K
end temp. absorber tube 4	666.36 K
temp. at heat exchanger	666.36 K
mass flow	18.11 $m^3 s^{-1}$
computational time	39.46 s
finished after	-
valve position at row 1	0.63
valve position at row 2	0.82
valve position at row 3	0.82
valve position at row 4	0.72

Table A.94: Data corresponding to the simulation of Cherek's valve control for fast schadow introduction and a network of 4 tubes, when using $\Delta t = 0.5$ s.

A.4. Network - Molten Salt

Design Point
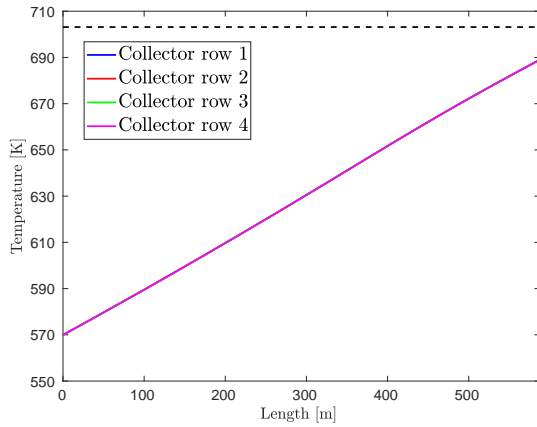
Figure A.95: Design point for a network of 4 tubes and molten salt.

Design point - without Shadow -	
inflow temp.	569.97 K
end temp. absorber tube 1	688.98 K
end temp. absorber tube 2	688.98 K
end temp. absorber tube 3	688.98 K
end temp. absorber tube 4	688.98 K
temp. at heat exchanger	677.3 K
mass flow	24.15 $m^3 s^{-1}$

Table A.95: Data corresponding to the design point for a network of 4 tubes and molten salt.
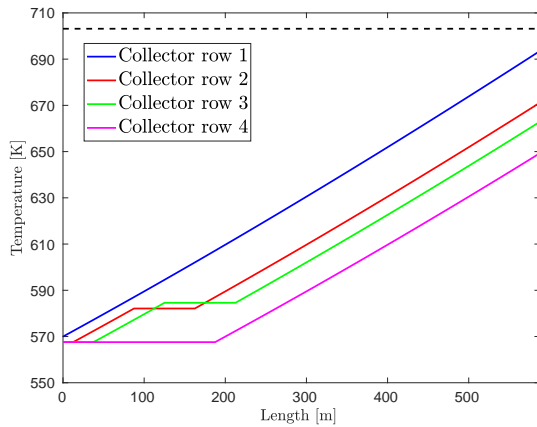
Figure A.96: Design point for a network of 4 tubes and molten salt with shadow.

Design point - with Shadow -	
inflow temp.	567.57 K
end temp. absorber tube 1	693.48 K
end temp. absorber tube 2	671.11 K
end temp. absorber tube 3	662.86 K
end temp. absorber tube 4	649.25 K
temp. at heat exchanger	678.93 K
mass flow	24.13 $m^3 s^{-1}$

**Table A.96:** Data corresponding to the design point for a network of 4 tubes and molten salt with shadow.

Mirror Control
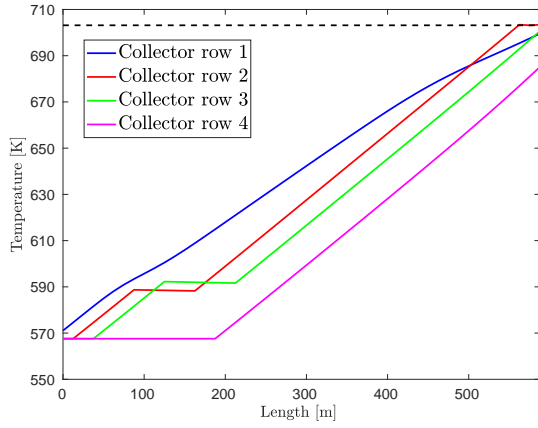
**Figure A.97:** Result of the mirror control with slow shadow introduction for a network of 4 tubes.

Mirror Control - Slow Shadow -	
g	3
$\tilde{g}$	5
end temp. absorber tube 1	699.52 K
end temp. absorber tube 2	703.39 K
end temp. absorber tube 3	700.55 K
end temp. absorber tube 4	685.06 K
temp. at heat exchanger	701.87 K
mass flow	16.35 $m^3 s^{-1}$
computational time	188.64 s
finished after	-
defocused mirrors in row 1	0
defocused mirrors in row 2	2
defocused mirrors in row 3	0
defocused mirrors in row 4	0

Table A.97: Data corresponding to the simulation of the mirror control with slow schadow introduction for a network of 4 tubes.

## Mirror Control with calculated defocus number
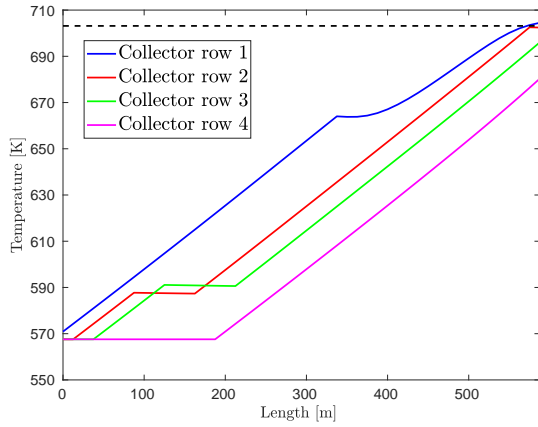
Figure A.98: Result of the mirror control with calculated defocus number and slow shadow introduction for a network of 4 tubes.

Mirror Control with $N_{\mathbf{defocus}}$ - Slow Shadow -	
end temp. absorber tube 1	704.49 K
end temp. absorber tube 2	702.44 K
end temp. absorber tube 3	696.01 K
end temp. absorber tube 4	680.32 K
temp. at heat exchanger	701.19 K
mass flow	17.12 $m^3 s^{-1}$
computational time	207.65 s
finished after	-
defocused mirrors in row 1	20
defocused mirrors in row 2	1
defocused mirrors in row 3	0
defocused mirrors in row 4	0

Table A.98: Data corresponding to the simulation of the mirror control with calculated defocus number and slow schadow introduction for a network of 4 tubes.

Mirror Control with weather forecast
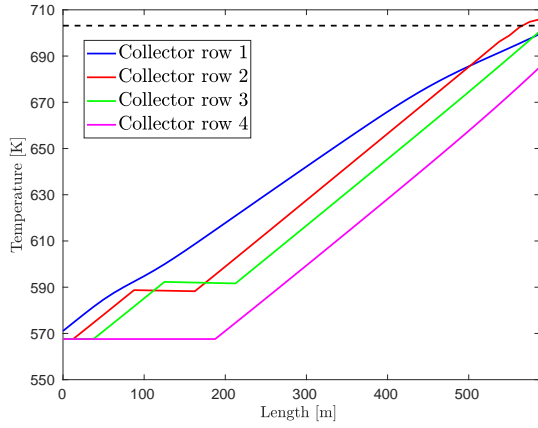
Figure A.99: Result of the mirror control with weather forecast and slow shadow introduction for a network of 4 tubes.

Mirror Control with weather forecast - Slow Shadow -	
g	3
$\tilde{g}$	5
end temp. absorber tube 1	699.54 K
end temp. absorber tube 2	705.92 K
end temp. absorber tube 3	700.69 K
end temp. absorber tube 4	685.19 K
temp. at heat exchanger	701.87 K
mass flow	16.33 $m^3 s^{-1}$
computational time	157.33 s
finished after	-
defocused mirrors in row 1	0
defocused mirrors in row 2	4
defocused mirrors in row 3	0
defocused mirrors in row 4	0

Table A.99: Data corresponding to the simulation of the mirror control with weather forecast and slow schadow introduction for a network of 4 tubes.

## Mirror Control with calculated defocus number and weather forecast
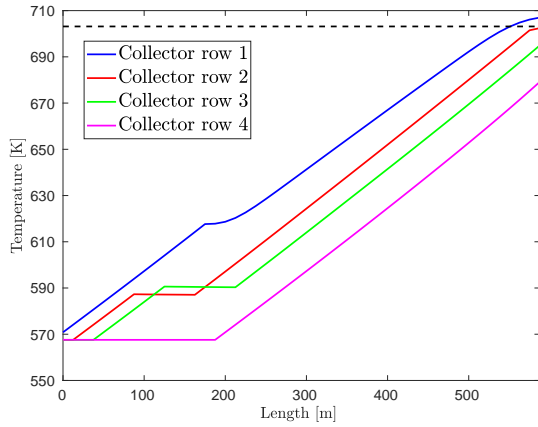
Figure A.100: Result of the mirror control with calculated defocus number, weather forecast and slow shadow introduction for a network of 4 tubes.

Mirror Control with $N_{\textbf{defocus}}$ and weather forecast - Slow Shadow -	
end temp. absorber tube 1	706.99 K
end temp. absorber tube 2	702.42 K
end temp. absorber tube 3	694.92 K
end temp. absorber tube 4	679.15 K
temp. at heat exchanger	701.04 K
mass flow	17.5 $m^3 s^{-1}$
computational time	202.15 s
finished after	-
defocused mirrors in row 1	33
defocused mirrors in row 2	0
defocused mirrors in row 3	0
defocused mirrors in row 4	0

Table A.100: Data corresponding to the simulation of the mirror control with calculated defocus number, weather forecast and slow schadow introduction for a network of 4 tubes.
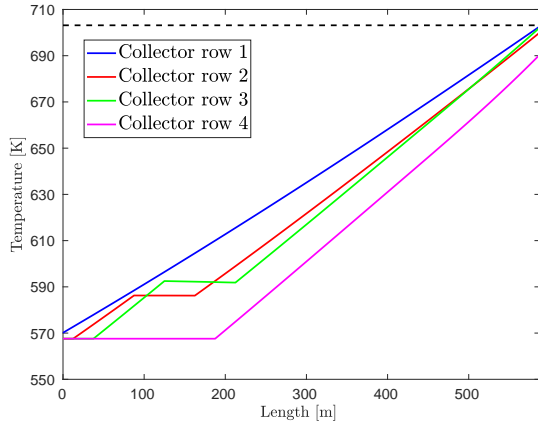
Valve Control

Figure A.101: Result of the valve control with slow shadow introduction for a network of 4 tubes.

Valve Control - Slow Shadow -	
g	3
$\tilde{g}$	5
end temp. absorber tube 1	702.65 K
end temp. absorber tube 2	699.99 K
end temp. absorber tube 3	702.14 K
end temp. absorber tube 4	690.41 K
temp. at heat exchanger	701.2 K
mass flow	18.19 $m^3 s^{-1}$
computational time	167.11 s
finished after	-
valve position at row 1	0.63
valve position at row 2	0.84
valve position at row 3	1
valve position at row 4	0.96

Table A.101: Data corresponding to the simulation of the valve control with slow schadow introduction for a network of 4 tubes.

Valve Control with weather forecast

Valve Control with weather forecast - Slow Shadow -	
g	3
$\tilde{g}$	5
end temp. absorber tube 1	702.66 K
end temp. absorber tube 2	700.04 K
end temp. absorber tube 3	702.18 K
end temp. absorber tube 4	690.23 K
temp. at heat exchanger	701.29 K
mass flow	18.19 $m^3 s^{-1}$
computational time	180.05 s
finished after	-
valve position at row 1	0.63
valve position at row 2	0.84
valve position at row 3	1
valve position at row 4	0.96
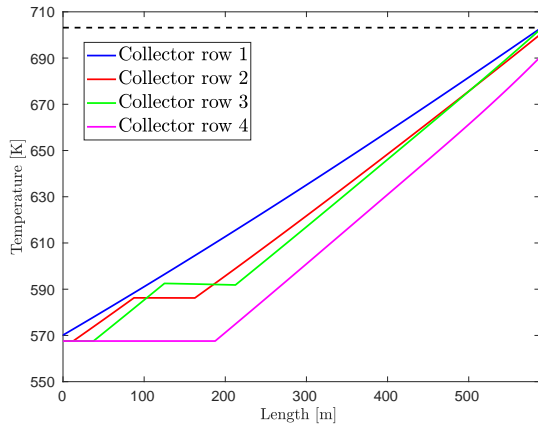
Figure A.102: Result of the valve control with weather forecast and slow shadow introduction for a network of 4 tubes.

Table A.102: Data corresponding to the simulation of the valve control with weather forecast and slow schadow introduction for a network of 4 tubes.

A.5. Matlab Code

The Matlab code of the described controls, built into the code of Cherek, is enclosed with the thesis in form of a DVD.

To be able to use the code in Matlab, the folders *code*, *InitialData* and *ClosureEquations* must be added to the file path in Matlab. The initial settings for the scenarios described here are sorted in the subfolders *InitialData/Oil* and *InitialData/Salt*. The data for oil are also already available in the parent folder. For the use of molten salt as heat transfer fluid these must be exchanged accordingly. Depending on the desired control or application some parameters have to be set in the control files (e.g. *annikaMirrorControl.m*) or the main file *Setup.m*. Finally, the simulation can be started by a call such as:

```
Setup(NetworkSetupLaAfricana,'TherminolVP1','annikaMirrorControl','upwind')
```

References

[1] Image. Online available at `https://en.grupotsk.com/images/uploads/proyectoimage/408/imagen/at10-199.jpg`; accessed on March 19, 2019.

[2] John J. Burkhardt III, Garvin A. Heath, and Craig S. Turchi. Life cycle assessment of a parabolic trough concentrating solar power plant and the impacts of key design alternatives. *Environmental science & technology*, 45(6):2457–2464, 2011.

[3] Therminol Heat Transfer Fluids by Solutia. Inc. therminol vp 1, 2012.

[4] Matthias Cherek. Regulating the temperature in a network of tubes in solar thermal power plants. Bachelor thesis at RWTH Aachen University, 2018.

[5] European Commission. A policy framework for climate and energy in the period from 2020 to 2030. Website, 2014. Online available at `http://eur-lex.europa.eu/legal-content/EN/ALL/?uri=CELEX:52014DC0015`; accessed on April 23, 2018.

[6] Taqiy eddine Boukelia and Mohamed-Salah Mecibah. Parabolic trough solar thermal power plant: Potential, and projects development in algeria. *Renewable and Sustainable Energy Reviews*, 21:288–297, 2013.

[7] Isabel Llorente García, José Luis Álvarez, and Daniel Blanco. Performance model for parabolic trough solar thermal power plants with thermal storage: Comparison to operating plant data. *Solar Energy*, 85(10):2443–2460, 2011.

[8] Michael Geyer, Eckhard Lüpfert, Rafael Osuna, Antonio Esteban, Wolfgang Schiel, Axel Schweitzer, Eduardo Zarza, Paul Nava, Josef Langenkamp, and Eli Mandelberg. Eurotrough-parabolic trough collector developed for cost efficient solar power generation. In *11th International symposium on concentrating solar power and chemical energy technologies*, pages 04–06, 2002.

[9] Hubertus Th Jongen, Klaus Meer, and Eberhard Triesch. *Optimization theory*. Springer Science & Business Media, 2007.

[10] M. J. Montes, A. Abánades, J. M. Martínez-Val, and M. Valdés. Solar multiple optimization for a solar-only thermal power plant, using oil as heat transfer fluid in the parabolic trough collectors. *Solar Energy*, 83(12):2165–2176, 2009.

[11] U.S. Department of Energy. Concentrating solar power projects. Website. Online available at `https://www.nrel.gov/csp/solarpaces/project_detail.cfm/projectID=236`; accessed on February 12, 2019.

[12] J. Ignacio Ortega, J. Ignacio Burgaleta, and Félix M. Téllez. Central receiver system solar power plant using molten salt as heat transfer fluid. *Journal of Solar energy engineering*, 130(2):024501, 2008.

[13] Robert Pitz-Paal, Jürgen Dersch, Barbara Milow, Félix Téllez, Alain Ferriere, Ulrich Langnickel, Aldo Steinfeld, Jacob Karni, Eduardo Zarza, and Oleg Popel. Development steps for parabolic trough solar power technologies with maximum impact on cost reduction. *Journal of Solar Energy Engineering*, 129(4):371–377, 2007.

[14] Andreas Poullikkas. Economic analysis of power generation from parabolic trough solar thermal plants for the mediterranean region—a case study for the island of cyprus. *Renewable and sustainable Energy reviews*, 13(9):2474–2484, 2009.

[15] V. Siva Reddy, S. C. Kaushik, and SK. Tyagi. Exergetic analysis and performance evaluation of parabolic trough concentrating solar thermal power plant (ptcstpp). *Energy*, 39(1):258–273, 2012.

[16] S. Rohani, T. P. Fluri, F. Dinter, and Peter Nitz. Modelling and simulation of parabolic trough plants based on real operating data. *Solar Energy*, 158:845–860, 2017.

[17] Manohar S Sohal, Matthias A Ebner, Piyush Sabharwall, and Phil Sharpe. Engineering database of liquid salt thermophysical and thermochemical properties. Technical report, Idaho National Laboratory (INL), 2010.

[18] Fredi Tröltzsch. *Optimal control of partial differential equations: theory, methods, and applications*, volume 112. American Mathematical Soc., 2010.